Institut für Chemie

Sequence Dependency of Photon- and Electron Induced DNA Strand Breaks

Dissertation

zur Erlangung des akademischen Grades

Doctor rerum naturalium (Dr. rer. nat.)

vorgelegt der Mathematisch-Naturwissenschaftlichen

Fakultät der Universität Potsdam

von

Stefanie Vogel

Eingereicht am 19.06.2018

Published online at the
Institutional Repository of the University of Potsdam:
URN urn:nbn:de:kobv:517-opus4-419669
http://nbn-resolving.de/urn:nbn:de:kobv:517-opus4-419669

Diese Arbeit ist vom Januar 2015 bis Juni 2018 als kooperatives Projekt an der Universität Potsdam, der Bundesanstalt für Materialforschung und -prüfung und der Humboldt Universität zu Berlin im Rahmen der Graduiertenschule School of Analytical Sciences Adlershof entstanden.

Gutachter: Prof. Dr. Ilko Bald
Prof. Dr. Thomas Schlathölter
Prof. Dr. Steen Brøndsted Nielsen

Abstract

Deoxyribonucleic acid (DNA) is the carrier of human genetic information and is exposed to environmental influences such as the ultraviolet (UV) fraction of sunlight every day. The photostability of the DNA against UV light is astonishing. Even if the DNA bases have a strong absorption maximum at around 260 nm/4.77 eV, their quantum yield of photoproducts remains very low [1]. If the photon energies exceed the ionization energy (IE) of the nucleobases (~8-9 eV) [2], the DNA can be severely damaged. Photoexcitation and -ionization reactions occur, which can induce strand breaks in the DNA. The efficiency of the excitation and ionization induced strand breaks in the target DNA sequences are represented by cross sections. If Si as a substrate material is used in the VUV irradiation experiments, secondary electrons with an energy below 3.6 eV are generated from the substrate. This low energy electrons (LEE) are known to induce dissociative electron attachment (DEA) in DNA and with it DNA strand breakage very efficiently. LEEs play an important role in cancer radiation therapy, since they are generated secondarily along the radiation track of ionizing radiation.

In the framework of this thesis, different single stranded DNA sequences were irradiated with 8.44 eV vacuum UV (VUV) light and cross sections for single strand breaks (SSB) were determined. Several sequences were also exposed to secondary LEEs, which additionally contributed to the SSBs. First, the cross sections for SSBs depending on the type of nucleobases were determined. Both types of DNA sequences, mono-nucleobase and mixed sequences showed very similar results upon VUV radiation. The additional influence of secondarily generated LEEs resulted in contrast in a clear trend for the SSB cross sections. In this, the polythymine sequence had the highest cross section for SSBs, which can be explained by strong anionic resonances in this energy range. Furthermore, SSB cross sections were determined as a function of sequence length. This resulted in an increase in the strand breaks to the same extent as the increase in the geometrical cross section. The longest DNA sequence (20 nucleotides) investigated in this series, however, showed smaller cross section values for SSBs, which can be explained by conformational changes in the DNA. Moreover, several DNA sequences that included the radiosensitizers 5-Bromouracil (^{5Br}U) and 8-Bromoadenine (^{8Br}A) were investigated and the corresponding SSB cross sections were determined. It was shown that ^{5Br}U reacts very strongly to VUV radiation leading to high strand break yields, which showed in turn a strong sequence-dependency. ^{8Br}A, on the other hand, showed no sensitization to the applied VUV radiation, since almost no increase in strand breakage yield was observed in comparison to non-modified DNA sequences.

In order to be able to identify the mechanisms of radiation damage by photons, the IEs of certain DNA sequences were further explored using photoionization tandem mass spectrometry. By varying the DNA sequence, both the IEs depending on the type of nucleobase as well as on the DNA strand length could be identified and correlated to the SSB cross sections. The influence of the IE on the photoinduced reaction in the brominated DNA sequences could be excluded.

Zusammenfassung

Desoxyribonukleinsäure (DNA) ist als Träger der menschlichen Erbinformation täglich vielen Einflüssen ausgesetzt. Diese Einflüsse können Teil unserer Umwelt sein, wie der ultraviolette (UV) Anteil des Sonnenlichts. Die Photostabilität der DNA gegen UV-Licht ist erstaunlich, denn trotz eines starkes Absorptionsmaximum der DNA-Basen bei etwa 260 nm/4,77 eV, bleibt ihre Quantenausbeute an Photoprodukten sehr gering [1]. Überschreiten die Photonenenergien die Ionisationsenergie (IE) der Nukleinbasen (~ 8-9 eV) [2], kann die DNA schwer geschädigt werden. Es treten Anregungs- und Ionisierungsreaktionen auf, die zu Strangbrüchen in der DNA führen. Die Effizienz der induzierten Strangbrüche in den untersuchten DNA-Sequenzen wird durch Wirkungsquerschnitte dargestellt. Wird in den Bestrahlungsexperimenten Silizium als Substratmaterial verwendet, werden aus dem Substrat zusätzliche Sekundärelektronen mit einer Energie unter 3,6 eV erzeugt, die weiteren Schaden an der DNA verursachen. Diese niederenergetischen Elektronen (LEE) sind dafür bekannt, dissoziative Elektronenanlagerung (DEA) und damit Strangbrüche in der DNA zu erzeugen. LEEs entstehen sekundär entlang des Strahlungsweges von ionisierender Strahlung im biologischen Gewebe, wenn in der Behandlung der Krankheit Krebs Strahlentherapie eingesetzt wird.

Im Rahmen dieser Arbeit wurden verschiedene Einzelstrang-DNA-Sequenzen mit 8.44 eV Vakuum-UV (VUV) Licht bestrahlt und Wirkungsquerschnitte für Einzelstrangbrüche (SSB) bestimmt. Ein Teil der Sequenzen wurde außerdem sekundär erzeugten LEEs ausgesetzt, die einen zusätzlichen Beitrag zu den SSBs liefern. Als erstes wurde der Wirkungsquerschnitt für SSBs in Abhängigkeit der Nukleinbasen bestimmt. Hierbei weisen sowohl die DNA Sequenzen, die nur ein Sorte an Nukleinbasen besitzen als auch die gemischte Sequenzen sehr ähnliche Werte auf. Durch den zusätzlichen Einfluss der LEEs hat sich wiederum für die DNA Sequenzen mit nur einer Sorte an Nukleinbasen ein stark ausgeprägter Trend gezeigt. Die Polythymin-Sequenz weist den höchsten Wirkungsquerschnitt für SSBs auf, was durch ausgeprägte anionische Resonanzen in diesem Energiebereich begründet werden kann. Des Weiteren wurden Wirkungsquerschnitte für SSBs in Abhängigkeit Sequenzlänge ermittelt. Dabei ergab sich eine Erhöhung der SSBs im gleichen Maße wie die Vergrößerung des geometrischen Wirkungsquerschnitts. Die längste DNA Sequenz (20 Nukleotide), die in dieser Reihe untersucht wurde, zeigte hingegen kleinere Werte für den SSB Wirkungsquerschnitt, was durch Konformationsänderungen in der DNA erklärt werden kann. Einige der untersuchten DNA Sequenzen wurden zusätzlich mit den Radiosensibilisatoren 5-Bromouracil (^{5Br}U) und 8-Bromoadenine (^{8Br}A) modifiziert und entsprechende SSB Wirkungsquerschnitte bestimmt. Hierbei hat sich gezeigt, dass ^{5Br}U mittels einer hohen Strangbruchausbeute sehr stark auf VUV Strahlung reagiert, wobei das Ausmaß der Reaktion stark sequenzabhängig ist. ^{8Br}A hingegen, weist keine Sensibilisierung gegenüber der verwendeten VUV Strahlung auf, da keine Erhöhung der Strangbruchausbeute gegenüber unmodifizierten DNA Sequenzen ersichtlich ist.

Um die Mechanismen der Strahlenschädigung durch Photonen besser einschätzen zu können, wurden zusätzlich die IEs bestimmter DNA Sequenzen mit Hilfe der Photoionisations-Tandem-Massenspektrometrie untersucht. Durch Variation der DNA-Sequenzen konnte sowohl ein Trend der IEs in Abhängigkeit der Nukleinbasen und der DNA-Stranglänge identifiziert und als auch eine Abhängigkeit der Reaktivität von ^{5Br}U von seinem IE in der entsprechenden DNA Sequenz ausgeschlossen werden. Die IE Trends und die Wirkungsquerschnitte für SSBs wurden abschließend in Korrelation gebracht.

Content

Abbreviations

^{8Br}A	8-Bromoadenine
^{5Br}U	5-Bromouracil
8-oxoG	8-Oxoguanine
A	Adenine
A	Area
abs.	Absolute
AD	Auto detachment
AFM	Atomic force microscopy
APEX	Atmospheric pressure experiment
Ar	Argon
C	Cytosine
CaF_2	Calcium fluoride
Co	Cobalt
d	Diameter
DEA	Dissociative electron attachment
DI	Dissociative ionization
DISCO	Dichroism, Imaging and mass Spectrometry for Chemical and biological systems
DNA	Deoxyribonucleic acid
DSB	Double strand break
dsDNA	Double stranded DNA
E	Energy
e^-	Electron
EC	Electron capture
EA	Electron affinity
EA_a	Adiabatic electron affinity
EDTA	Ethylenediaminetetraacetic acid
EF	Enhancement factor
E_{ox}	Oxidation potential
E_{ph}	Energy of a photon
ESI	Electrospray ionization
F	Fluence
h	Planck constant
G	Guanine
H·	Hydrogen radical
H^+	Proton
H_2	Hydrogen
H_2O	Water
H_2O_2	Hydrogen peroxide
HOMO	Highest occupied molecular orbital
HPLC	High pressure liquid chromatography

I	Current
IMS	Ion mobility spectrometry
IE	Ionization energy
IE_a	Adiabatic ionization energy
IE_v	Vertical ionization energy
l	Length
LEE	Low energy electrons
LET	Linear Energy Transfer
M	Molecular ion
$MgCl_2$	Magnesium chloride
mRNA	Messenger RNA
MS	Mass spectrometry
n	Number
N	Number of AFM images
n_{ph}	Number of photons
n_{SSB}	Number of SSBs
NB	Nucleobase
ND	Neutral dissociation
nt	Nucleotide
OH·	Hydroxide radical
P	Power
r	Radius
R	Resistance
R_{Diode}	Responsivity of the photodiode
RNA	Ribonucleic acid
σ_{SSB}	Cross section for SSBs
σ_n	Standard error
σ_A	Geometrical cross section
Si	Silicon
SOLEIL	Source optimisée de lumière d'énergie intermédiaire du LURE
SSB	Single strand break
ssDNA	Single stranded DNA
T	Thymine
t	Irradiation time
TAE	Tris-Acetate-EDTA
TNI	Transient negative ion
TTL	Transistor-transistor logic
UHV	Ultra-high vacuum
U	Uracil
U	Bias
UV	Ultraviolet
υ	Wave frequency

VAE	Vertical electron attachment energy
VD	Vertical detachment
VDE	Vertical detachment energy
VUV	Vacuum-ultraviolet
XPS	X-ray photoelectron spectroscopy
z	Charge state

1 Introduction

Deoxyribonucleic acid (DNA) as the carrier of all human genetic information [3] is exposed to many influences every day, which can cause severe structural damages leading to serious detrimental effects on its functionality. These influences can be part of the environment we live in such as the ultra violet (UV) fraction of the sunlight [4], natural or artificial radioactive radiation [5] or chemical substances such as the smoke of a cigarette [6]. Especially the photostability of DNA against UV light is extremely important for the existence and consistency of life itself. Even if the DNA bases have a strong absorption in the UV region (300 nm-200 nm), their quantum yield of photoproducts remains very low [1]. The incoming photon energy is effectively converted into vibrational energy and can either be distributed intra- or intermolecularly, before photochemical reactions can occur [7]. Despite the very effective non-radiative decay of the nucleobases, oxidation of the nucleobases such as the formation of 8-oxoguanine (8-oxoG) [8] or the formation of photoproducts such as the very prominent cyclobutane dimer or the (6-4) photoproduct emerge in the UV range [9]. Generally various modifications of the DNA components are feasible. Going to higher photon impact energies and exceeding the ionization energies (IEs) of the nucleobases (~ 8-9 eV) [2,10] single strand breaks (SSBs) and double strand breaks (DSBs) become dominant.

Although the body has highly effective repair mechanisms that can fix many of these defects [11], some remain irreparable. The ultimate way of the cell to deal with these damages is to initiate its own death, the apoptosis, to avoid further changes in the DNA code [12]. If the body fails to repair the DNA damage and the apoptosis cannot be initiated, the defect can change the genetic code and cause a mutation of the cell. This is often the beginning of the disease cancer, where the balance between cell growth and division and the cell death is disturbed to the point that biological tissue grows uncontrolled within the body. In developed countries, cancer is the second most common cause of death [13]. Thus, huge research effort is made to improve the medical treatment and to develop new treatment procedures [14], which classically consist of surgery, chemo- and radiotherapy. They are usually combined and adapted to the patients' needs to reach the optimal treatment effect. The surgical removal of the carcinogenic tissue, for example, is usually combined with the application of chemotherapeutics such as cisplatin [15]. If some tumor cells have not been removed by the surgery or have already spread in the body (metastasis), this drug is used to create cross links in the DNA double helix to keep the cells from replicating and induces the cell death [15]. Often, however the tumor has grown in a way rendering it inoperable as vital organs would otherwise become damaged by a surgery. In most cases radiotherapy can be a choice. This type of cancer therapy exploits the interaction of ionizing radiation, such as electron, photon or particle radiation, with biological matter. Depending on the radiation type and energy, different penetration depths and energy distribution of the incoming particle in the tissue can be reached and adapted to the position and the size of the tumor. The ionizing radiation generates

secondary particles such as electrons [16] and radicals [17] *via* collision reactions with the molecules of the cells along the radiation track. These secondary particles are causing the main damage in the DNA.

Electrons are mainly produced along the radiation track with an energy of 0-20 eV showing a maximum at around 10 eV [16]. Below an energy of 15 eV these low energy electrons (LEEs) can damage the DNA very effectively *via* dissociative electron attachment (DEA) [18]. In the DEA process a transient negative ion (TNI) is formed by the attachment of an electron to a formerly unoccupied molecular orbital at a specific energy. The decay of the TNI can lead to a fragmentation of the molecule yielding an anion and one or more neutral fragments. The nucleobases can basically function as antennas for LEEs [10,19–21]. This way, electrons can induce a bond cleavage in the DNA backbone that corresponds to a SSB [22–24]. If two SSBs in close proximity within one double stranded DNA strand (dsDNA) occur, they form a DSB, which cannot be repaired by the body and the cell apoptosis is initialized [12].

The generation of electrons along the radiation track and the DNA damaging DEA mechanism are well established processes. So far it was not well-established whether photons below 10 eV are able to induce DNA strand breaks as well. Still, it is known that photons in the UV energy regime can affect the DNA by excitation and ionization [25] and by further oxidation reactions such as the formation of cyclobutane pyrimidine dimers [26]. At energies equal to or higher than 4.7 eV electronic excitation within the DNA can occur [1] and initial experiments in the framework of my master thesis demonstrated photo-induced DNA strand breaks at an energy of 6.5 eV and higher, however with small cross sections [25]. The strand break cross sections are expected to rise considerably when approaching the IE of the DNA components at around 8-11 eV [2,10,27,28]. In the case of the photon energy being lower than the IE, electronic excitations and oxidation reactions are very likely to occur. If the photon energy exceeds the IE of the DNA, an electron can be ejected from the highest occupied molecular orbital (HOMO) or even higher states of the DNA molecule. Precursors for DNA damage sites could be formed this way and thus induce DNA strand breakage [25]. The processes going on in this energy regime need to be further explored. The aim of this thesis is also to compare the photon induced strand breakage around the IE with the corresponding processes induced by electrons in the same energy regime.

The group of secondary particles with the highest detrimental effect besides the electrons in the cells [29,30] are radicals. They mainly arise from the interaction of the ionizing radiation with water and oxygen in the cells [17] resulting in major oxidative damage that also leads to SSBs and DSBs. Carcinogenic cells however are hypoxic: they are deprived of oxygen [30,31]. Thus, less radicals can be formed decreasing the sensitivity of cancer cells against radiation.

To overcome this problem, radiosensitizing agents can be used. They are preferentially accumulated in cancer cells, since these cells have a higher metabolism and replication rate than healthy cells. One example of radiosensitizing agents are halogenated nucleobases [32] such as 5-bromouracil (^{5Br}U) and 8-bromoadenine (^{8Br}A), which are known

to have strong resonances in the LEE energy range that are needed to induce the DEA process and thus, an effective SSB formation [33–35]. By increasing the amount of SSBs in the DNA in such a way, the probability of forming a DSB becomes more likely, too, which in turn leads to an increased probability of cell apoptosis. This way, cancer cells experience a higher amount of DNA damage than healthy cells. Hence, the given radiation dose can be lowered and side effects minimized.

To better understand the underlying mechanisms in the interaction of DNA with LEE radiation and VUV photons, short single stranded DNA (ssDNA) sequences were used as DNA model systems in this thesis. The strand breakage was studied in DNA sequences of various lengths and nucleobase composition upon irradiation at a VUV energy of 8.44 eV. The amount of SSBs is determined as absolute cross section for SSBs, i.e. the probability of a SSB to occur after being hit from a corresponding particle (a photon or an electron). The absolute values are directly accessible, since the SSBs are determined on a single-molecular level. Otherwise mainly relative or effective values are determined, because it remains technically very difficult [36]. The single-molecular level was achieved by incorporating the target DNA sequences into a 2D origami nanostructure. The DNA origami nanostructures have been invented by Rothemund *et al*. [37]. To visualize the DNA target sequences within the DNA origami nanostructure, the DNA origami nanostructure has to be adsorbed onto a substrate first. Then, the target DNA sequence must be labelled with a protein. This way, atomic force microscopy (AFM) can be applied to visualize the ssDNA sequences. If the DNA sample is irradiated and a SSB occurs, the target DNA sequence is cleaved in the DNA backbone and hence, loses its binding site to the protein. Now the target DNA sequence cannot be visualized anymore. This way, intact and broken DNA sequences can be distinguished [38] and the absolute number of SSBs determined. Since the DNA damage caused by ionizing radiation in cancer cells is reduced at hypoxic conditions, radiosensitizers are used. To elucidate the effect of radiosensitizers on VUV induced DNA strand breaks, some selected target DNA sequences were modified with the radiosensitizers ^{5Br}U and ^{8Br}A. Both radiosensitizer molecules have a halogen substitution at the nucleobase to increase their electrophilicity to act as a strong electron trap. The DNA sequences modified with the radiosensitizers were also incorporated into DNA origami nanostructures to determine the cross sections for SSBs under the same irradiation conditions as for the non-modified target DNA sequences. From the relation of the cross sections for SSBs of the non-modified to the modified target DNA sequences, enhancement factors were calculated to estimate the increase of SSB formation in the modified DNA sequences and hence, their potential as radiosensitizer in medical treatment. Herein, vacuum ultraviolet (VUV) photon radiation with an energy of 8.44 eV was chosen as the main radiation type and energy, since this energy is around the ionization threshold of the nucleobases [2]. Ionization is a threshold process, therefore it is expected that also the SSB cross section increases considerably at photon energies exceeding the IE of the nucleobases. To better estimate the IE of the whole DNA sequence, photoionization tandem mass spectrometry was applied on the short DNA sequences investigated in this thesis. By varying the DNA sequence, an IE trend depending on the nucleobase composition and DNA strand length could be identified.

The photon radiation can also be directed on a substrate that is not transparent to this photon energy (8.44 eV). If the photon energy exceeds the work function of the substrate material, secondary electrons can be generated from the substrate surface. This can be exploited as an indirect radiation giving additional DNA damage, when the used substrate is covered by DNA origami nanostructures with target DNA sequences. This way, additional LEE radiation with an energy below 3.6 eV was produced and its effect on the target DNA sequences determined.

The influence of radiation on the DNA was already investigated by different approaches from a macroscopic view at the patient in clinical trials to a microscopic picture of the DNA building blocks obtained in gas phase experiments. In clinical trials the chemotherapeutics can be tested in combination with ionizing radiation to estimate the success of the treatment by the shrinking of the tumor size [39]. This way, the result of the apoptosis in the carcinogenic tissue can be observed, but not the reactions in the tumor cells themselves. In vitro studies allow to investigate the interaction of cells with radiation or/and chemotherapeutics and to study their survival rate and proliferation *via* cell viability and clonogenic assays. Many cancer cell lines can be screened here, but how the DNA itself reacts on the treatment remains unknown. The investigation of even smaller cell subunits such as the DNA itself can be performed in the condensed phase with the help of plasmid DNA, which was extracted from viruses [40]. Prepared as a thin film on a substrate, the SSB and DSB yield after irradiation can be determined by gel electrophoresis. In this way, a qualitative statement about the strand break yield can be made, but it is very much depending on the preparation method applied [41,42]. If short artificial oligonucleotides are irradiated instead of the plasmid DNA, the DNA fragments can be analyzed by using high-performance liquid chromatography (HPLC) to identify the damage sites and quantify their amount [43]. Only very small oligonucleotides can be analyzed with this technique. Otherwise the damage sites cannot be distinguished anymore. The irradiation of the oligonucleotides is also conducted as a DNA thin film on a substrate, where the preparation still has strong influence on the results. Going to the building blocks of the DNA such as the nucleobases themselves, investigations with crossed electron/molecular beam experiments deliver fragmentation patterns and anion resonances of the molecule, but isolated in the gas phase [44]. This method is limited to the size of the investigated system and the ability of the molecule to evaporate without degradation. So far, this was only possible for very small DNA systems, such as DNA building blocks or single nucleotides [45]. The results obtained in this type of experiments might be very different to those obtained in a more natural environment of the DNA, since already solvent molecules, which are coordinated to a molecule, allow many more ways for a molecule to distribute its energy and change the resonance energies and fragmentation pattern [46]. The research approach used in this thesis is based on the DNA origami technique [37,38] and is building a bridge between the investigation of SSBs and DSBs of the plasmid DNA and the investigation of short oligonucleotides with HPLC. The DNA origami technique allows the preparation of sublayer coverage of DNA nanostructures on the substrate to analyze the number of SSBs on a single molecule level. Several DNA sequences can be investigated at the same time under the same experimental conditions. The cross sections for SSBs determined in this thesis are even relevant for

clinical trials, since they give basic information for simulation of the interaction of biological matter with radiation.

In the following chapters the theoretical basics of the presented work are shown. First, the composition and structure of the DNA in the natural media, the condensed and the gas phase is discussed. Higher order DNA structures are introduced and characteristics of the DNA such as electronic properties, photostability and possible DNA damage sites described. In the next chapter the photon and electron induced processes in the condensed and in the gas phase DNA are discussed in detail. The main focus lies on the description of the photoionization and the DEA process compared with the state of the art. In this context, also the radiosensitizing effect of ^{5Br}U and ^{8Br}A in DNA is elaborated. The fourth chapter introduces the methods used in this thesis. The DNA origami technique, the VUV and LEE irradiation experiments and tandem mass spectrometry investigations are explained in detail. In the fifth and the sixth chapter the results of this thesis regarding the VUV and LEE irradiation investigations and the photoionization tandem mass spectrometry experiments are shown and compared to the results of other working groups applying similar DNA systems. In the last chapter, the work presented in this thesis is summarized and a short outlook is given.

2 Basics of deoxyribonucleic acid (DNA)

DNA as the carrier of our genetic information can be found in the cell of every living organism from the smallest bacteria to plants and the human being. The biological information that builds the foundation for the characteristics and appearance of every organism is stored in long polynucleotide DNA chains within the cell nucleus in eukaryotes or free in the cytoplasm in prokaryotes. The genetic information such as the composition of a protein is encoded in sections of the DNA chain. For the protein to be made out of this information, the corresponding DNA sequence has first to be transcribed by the enzyme ribonucleic acid (RNA) polymerase into the messenger RNA (mRNA). The ribosome translates then in turn the mRNA into a chain of amino acids, which folds into the corresponding protein [3]. If the nucleobase experiences a chemical modification e.g. through radical formation caused by ultraviolet radiation from the sun, the transcription will lead to mismatches in gene expression that can cause mutation and cancer [4]. The short DNA sequences used in this thesis serve as model systems to study the DNA damage caused by VUV and LEE radiation. A more detailed description of the DNA damage will be given in chapter 2.4.

2.1 Structure and properties in the condensed phase

The structure of DNA was discovered by Watson and Crick in 1953 [47] and is displayed in figure 1. A high number of nucleotides, which consist of three components, assemble a single polynucleotide chain. The nucleobase component is connected to a deoxyribose moiety (sugar unit) by a glycosidic bond that in turn is bound to a phosphate unit. The phosphate unit of each single nucleotide forms a phosphodiester bond to the neighboring sugar unit to create the backbone of the polynucleotide chain. The opposite nucleobases in the polynucleotide chains form a link *via* hydrogen bonding to create the typical double helical structure of the DNA. This interlink between the two chains is called a Watson-Crick base pair and is formed between the nucleobases adenine (A) and thymine (T), and guanine (G) and cytosine (C). Two hydrogen bonds are formed between A-T, while G-C base pairs are connected by three hydrogen bonds. In RNA T would be replaced by uracil (U), which has basically the same structure as T, but is lacking the methyl group. Between neighboring nucleobases within one polynucleotide chain ππ-stacking interactions occur [48]. They are based on attractive, non-covalent interactions of the π-system of the aromatic rings and give additional stability to the double helical DNA structure. Furthermore, the polarity of the phosphate group, which leads to Coulomb repulsion contributes to the double helical DNA structure, whereas these forces are weakened by the solvation of the backbone.

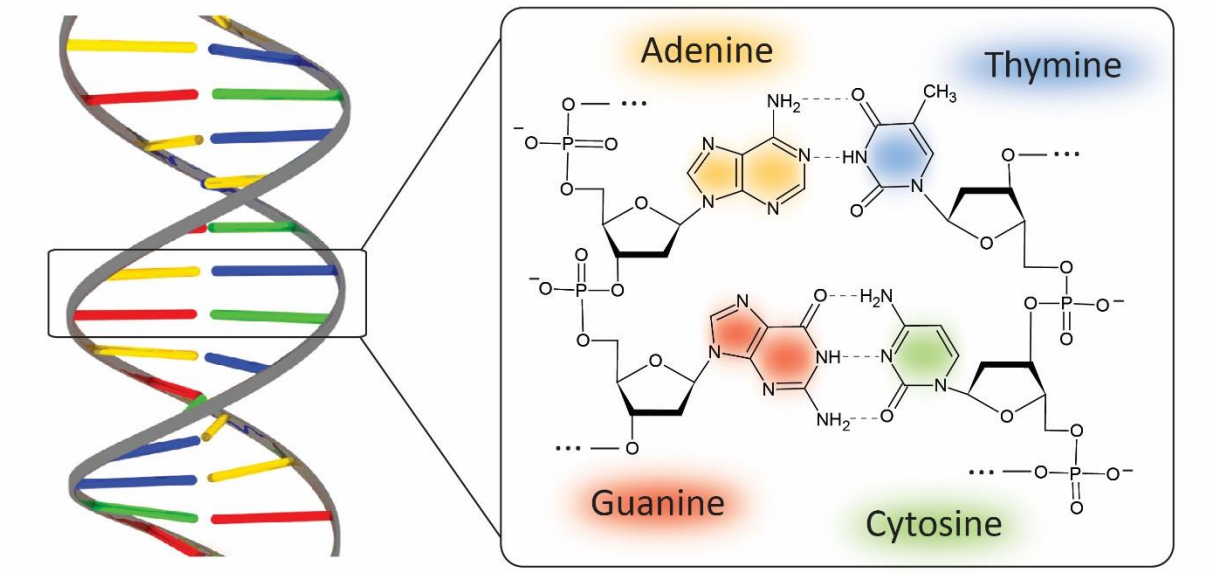

Fig. 1 Scheme of B-DNA double helix and its molecular structure.

In physiological media the DNA molecule is fully hydrated and exists in its right-handed B-form (fig.1). It has a diameter of 2 nm and a distance between base pairs along the helix axis of 0.34 nm [49]. Under reduced humidity or high salt concentrations the number of water molecules per nucleobase is decreasing and the DNA will change its conformation. The two most common structures under these conditions are the A- and the Z- form of the DNA [50]. The A-DNA structure is very similar to the B-form. The double helix formed here is also right-handed, but more compact in its structure. The diameter is a little larger with 2.3 nm, but the distance between adjacent bases along the axis is shorter with 0.24 nm [51]. The diameter of Z-DNA is smaller (1.8 nm) and the distance between bases along the axis is 0.46 nm [52]. This structure is left-handed and is only a transient structure being involved in biological activity [53].

Tab. 1 DNA type and their diameter, base distance and chirality.

DNA type	**Diameter**	**Base distance**	**Chirality**
B-form	2 nm	0.34 nm	right-handed
A-form	2.3 nm	0.24 nm	right-handed
Z-form	1.8 nm	0.46 nm	left-handed

Due to the dry and high salt conditions in the presented VUV and LEE irradiation experiments, an A-form of the DNA is more likely to be present than a B-DNA conformation. Still, the considered DNA sequences are single stranded so that the exact conformation is unknown. A rough estimation of the geometrical cross section (σ_A) can be calculated from the length of the DNA sequence (l) and its diameter (d) assuming an A-DNA conformation and a simplified rectangular projection of the DNA strand:

$$\sigma_A = l \cdot d \quad (1)$$

Tab. 2 Length and geometrical cross section of the oligonucleotides calculated from equation 1.

Number of nucleotides	Length in 10^{-9} m	Geometrical cross section in 10^{-18} m²
4	0.96	2.2
8	1.92	4.4
12	2.88	6.6
16	3.84	8.8
20	4.80	11.0

2.2 Structure and properties in the gas phase

The photo ionization tandem mass spectrometry (MS) experiments presented in this thesis are performed in the gas phase. In comparison to the DNA in the condensed phase, the molecule in the gas phase is isolated. No intermolecular interactions with surrounding solvent molecules are possible, which prevents changes in the DNA structure. Moreover, in the gas phase the shielding of the Coulomb repulsion between the phosphate groups through the solvent molecules is reduced and leads to an elongated DNA structure. Still, the structure in the gas phase refers more to the structure in solution than one can expect. The time needed to rearrange the structure in big molecules such as the DNA to find the absolute energy minimum is usually longer than the duration of a typical electrospray ionization (ESI) MS experiment (microsecond timescale) [54]. Hence, the rearrangement is more likely to result in a metastable structure (submillisecond timescale) [54] corresponding to a local energy minimum with a longer lifetime than is needed for ESI MS experiments.

Molecular dynamic simulations of 12mer and 16mer ds oligonucleotides showed that the helical structure is preserved in the gas phase, but the plane stacking of the nucleobases in the double helix gets distorted and the structure stretches along the axis [55]. One possible explanation for this could be a change in the hydrogen bonding behavior. Under dehydrating conditions the nucleobase C tends to change its structure from a keto-amino to an enol-amino form followed by preferable binding to A instead of G [56]. Even if the Watson-Crick hydrogen bonding becomes less feasible, due to higher Coulomb repulsion in the DNA backbone and the corresponding structural adaptions, different channels to stabilize the DNA structure through hydrogen bonding are available.

According to the work of Hoaglund *et al.* [57] the unfolding of the oligonucleotide (i.e. DNA sequence) starts, as soon as more than 50 % of the phosphodiester linkages are charged. Hence, the 10mer single stranded oligothymidine studied in ion mobility setup displayed conformational changes with increasing negative charge. Low negative charge states (z = -2 and -4) show lower drift times than higher negative charge states (z = -6 and -7), which can be related to more compact- and elongated conformations of the oligonucleotide, respectively. To summarize, the higher the charge states, the higher the Coulomb repulsion within the molecule and it becomes stretched.

The work of Phillips *et al*. [58] applied tandem mass spectrometry on dinucleotides and indicates the formation of a coiled structure. Dinucleotides with a z = -1 charge ($[MH]^-$) show hydrogen bonding between the sugar units of both nucleotides. Additionally, one nucleobase of the dinucleotide can form a hydrogen bond to the phosphate group that connects the two nucleotides. For a dinucleotide with a z = +1 charge (MH^+) the phosphate anion is protonated and the nucleobases are sharing a proton *via* hydrogen bonding. Even more stabilization is achieved *via* hydrogen bonding of the hydroxide group of the phosphate and nucleobase. This way very compact tertiary structures are created [58].

Oligonucleotide length dependent investigations have been performed in this thesis where structural changes of the DNA strand in the gas phase might play a major role. Further discussion will be presented in chapter 6.

2.3 Higher order structures – DNA origami nanostructures

The DNA sequences investigated in the presented work are incorporated in 2D DNA origami nanostructures to perform measurements on a single molecular level to determine absolute values for the DNA strand break. The development of 2D and 3D higher order DNA structures [59] has strongly increased, since DNA can be artificially synthesized [60]. Complex DNA structures can serve as templates e.g. in the fields of biosensing [61], plasmonics [62] or theranostic applications [63,64]. In the present research approach triangular shaped DNA nanostructures invented by Rothemund [37] were used due to their high stability under dry and wet conditions and their low clustering tendency during the adsorption process on a substrate. The DNA origami triangle consists of three trapezoids that are connected at the short ends to from the corners of the triangle. They are produced in a self-assembling process via a hybridization reaction between a long circular viral scaffold strand (7249 nt) and a set of 208 short artificial ssDNA sequences (32 nt, staple strands) as visualized in figure 2. The DNA sequences of the staple strands are only complementary to different parts of the DNA sequence of the scaffold strand and therefore, staple the scaffold strand into the desired shape. The staple strands can be extended by an additional DNA sequence, which is not incorporated into the DNA nanostructure but is protruding from the nanostructure surface. This extended DNA sequence is the target DNA sequence in the irradiation experiments in the condensed phase in this thesis. With this technique two or more DNA sequences can be investigated at the same time and under the same experimental conditions. Since only a submonolayer coverage is needed to analyze a sufficient amount of DNA origami nanostructures, a minimum of material is required. The triangular DNA origami nanostructures have a side length of 127 nm and can be visualized by AFM and this way, be used as a tool for single molecule measurements [25,38].

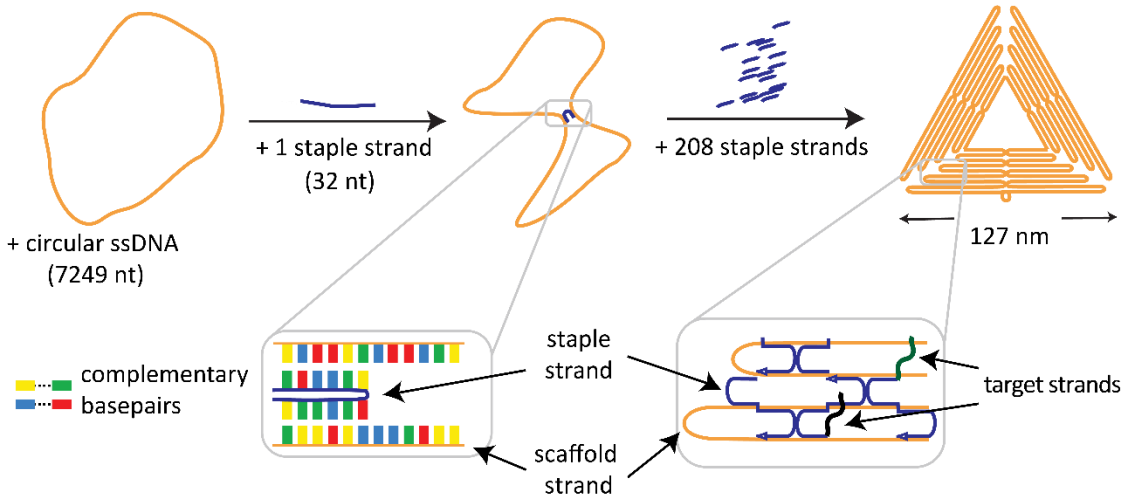

Fig. 2 Scheme of the formation of a triangular DNA origami nanostructure and its modification with target DNA sequences.

2.4 Photostability and DNA damage

The presented work investigates the strand breaks in short, artificial oligonucleotides induced by UV light, more precisely in the VUV range at 8.44 eV. The photostability of the DNA against UV light (380 nm-100 nm/3.26 eV-12.4 eV) is extremely important for the existence and consistency of life itself. Even if the DNA bases have a strong absorption at the wavelength of 300 nm-200 nm (4.13 eV-6.2 eV) with a maximum at around 260 nm/4.77 eV, their quantum yield of photoproducts remains very low [1]. The excitation occurs at these photon energies from the electronic ground state (π or n) into the excited (π* or n*) state of the nucleobases. The π* state decays into a n-π* dark state and relaxes then within 1 to 2 ps into the electronic ground state *via* a conical intersection [65]. The incoming photon energy is effectively converted into vibrational energy of the hydrogen bond that can either be distributed intra- or intermolecularly, before photochemical reactions can occur [7]. In ssDNA no hydrogen bonding between nucleobases exists. Consequently, the non-radiative deactivation pathway is one to two orders of magnitude slower than in dsDNA, but still very effective [1].

Despite the very effective non-radiative decay of the nucleobases, oxidation of the nucleobases such as the formation of 8-oxoguanine [8] or the formation of photoproducts such as the very prominent cyclobutane dimer or the (6-4) photoproduct emerge in the UV photon range [9]. Generally various modifications of the nucleobases, the sugar or the phosphate unit are possible (fig.4a). At higher photon impact energies, which exceed IEs of the nucleobases (~8-9 eV) [2,10] SSBs and DSB become dominant. Generally various modifications of the nucleobases, the sugar or the phosphate unit are feasible (fig.3a), but do not necessarily lead to a mutation, since they can be repaired enzymatically. To induce a SSB, the C-O bond between the sugar unit and the neighboring phosphate unit between two nucleotides has to be cleaved (fig.3b). Hence, two SSBs occurring in a close

proximity to each other will than induce a DSB in the DNA. DNA cross links occur e.g. after the administration of cytostatic drugs such as cisplatin in cancer therapy [66]. DSBs cannot be repaired enzymatically and cisplatin induced cross links constrain the repair mechanism; both are leading to cell apoptosis, the so called cell death that is desired in cancer therapy.

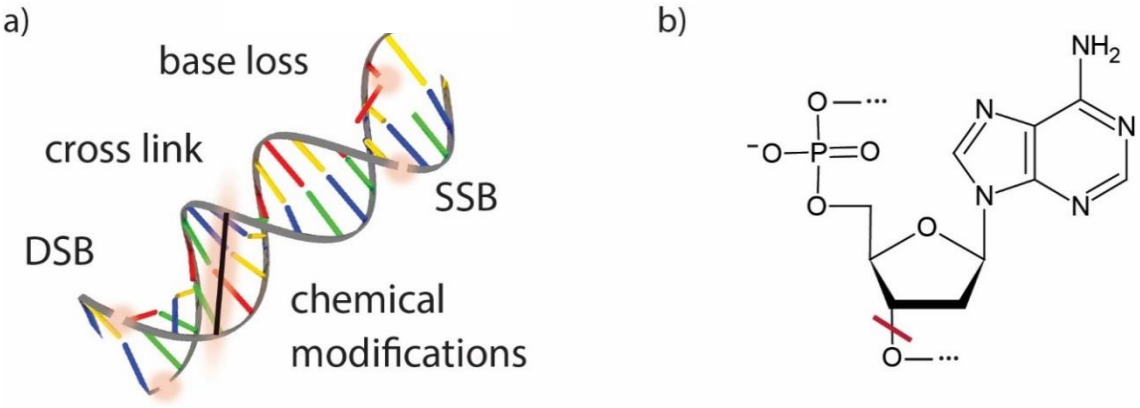

Fig. 3 a) Scheme of general damage forms that can occur at a DNA strand, b) formation of a SSB at an adenosine nucleotide in the DNA, marked with a red line.

The photon irradiation energy used in this work can be assigned to the UVC light or VUV radiation (200-10 nm/6.2-124 eV) [67]. Photoexcitation and photo ionization processes can take place in this energy regime leading to diverse chemical reactions in the DNA sequence such as the single strand breakage that is investigated in this work. The photoexcitation and photoionization process is further explained in chapter 3.3.

2.5 Charge transfer through DNA

A major focus of the present thesis is the dependency of the strand breakage on the DNA sequence. Positive or negative charges that are introduced through ionization and electron attachment reactions can migrate through the DNA strand to react at preferable positions within the DNA sequence. The electronic conductivity of DNA was proposed for the first time by Eley *et al.* [68] in 1962 and is since then a part of an ongoing discussion of DNA being a molecular wire [69]. The stacked nucleobases in the DNA strand feature a π-system in their aromatic rings that is delocalized over several nucleobases making a charge transfer through the helices theoretically possible [68,70]. Two main charge transfer mechanisms are known, the tunneling process over several base pairs, as described by Marcus *et al.*[71]; and the hopping mechanism, as suggested by Giese *et al.* [72]. Both mechanisms are displayed in figure 4.

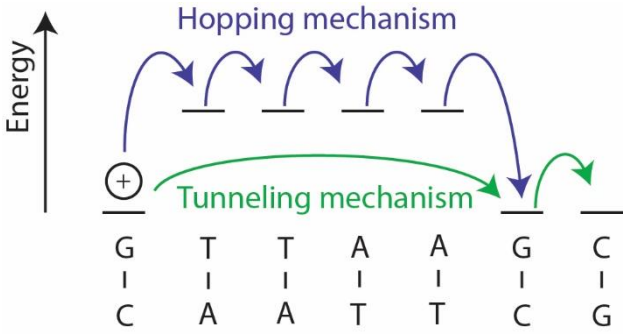

Fig. 4 Scheme of charge transfer mechanisms in DNA; hopping mechanism is marked in blue and the tunneling mechanism marked in green.

In the tunneling mechanism the charge transport occurs from one G as a charge donor to another G as the charge acceptor in one step over a bridge of A:T base pairs *via* the tunneling effect (fig.4). The whole system is considered as delocalized. The charge transfer velocity decreases exponentially with the distance between donor and acceptor and occurs only if the donor has a lower energy level than the bridge [68]. An alternative charge transfer mechanism that better explains small distance dependencies is the hopping mechanism. Here, the charge transfer takes place stepwise and the charge is shortly localized on each nucleobase. The charge transfer velocity depends on the number of steps. Furthermore, it can only take place, if the vibrational states of the donor are in resonance with those of the DNA helix.

Using ionizing radiation or even UV radiation [73], a charge can be induced directly in the nucleobases. G has the lowest IE among the nucleobases [2] and serves as an electron donor as well as an electron trap [74], since it has also the lowest oxidation potential (E_{ox}) among the nucleobases [75]. As a bridge for the electron to be transferred from the electron donor to the acceptor, the nucleobase A is considered, since it has only a slightly higher IE than G [2]. Joseph *et al.* [76] introduced anthraquinone in the DNA sequence, which gets oxidized easily under UV radiation releasing a radical cation and thus, creating an electron hole. The radical cation can migrate through the DNA sequence *via* the hopping mechanism until a reaction with water or molecular oxygen at the nucleobases occurs. This results in a chemical reaction, which leads to a strand break, if the DNA sequence is treated with piperidine. This way, the charge transfer to the preferential oxidation sites could be observed. The investigation of the dsDNA sequence 5'-d($A_3(TG)_4A_3T_2$:$T_3(AC)_4T_3A_2$) indicated that the walk of the charge is random from the electron donor to the acceptor, since all G sites were cleaved equivalently in this study. If the G nucleobases are considered as potential energy wells, all possess the same energy, since they are cleaved to the same degree (fig.5a). The G nucleobase can also be converted from a trap to a bridge, if a GG stack is introduced that has an even lower IE [77]. Considering again the potential energy landscape of the nucleobases, the GG stack has a lower potential energy than the G nucleobases and thus serves as a trap, whereat the G nucleobases become a bridge (fig.5b). If additionally the oxidized form of G, 8-oxoG is introduced in the DNA sequence, the GG stack will be translated into a bridge as well, because 8-oxoG is highly

reactive due to its low IE [77] and low E_{ox} [78]. The potential energy is now even lower than the one of the GG stack and thus the 8-oxoG becomes an even deeper trap (fig.5c). The electron transfer in a DNA sequence can also be blocked by a barrier. A d(T_4) DNA sequence would serve as such a barrier (fig.5d). Joseph *et al.* [76] separated the electron donor and 8-oxoG by such a d(T_4) DNA sequence and observed no strand cleavage at the 8-oxoG site. Hopping would be the preferential process to reach the nucleobase with the lowest IE, but potential barriers cannot be overcome.

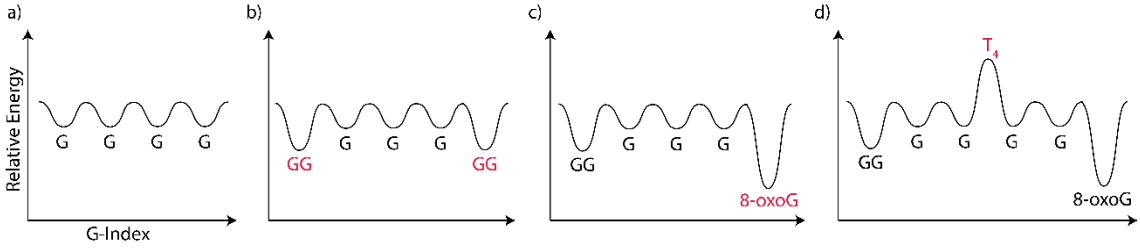

Fig. 5 Scheme of the potential energy landscape for different oligomers, all G, GG or 8-oxoG nucleobases are separated by C or T nucleobases; the x-axis (G-Index) represents schematically the position of the G, GG or 8-oxoG along the DNA sequence [77].

These examples show that the electron transfer within a DNA sequence is highly depended on the nucleobase composition. The DNA sequences can be considered as a potential energy landscape with low lying potentials serving as an electron trap (G, GG or 8-oxoG) and higher lying potential serving as barrier (T) for the charge [76,79] (fig.5). The electron can hop over the bridges from the donor to the trap, if its further movement is not blocked by a barrier. Hopping will be always the preferential process compared to the oxidation of a base, since it is the faster process [76,79].

The described charge transfer processes are the basis of the activation of the radiosensitizer ^{5Br}U, a therapeutic agent in cancer therapy. There, G is supposed to serve as an electron donor, initiating the charge transfer process to ^{5Br}U that finally can lead to a strand break in DNA [73,80].

3 Photon and electron induced processes in DNA

In the present work short DNA sequences are investigated on their DNA strand breakage caused by VUV and LEE radiation. LEE radiation is generated along the radiation track [16,17,81] in cancer radiation therapies, when highly ionizing radiation is directed on tumor tissue. In this section the different methods applied in cancer radiation therapies are introduced and the basic collision processes of the ionizing radiation with molecules and atoms along the radiation track are generally explained. In the applied LEE energy range of below 3.6 eV, DEA is the dominant process. VUV light on the other hand is applied at an energy of 8.44 eV. At this energy the photo excitation and ionization [25] process occur. All processes are presented in greater detail and a state of the art of the current literature is given. Since radiation therapy is less effective in hypoxic cancer cells than in oxic healthy cells, radiosensitizing molecules are used to increase the DNA damage yield in the cancer treatment. Hence, the two radiosensitizers ^{5Br}U and ^{8Br}A and their effect on the DNA strand breakage are introduced at the end of this chapter.

3.1 Cancer radiation therapies

Radiotherapy is a substantial part of cancer treatment. The classical radiotherapy uses highly ionizing radiation in the energy range of MeV to direct it on the carcinogenic tissue. This way, secondary particles will be generated along the radiation track [16,17,81], which are causing the actual damage in the cells and therefore of the DNA. One type of these secondary particles are LEEs, which in the framework of this thesis are investigated with respect to their influence on the strand breakage of certain target DNA sequences.

At the patient the radiotherapy can be implemented either from the inside or outside of the body. A linear accelerator generates electrons nearly at the speed of light. They can be directed to the tumor from the outside, but don't have a deep penetration depth. The generated electrons can also be braked by a wolfram plate and in this way, converted into hard X-rays (30 keV-1 MeV [82]). These highly energetic photons have a very high penetration depth so that they can even go through the body. On their way through the biological tissue they will deposit a lot of energy [83] and are thus the most effective at a depth of 3 cm [84].

Technically even more challenging are the ion beam therapies. Fast particles such as protons, carbon, helium or other ions are accelerated and directed to the tumor. They can be bunched in a sharper way and have a defined penetration depth. Depending on their velocity and energy they can penetrate up to 30 cm into the tissue [84]. Most of the energy can be placed in the tumor and the surrounding tissue is preserved to reduce the side effects of the radiation therapy.

Brachytherapy or radionuclide therapy are possible options to treat the tumor from the inside of the body. Radiation sources, such as ^{60}Co that emitting γ-radiation [85], are placed near or directly into the tumor. Both, brachytherapy and radionuclide therapy use drugs that have an instable core, which decays and emits ionizing radiation. Due to the high metabolism of cancer cells, these drugs can be accumulated mainly in the carcinogenic tissue [83].

It is important to understand the process of energy deposition and distribution in the tissue through the different radiation types and the consequences of these processes in the DNA. The linear energy transfer (LET) describes the energy loss due to ionization reactions, which in turn depend on the charge, the velocity and the energy of the particle and the density and IE of the surrounding material. Collision with the atomic cores and the release of electromagnetic radiation plays a major role. The LET is often displayed as a function of the path length through a medium, which is very characteristic for different radiation types. With the LET the dimension of the damage in the tissue can be estimated and the radiation therapy adapted to the patient's needs [86].

3.2 Collision processes in atoms and molecules

The DNA strand breakage investigated in the present work is mainly induced by secondary particles produced along the radiation track [16,17,81] of ionizing radiation in cancer radiation therapies. Depending on the type and energy of the primary beam in the cancer treatment, different processes to generate secondary particles in the tissue can occur. Primary electron radiation affects the atoms or molecules in the radiation track directly through inelastic collisions, which results in excitation or ionization reactions. Herein, additional δ-electrons are generated, which still have a very high energy to induce further ionization events. If the incoming electron just passes the atomic shell, it will experience a radial acceleration, which leads to additional electromagnetic radiation emission [86]. In comparison, the effect of primary photon radiation depends on its energy. A photon impact energy above 1.022 MeV leads mainly to the pair formation effect [87]. If the atomic shell of an atom/molecule along the radiation track gets hit by a photon, an electron can be ejected. Does the photon instead collide with the core of an atom, its energy is transformed into an electron and a positron. The positron can in turn recombine with an electron to release a secondary photon, which can react in additional secondary processes. At photon energies between 0.1 and 1 MeV the Compton effect is dominant [88]. Elastic collisions between the incoming photon and the atomic shell can occur. The amount of the energy transfer of the photon to the electron in the atomic shell depends on the angle of the collision. If enough energy is transferred, an ionization can take place. At energies below 100 keV the photoelectric effect is prevailing [89]. Herein, the energy of the photon will be fully absorbed by the colliding atom or molecule and an ionization event can occur accompanied by the release of an electron close to the core of the atom or molecule. A recombination process within the atom or molecule will release energy in form of a secondary photon, which can reject another electron from the same system. This

process is called an Auger process or cascade [90]. If the energy is instead transferred to a valence electron of a neighboring atom or molecule, the process is referred to as an interatomic Coulomb decay [91]. Due to the described collision processes, cascades of secondary electrons and photons are released, which can induce further reactions.

Particle radiation deposits most of its energy after falling below a certain velocity limit resulting in a Bragg peak. Depending on the radiation energy the Bragg maximum can be focused on a certain depth in the tissue. Here also mainly ionization reactions along the radiation tracks take place and secondary electrons are generated. Other fission products will induce additional ionization events along their tracks and release even more secondary electrons [86].

Ionizing radiation is the base of all radiotherapy. Independent of the type of medical irradiation treatment, they are all exploiting the same indirect effect of generating secondary particles through collision processes within the tissue. Ionization products along the radiation track are mainly electrons [16] with an energy lower than the primary beam. Another important reaction occurring inside the irradiated body cells is the water radiolysis (eq.1). This way hydroxide radicals (OH·) are generated, which are known to induce a high amount of damage in the cell [29]. Other reaction products are LEEs, hydrogen radicals (H·), protons (H^+), hydrogen peroxide (H_2O_2) and hydrogen itself, which are able to damage the DNA [17].

(1) H_2O + ionizing radiation ⇉ OH·, e^-, H·, H^+, H_2O_2, H_2

This work focusses on the interaction of photons at the energy of 8.44 eV and LEEs of an energy below 3.6 eV with the DNA molecule. While electrons below the energy of 10 eV are already known, to induce DNA damage very effectively, barely any data exists about photon induced reactions in this energy regime. At this energy photons can induce excitation and ionization events in the DNA molecule, which can result in dissociation reactions leading to strand breakage in the DNA, which is further discussed in the following section 3.3. The reaction of electrons of such a low energy with the DNA has already been investigated intensively. DEA to DNA and the corresponding dissociation reactions are well established and presented in section 3.6.

3.3 Photoinduced dissociative reactions in DNA

The VUV irradiation energy used in the present work is 8.44 eV and known to induce SSBs in short oligonucleotides [25]. The initial steps for strand breakage are photoexcitation and ionization events. In previous work SSBs were also detected at even lower energies such as 6.5 eV and 7.29 eV [25]. To induce a SSB, the C-O bond between the sugar unit and the phosphate unit or the P-O bond within the phosphate unit in the DNA backbone has to be cleaved. The binding strengths of these bonds are 3.71 eV and 3.47 eV, respectively [92]. This is the minimum energy that a photon has to possess to induce a fragmentation of these bonds and thus, a SSB. The higher the energy of the photon, the higher the molecule can be excited or even ionized and more fragmentation channels open. The important photon energy value to differ between the aforementioned reactions is the IE of the DNA molecule. Below this value only photoexcitation events take place. At energies above the IE of the DNA the additional process of the photoionization occurs. The IE of the DNA nucleobases [2,10] and other DNA components such as deoxyribose [27] or a 2'-deoxyribose 5'-phosphate [28] are listed in table 3.

Tab. 3 Vertical ionization energies of the different DNA components.

DNA component	**IE_v in eV**
Adenine	8.44[a] / 8.38[b]
Cytosine	8.94[a] / 8.95[b]
Guanine	8.24[a] / 8.09[b]
Thymine	9.15[a] / 9.13[b]
Deoxyribose Isomers	9.60 - 10.06[c]
2'-Deoxyribose 5'-phosphate	11.32[d]

[a] Cauët *et al.*[2], [b] Gallandi *et al.*[10], [c] Gosh *et al.*[27], [d] Colson *et al.* [28].

The photoexcitation and the photoionization processes leading to different dissociative reactions are displayed in figure 6 and are further explained with the example of the DNA sequence 5'-d(A_{12}) at the equations 2 and 3.

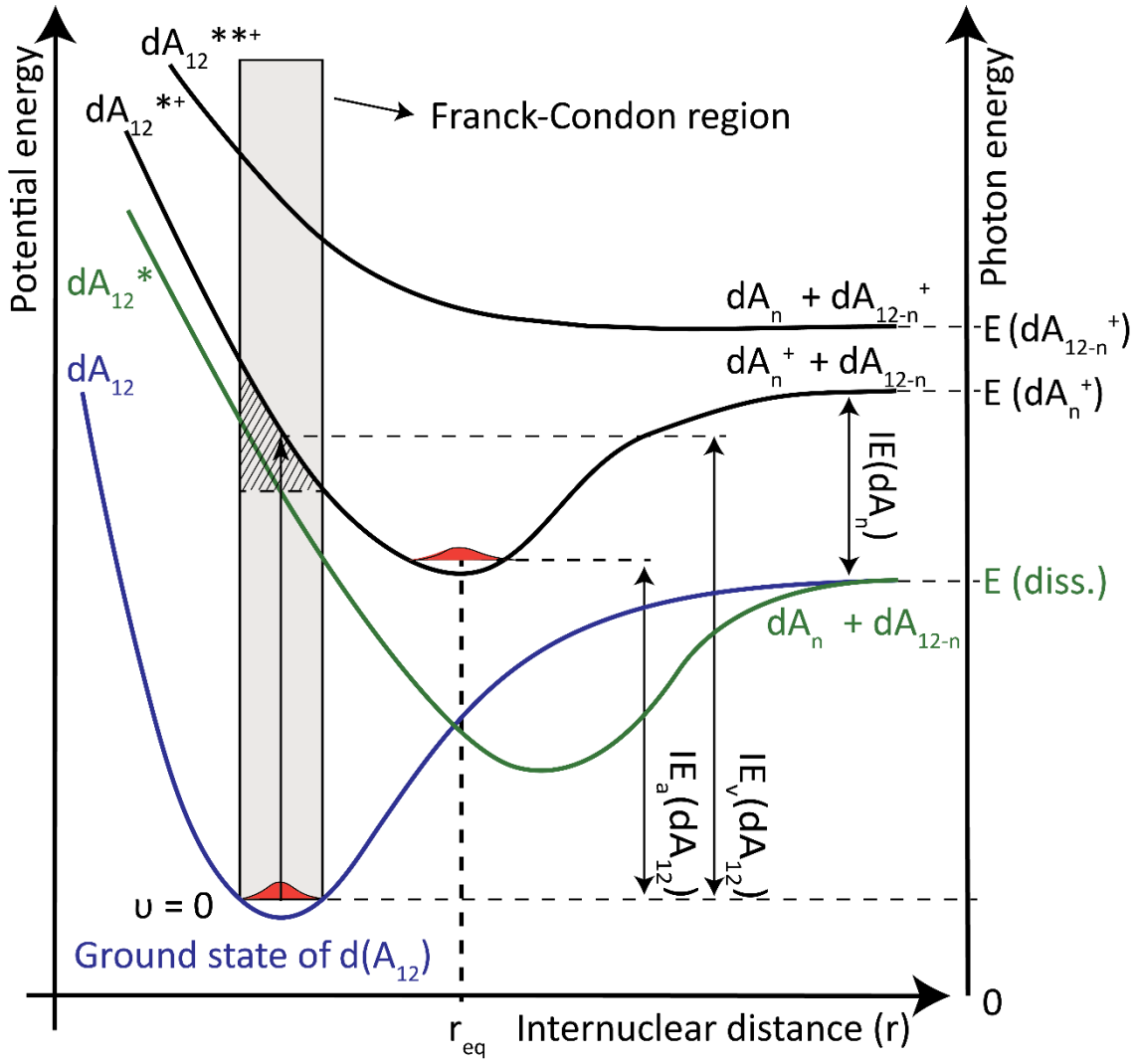

Fig. 6 Schematic potential energy diagram of the dissociative electronic excitation and ionization processes of the DNA sequence 5'-d(A12). The molecule can be promoted from neutral ground state (blue line) to an electronically excited state (green) via a vertical Franck-Condon transition by the absorption of an incoming photon. This can result in a neutral fragmentation by forming two fragments dA_n and dA_{12-n}. Another pathway could be a combined excitation and ionization into even higher cationic excited states (black) resulting in a neutral dA_n and a positively charged fragment dA^+_{12-n}; IE_a - adiabatic ionization energy, IE_v - vertical ionization energy.

In figure 6 the electronic ground state of the DNA sequence 5'-d(A_{12}) is displayed in blue. If a photon with an energy below the IE of the molecule is absorbed, the molecule will be promoted into an excited state, which is illustrated marked in green in figure 6. The transition will happen vertically within the Frank-Condon region. The better the overlap between the wave functions of both electronic states, the higher is the probability of this transition to happen. If the lifetime of the electronic state exceeds the time of the molecular vibration (around 10 fs), a neutral fragmentation might occur (eq.2).

$$(2) \qquad dA_{12} \xrightarrow{h\upsilon} dA^*_{12} \rightarrow dA_{12-n} + dA_n \qquad \textit{Neutral Dissociation}$$

In equation 2 the neutral dissociation, which leads to a neutral fragmentation of the DNA sequence 5'-d(A_{12}) to the dA_{12-n} and dA_n fragments is displayed. This fragmentation would correspond to a SSB of the DNA sequence. If the potential energy curves of the electronically excited stated and the ground state cross, the molecule might decay within a non-radiative pathway occurring *via* a conical intersection du to very strong vibrational coupling [93]. The additional energy absorbed from the incoming photon might also be transferred into other DNA damages than the SSB, e.g. base loses or other chemical modifications.

According to the IEs of the DNA components, the nucleobases G (8.24 eV) and A (8.44 eV) have the highest probability to be ionized under the conditions applied in the present work because they have an IE below or equal to the energy of the used photon radiation. In the case of the DNA sequence 5'-d(A_{12}) the dissociative ionization, displayed in equation 3, will lead to the neutral fragment 5'-d(A_n) and the positively charged fragment 5'-d(A^+_{12-n}). Higher excited states will lead to different dissociative pathways and fragments.

$$(3) \qquad dA_{12} \overset{h\upsilon}{\rightarrow} dA_{12}^{*+} + e^- \rightarrow dA_{12-n}^{+} + dA_n + e^- \qquad \textit{Dissociative ionization}$$

To form a SSB in the DNA strand *via* an ionization reaction, a positive charge will be induced the most likely on a nucleobase first. An electron could than migrate from the DNA backbone to the nucleobase, releasing a positive charge in the DNA backbone, which can result in the cleavage of the C-O bond between the sugar and phosphate unit (fig.4).

In this work only SSBs are considered. Other types of DNA damages will also occur, but cannot be detected within the design of the experiment. In the following sections (3.4 and 3.5) experimental results of the single strand breakage in DNA in the condensed phase as well as in the gas phase of other working groups will be introduced.

3.4 Investigations of SSBs caused by VUV light in ssDNA

One technique to study DNA damage in thin films of calf thymus DNA on a molecular level is X-Ray photoelectron spectroscopy (XPS) as performed in a study by Gomes *et al.* [94]. It was shown that above a photon impact energy of 6.9 eV a strong degradation of the amine groups of the nucleobases, which are not involved in hydrogen bonding, occurs. It was suggested that electrons are ejected at the nucleobases under 6.9 eV photon energy. These electrons can directly attach to the nitrogen groups of the nucleobases to form TNIs, which can in turn relax *via* autodetachment of an electron (detailed description in section 3.6). The released electrons will have a lower energy than the incoming photon and can migrate through the nucleotide inducing bond cleavage in the phosphodiester groups. The 2'-deoxyribose 5'-phosphate group was shown to have an IE of 11.32 eV [28] and it was demonstrated in the study of Gomes *et al.* [94] that the degradation of the phosphodiester bond is induced very effectively below 4.2 eV despite the high IE of this group. With the scission of the phosphodiester bond, which is the connection between the sugar and the phosphate unit constituting the DNA backbone, a SSB is formed. The formation of SSBs in different DNA sequences is the main focus of this work and is intensively investigated in this thesis.

In 1994 Hieda *et al.* [95] were the first to analyze VUV-induced DNA strand breakage in plasmid DNA. The naturally supercoiled structure of the plasmid DNA changes into a linear structure when a SSB occurs and is cleaved into smaller linear fragments by double strand breaks (DSBs). This structural behavior of plasmid DNA is exploited in the gel electrophoresis analysis to separate the different fractions and analyze the DNA damage quantitatively by staining the DNA with a fluorescent dye and measuring the fluorescence yield. At a photon energy of 8.3 eV a cross sections for SSBs of $\sigma = 8.1 \cdot 10^{-15}$ cm² was found in these experiments [95]. Prise *et al.* [96] irradiated plasmid DNA in the energy regime from 7 to 150 eV with synchrotron-generated VUV light. The same gel electrophoresis analysis and fluorescence quantification was used to determine the cross sections for SSBs. Relevant results in the context of this thesis are the cross section for SSBs at 8 eV with $\sigma = 7 \cdot 10^{-15}$ cm² and at 11 eV with $\sigma = 2 \cdot 10^{-14}$ cm² [96]. Wehner *et al.* [97] performed the same type of experiment with irradiation energies of 7.75 eV, 6.5 eV, 5.6 eV and 4.9 eV with air dried plasmid DNA and at 4.9 eV with plasmid DNA in solution. For the irradiation at 4.9 eV a mercury lamp and for the higher photon energies a gallium phosphide diode was used. The cross section for SSBs in the previously mentioned studies are increasing with the photon energy. The study by Prise *et al.* [96] represents an exception, because the values for SSBs at 6.53 eV with and at 7.75 eV are $\sigma = (4.4 \pm 0.1) \cdot 10^{-19}$ cm² and $\sigma = (1.5 \pm 0.1) \cdot 10^{-17}$ cm², respectively, and thus are considerably lower [97]. The cross sections for SSBs presented so far in a photon irradiation energy range from 6.53 eV up to 11 eV differ in their values by five orders of magnitude. On the one hand different photon irradiation energies induce different reactions in the DNA strand. The closer the value of the photon irradiation energy is to the IE of DNA molecules, the higher is the probability to induce an ionization in the molecule that results more likely in a SSB than an electronic excitation, which is more likely to follow a non-dissociative pathway [1] as

described in section 2.4. Besides, with this technique only the first SSB appearing in the plasmid DNA will be detected. Thus, the amount of SSBs underestimated. On the other hand different plasmid DNA types were used for the experiments, which might react, due to their different DNA sequences, differently with the photon irradiation. Another important role plays the preparation of the dry plasmid DNA samples. The temperature [42] of the substrate and the buffer [41] used for the adsorption of the plasmid DNA play an important role in thin film adsorption quality. If the DNA is clustering or the film is too thick, the irradiation is not homogeneous and the quantification of the strand breakage not representative. These problems can be overcome with the DNA origami technique [38] as described in section 2.3. The distribution of the DNA origami nanostructures is rather homogeneous on the substrate surface and single triangular structures are visible on AFM images to be analyzed on a single molecule level, which allows to determine absolute values here. In the framework of my master thesis, the DNA origami technique was used to incorporate ssDNA strands and irradiate them with 8.44 eV VUV light to determine the cross sections for SSBs [25]. The cross sections for SSBs of the DNA sequences 5‘-d(TT(ATA)$_3$TT) and 5‘-d(TT(CTC)$_3$TT) were evaluated to be $\sigma = (2.8 \pm 0.2) \cdot 10^{-16}$ cm^2 and $\sigma = (2.2 \pm 0.4) \cdot 10^{-16}$ cm^2, respectively. The results of the discussed investigations are summarized in table 4.

Tab. 4 Cross sections for SSBs and the order of DNA damage of thin film VUV photon impact experiments.

DNA type		Photon energy in eV	Cross section for SSBs	Trend	
Plasmid		8.3	$8.1 \cdot 10^{-15}$ cm²	/	[a]
Plasmid		8	$7 \cdot 10^{-15}$ cm²	/	[b]
		11	$2 \cdot 10^{-14}$ cm²		
Plasmid		6.53	$(4.4 \pm 0.1) \cdot 10^{-19}$ cm²	/	[c]
		7.75	$(1.5 \pm 0.1) \cdot 10^{-17}$ cm²		
ssDNA	5‘-d(TT(ATA)$_3$TT)	8.44	$(2.8 \pm 0.2) \cdot 10^{-16}$ cm²	TT(ATA)$_3$TT	[d]
	5‘-d(TT(CTC)$_3$TT)		$(2.2 \pm 0.4) \cdot 10^{-16}$ cm²	> TT(CTC)$_3$TT	

[a]Hieda *et al*. [95], [b]Prise *et al*. [96], [c]Wehner *et al*. [97], [d]Vogel *et al*. [25].

3.5 Photoionization events in DNA and its components in the gas phase

Since VUV light with high brilliance is only available at synchrotron facilities, only a few investigations of the photoionization of DNA in this photon energy range exists. González-Magaña *et al.* [98] investigated the interaction of the oligonucleotide 5'-d(GCAT) with photons in the energy range of 10-570 eV and keV C^{q+} Ions with respect to their ionization and fragmentation behavior to find the molecular mechanisms underlying DNA radiation damage. At 15-20 eV photon irradiation a maximum of photoabsorption due to excitation of valence electrons is reached. The photofragmentation pattern of the protonated $(dGCAT+2H)^{2+}$ DNA sequence showed abundant signals of the G and A nucleobase in this photon energy region. Phillips *et al.* [58] performed investigations on dinucleotides with protonated nucleobases and the main process found here is the glycosidic bond cleavage between the sugar unit and the nucleobase accompanied by a proton transfer from the nucleobase to the sugar unit. Most likely C, A and G are protonated, because they have the highest proton affinity. Nucleotides containing these nucleobases have a high yield in nucleobase abstraction [98]. Phillips *et al.* [58] suggest also that the nucleobase abstraction induces the formation of a fragment based on the dehydrated sugar unit, which is a precursor for a bond cleavage in the DNA backbone. González-Magaña *et al.* [98] on the contrary propose that this exact fragment can also be formed without a previous nucleobase abstraction, since they found fragments containing the mass of the claimed fragment and an additional nucleobase. The presented results at low photon impact energies indicate that backbone lesions are indeed a possible dissociative pathway. Going to higher photon impact energies, the fragmentation pattern shifts with increasing irradiation energy to smaller fragments [98].

A photoionization study of different nucleotides with a photon impact energy of 118.2 nm/10.49 eV from Shin *et al.* [99] supports the suggested fragmentation pathway described before, in which the bond between the nucleobase and the sugar unit is the favored one to be cleaved at a photon energy of 10-15 eV [98]. Stable nucleobase fragments are formed and since these experiments are conducted with neutral nucleotides, a hydrogen transfer from phosphate group to the nucleobase takes place. A second suggested mechanism is the direct ionization of the nucleobase instead of the sugar unit, because the IE of the nucleobases [2,10] is much lower than the IE of the deoxyribose [27]. This assumption is also the basis for the photon irradiation experiments in the condensed phase as discussed in section 3.5 and as presented in this thesis, which investigated SSBs in ssDNA strands at 8.44 eV.

3.6 Dissociative electron attachment (DEA) to DNA

Not only photons but also electrons especially in a very low energy range (0-20 eV) are known to damage DNA very effectively. These secondary electrons are generated in a large numbers e.g. along the radiation track of 1 MeV proton radiation in water with a maximum energy of around 10 eV [16]. At the irradiation energy of 10 eV or below, the DEA process is the most effective dissociative pathway to occur [100]. The general DEA process is displayed in a schematic potential energy diagram in figure 7 with the DNA sequence 5'-d(A_{12}) as an example.

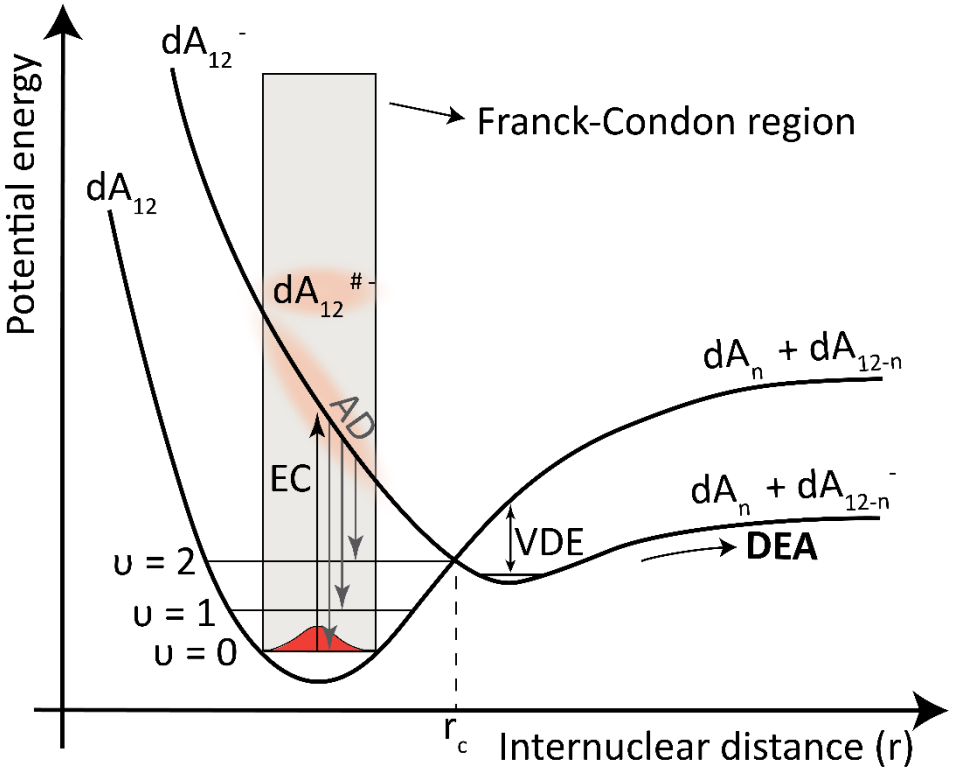

Fig. 7 Potential energy diagram illustrating dissociative electron attachment (DEA) to the DNA sequence 5'-dA_{12}. The neutral ground state is displayed below the anionic ground state. Vertical transitions between both states can occur in the Frank-Condon region, shown in grey. The incoming electron can attach (electron capture-EC) to the molecule to form a transient negative ion $dA_{12}^{\#-}$ (TNI), marked in orange. The TNI can relax via a direct reemission of the extra electron (autodetachment) or dissociate directly, if the life time of the formed TNI is equal to longer than one vibrational period of the molecule. Then a neutral fragment dA_n and a negative fragment dA_{12-n}^{-} are formed. Depending on the incident energy of the electron, different dissociative pathways within the molecule are accessible. The stable anion can decay via a vertical detachment from the anionic state to the ground state that is defined by the vertical detachment energy (VDE).

Electrons of an energy of 10 eV or below have the ability to attach to the DNA molecule to form a vibrationally or rotationally excited TNI. The electron energy must be resonant with the transition from neutral to the anionic state, and the wave functions of both, the

neutral ground state and the transient anionic state, must have a sufficient overlap for the vertical Franck-Condon transition to take place (fig.7). Different competitive processes for the decay of the TNI are possible. If the lifetime of the TNI is very short, it will just decay via autodetachment (AD). Herein, the electron detaches and the molecule goes back into its electronic ground state. If the lifetime of the TNI is longer than one vibrational period of the molecule (i.e., in the 10 fs time scale) and the bond is stretched over the equilibrium distance, the molecule will decay via a dissociation reaction, where a negative and one or more neutral fragments are formed. The valence anionic state can decay via vertical detachment (VD) into the ground state, if the vertical detachment energy (VDE) is reached, or dissociate by forming a neutral and an anionic fragment. In equation 4 the DEA process is displayed for the DNA sequence 5'-d(A_{12}).

$$dA_{12} + e^- \rightarrow dA_{12}^{\#-} \rightarrow dA_{12-n}^- + dA_n \qquad DEA \tag{4}$$

The 5'-d(A_{12}) DNA sequence captures an electron having a suitable energy to form the TNI $dA_{12}^{\#-}$ and dissociates into the negative fragment ion dA_{12-n}^- and the neutral fragment dA_n. The cross section for the DEA process is depending on the overlap of the neutral ground state wavefunction, the wavefunction of the TNI state and the probability of AD. Especially LEEs of an energy below 2 eV are very effective in inducing the DEA process [101].

Another process that has also to be considered, is the neutral dissociation triggered by an energy transfer from a scattered electron. An electron of a certain energy e_1^- attaches to the DNA molecule, but is released *via* AD, when the crossing point between neutral and anionic curve r_c is reached. If some of the energy from the electron is transferred during the electron attachment, the molecule is released in an electronically excited state, which could lead to a further dissociation reaction. This is exemplarily shown for the DNA sequence 5'-d(A_{12}).

$$dA_{12} + e_1^- \rightarrow dA_{12}^* + e_2^- \rightarrow dA_{12-n} + dA_n \quad e_1^- > e_2^- \quad ND \tag{5}$$

The 5'-d(A_{12}) DNA sequence captures an electron of a certain energy e_1^-, an energy transfer takes place and the molecule is promoted into an excited state, whereas the primary electron e_2^- is released possessing now less energy than before. The excited DNA sequence dA_{12}^* will then further dissociate into two neutral fragments. Here, it would be 5'-d($A_{12\text{-}n}$) and 5'-d(A_n), which corresponds to a SSB in the DNA backbone.

If the electron energy would even exceed the IE of the DNA, a dissociative ionization (DI) could occur. Herein, the incoming electron would eject another electron from the molecule and could promote it into an excited cationic state. One path of decay of the excited cation can then be the dissociation into a neutral and cationic fragment.

Many investigations of strand breakage in DNA caused by LEEs in the discussed energy regime have been performed. At the electron impact energy of 3-20 eV Boudaïffa *et al.* [18] discovered peaks for the incidence of SSBs and considered a mechanism, where the

electron attachment is accompanied by an electronic excitation to form a TNI that is named a core-excited resonance. The incoming electron can e.g. occupy a π*-orbital of the nucleobase and excites at the same time another electron from the π-orbital to the π*-orbital of the nucleobase [18]. The C-O bond between the base and the sugar in thymidine[102] or the DNA sequence GCAT [103] can be cleaved *via* the formation of core-excited resonances at higher electron energies. Aflatooni *et al.* [104] investigated the formation of resonances below 3 eV electron impact energy in the four DNA nucleobases and reported low lying π*-orbitals of the nucleobases. An electron can attach there without the excitation of another electron to form a TNI called shape resonance [104]. Ptasinska *et al.* [105,106] could experimentally prove that electrons with an energy below 3 eV can attach to the nucleobases, which results in the formation of the anion accompanied by an H abstraction. Additionally, it was shown that the H abstraction from the T nucleobase is favored at the N position that connects the sugar unit with the nucleobase [105]. These findings are confirmed by the gas phase DEA study of T and C from Denifl *et al.* [107]. Resonances coupled with an H loss at one of the nitrogen atoms of the nucleobases are observed and suggested to be very likely to appear from the same low lying π*-orbital of the nucleobases since they have the same energy range. Martin *et al.* [108] investigated the strand break formation in plasmid DNA in the energy range of 0-4 eV and could find peaks for SSBs, which proves that C-O bond rupture of the phosphodiester bond occurs also at these electron energies. Furthermore, it was demonstrated that a sugar radical is formed as the consequence of a T fragmentation with electron impact energies below 3 eV [109] . It was also suggested that LEEs can also attach to the low lying π*-orbital of the phosphate group to induce a cleavage directly in the backbone [19]. The possible damage sites are summarized in the following figure 8.

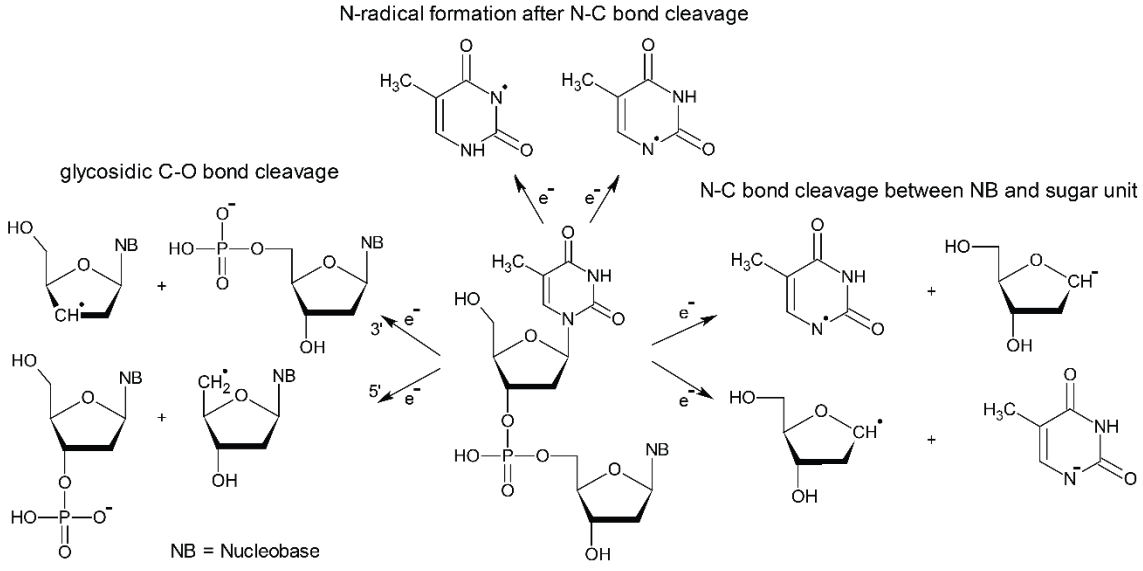

Fig. 8 Scheme of the radical formation and 3'- and 5'-bond cleavage of a dinucleotide underlying DEA; adapted from Ref. [102,105,109].

The possible mechanism of a cleavage of the phosphodiester bond induce by LEEs was intensively investigated by Simons and coworkers [100,110–114]. In figure 9 is schematically displayed that the π* orbital of the nucleobase (marked in red) has a potential energy that is around 1 eV higher than the neutral ground state of the glycosidic C-O σ bond at the equilibrium bond length of roughly 1.45 Å. To form e.g. a shape resonance, the incoming electron needs to have this energy of around 1 eV to attach to the molecule and create a TNI at the π*-orbital of the nucleobase. The configuration interaction of the π* orbital of the nucleobase and the C-O σ* orbital enables the electron to be transferred from the nucleobase to the phosphodiester bond. This electron transfer is thermodynamically driven, because the high electron affinity (EA) of the created phosphate radical, lowers the barrier of the electron migration process. Since the energy profile of the C-O σ* orbital is repulsive, the C-O σ bond rupture happens immediately after the charge transfer. The described procedure can be translated to the bond rupture at the C-N bond between sugar unit and the nucleobases, and the N-H bond at the nucleobases.

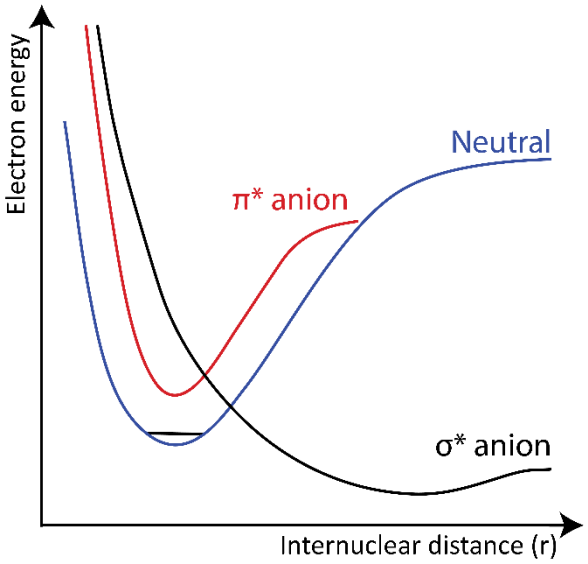

Fig. 9 Schematic potential Energy diagram of a DNA molecule in its neutral ground state (blue), its TNI with an electron in the π-orbital of* the *nucleobase (red) and an electron in the σ*-orbital of e.g. the C-O bond of phosphodiester bond (black); adapted from ref.* [101].

It was mentioned before that the electron can enter the system through the π*-orbital of the nucleobase or the π*-orbital of the phosphodiester bond. For electron energies below 2 eV the π*-orbital of the nucleobase is favored, because the π*-anion of the nucleobase has a lower energy (0.1-2 eV) than the π*-anion of the phosphodiester bond (> 2 eV). Electrons with higher energies could attach to both sites to induce a C-O bond rupture i.e. a SSB.

3.7 Experimental result for SSBs by LEEs in the condensed phase

In this thesis LEEs with an energy below 3.6 eV are generated from the Si substrate, while irradiated with 8.44 eV photon radiation. They can induce strand breaks in DNA very effectively, which was demonstrated in the section before (3.6). Boudaïffa *et al.* [18] were the first to systematically investigate plasmid DNA and the amount of SSBs and DSBs formed in the 3-20 eV electron impact energy range. The analysis of the DNA samples was conducted with gel electrophoresis and fluorescence measurements as already described in chapter 3.4. The number of SSBs was peaking at around 7.5-12.5 eV with an amount of $8.2 \cdot 10^{-4}$ SSBs per incident electron. At an energy of 3 eV the number of SSBs per incident electron is one order of magnitude lower. Martin *et al.* [108] investigated plasmid DNA thin films at an electron impact energy of 0-4 eV and found a sharp peak at 0.8 eV and a broad peak centered at 2.2 eV with a SSB yield of $\sigma = (1.0 \pm 0.1) \cdot 10^{-2}$ and $\sigma = (7.5 \pm 1.5) \cdot 10^{-3}$ per incident electron, respectively. These peaks were assigned to the formation of a shape resonance at the π^*orbital of the nucleobases and charge transfer to the phosphodiester bond in the DNA backbone followed by a cleavage of the bond as described by Barrios *et al.* [100]. Interestingly, no DSBs have been detected in the study of Martin *et al.* [108] and the values for the SSB formation are one to two orders higher than in the investigations of Boudaïffa *et al.* [18]. Another plasmid DNA strand break study was performed by Panajotovic *et al.* [115]. Cross sections for SSBs were determined in an electron impact energy range of 0.1-4.7 eV. It was shown that already at 0.1 eV SSBs can be induced. The highest cross sections in the investigated electron energy range were $\sigma = (24.8 \pm 0.2) \cdot 10^{-15}$ cm² at 1 eV and $\sigma = (18.0 \pm 1.7) \cdot 10^{-15}$ cm² at 2.2 eV. Schürmann *et al.* [116] investigated the formation of SSBs in the ssDNA sequence 5‘-d(TT(ATA)$_3$TT) with the help of the DNA origami technique [37,38] in the electron impact energy range of 0.5-9 eV and could find a slight maximum in the cross section for SSBs at 2 eV and a more pronounced peak at 7 eV with a cross section for SSBs of $\sigma = (5.9 \pm 0.3) \cdot 10^{-15}$ cm² and $\sigma = (11 \pm 3) \cdot 10^{-15}$ cm², respectively. The peak at lower energies could be assigned to the formation of a shape resonance and the peak at higher energies to a core excited resonance. At higher electron irradiation energies (8.8 eV) Kenny Ebel, Department of Physical Chemistry at Potsdam University (Vogel *et al.* [117]), Rackwitz *et al.*[23] and Keller *et al.*[118] did additional investigations of the SSB formation of ssDNA sequences. At 8.8 eV it was found that the DNA sequences 5‘-d(X$_{12}$) with X = A, C, G, T are giving cross sections for SSBs in the range of $\sigma = (5.4 \pm 2.1) \cdot 10^{-15}$ cm² to $\sigma = (8.9 \pm 2.8) \cdot 10^{-15}$ cm² with a trend of $T_{12} \geq A_{12} > C_{12} > G_{12}$ [117]. The LEE irradiation energy of 8.8 eV is sufficient to induce an electronic excitation during the electron attachment in the neutral molecule. A corresponding resonance was observed in electron impact experiments using DNA by both Schürmann *et al.* [116] and Boudaïffa *et al.* [18] with broad peaks at 6 eV to 9 eV and 7.5 eV to 12.5 eV, respectively. The DNA sequences 5‘-d(TT(GGG ATT)$_2$T) and 5‘-d(TGT GTG A)$_2$T), which were also irradiated at 8.8 eV show cross sections of $\sigma = (6.8 \pm 0.5) \cdot 10^{-15}$ cm² and $\sigma = (4.5 \pm 0.3) \cdot 10^{-15}$ cm², respectively [23]. Herein, the DNA sequence with the G nucleobases being organized next to each other instead of being separated by T nucleobases has a slightly higher cross section for SSBs. Since G-stacks

are known to be an electron trap in telomere sequences and their IE is lowered [119], they might also be damaged easier resulting in higher SSB yields. The results of this investigation still have similar values for the cross sections for SSBs such as the ones Schürmann *et al*. [116] have found at 2 eV electron irradiation energy. Another investigation from Solomun *et al*. [120] at an electron impact energy of 1 eV showed that the DNA damage was increasing with the number of Gs in the G-stack (n=1-4). At an even higher electron irradiation energy of 18 eV the cross section for SSBs increases by one order of magnitude. At this energy not only the DEA process plays a major role, but also the ionization of the molecule by electron impact, because the IEs of the DNA building blocks [2,10,27,28] have been exceeded. Li *et al*. [43] and Park *et al*. [121] investigated 10 eV LEE induced DNA damage on oligonucleotide trimers. The results display the DNA SSB formation in relation to the total damage sites. The trends of the different investigations gave opposite results. In Li's work [43] d(TTT) and d(TCT) were giving the highest and d(TAT) the lowest amount of damage while Park *et al.* [121] showed that d(TAT) was giving the highest and d(TCT) the lowest amount of DNA damage. All presented results are summarized in table 5.

Tab. 5 Cross sections for SSBs and order of DNA damage of thin film electron impact experiments, LEEs at 0.1-18 eV.

DNA type		LEE in eV	Cross section for SSBs in 10^{-15} cm²	Trend	
Plasmid		10	$8.2 \cdot 10^{-4}$ per incident e^-	/	[a]
Plasmid		0.8	$(1.0 \pm 0.1) \cdot 10^{-2}$ per incident e^-	/	[b]
		2.2	$(7.5 \pm 1.5) \cdot 10^{-3}$ per incident e^-	/	
Plasmid		0.1	(3.6 ± 1.1)	/	[c]
		1	(24.8 ± 0.2)		
		2.2	(18.0 ± 1.7)		
		4.7	(14.8 ± 1.6)		
		10	(10.8 ± 5.2)		
ssDNA	5‘-d(TT(ATA)$_3$TT)	0.5	(2.9 ± 0.6)	/	[d]
		2	(5.9 ± 0.3)		
		7	(11 ± 3)		
ssDNA	5’-d(A_{12})	8.8	(8.8 ± 0.9)	$T_{12} \geq A_{12} > C_{12} > G_{12}$	[e]
	5’-d(C_{12})		(7.7 ± 1.1)		
	5’-d(G_{12})		(5.4 ± 2.1)		
	5’-d(T_{12})		(8.9 ± 2.8)		
ssDNA	5‘-d(TT(GGG ATT)$_2$T)	8.8	(6.8 ± 0.5)	TT(GGG ATT)$_2$T > (TGT GTG A)$_2$T	[f]
	5‘-d(TGT GTG A)$_2$T)		(4.5 ± 0.3)		
ssDNA	5‘-d(TT(XTX)$_3$TT),	18			[g]
	X = A		(60 ± 9)	TT(ATA)$_3$TT > TT(CTC)$_3$TT > TT(GTG)$_3$TT	
	X = C		(27 ± 9)		
	X = G		(22 ± 9)		
ssDNA	d($A_{9-n}G_n$)$(dT)_{24}$, n = 1, 2, 3, 4	1	/	n = 4 > 3 > 2 > 1	[h]
Trimer	d(TXT), X = A, C, G, T	10	/	TTT > TCT > TGT > TAT	[i]
Trimer	d(TXT), X = A, C, G	10	/	TAT > TGT > TCT	[j]

[a]Boudaïffa *et al.* [18], [b]Martin *et al.* [108], [c]Panajotovic *et al.* [115], [d]Schürmann *et al.* [116], [e]Vogel *et al.* [117], [f]Rackwitz *et al.* [23], [g]Keller *et al.* [38], [h]Solomun *et al.* [120], [i]Li *et al.* [43], [j]Park *et al.* [121].

3.8 Radiosensitization with 5-bromouracil (^{5Br}U)

Often cancer cells are hypoxic in comparison to healthy oxic cells, and consequently they are 2.5-3 times less sensitive to ionizing radiation than normal tissue [122]. In hypoxic cells the oxygen level is decreased and less OH radicals are produced during the irradiation [123]. OH radicals are known to induce DNA damage very effectively [29] and to treat the cancer with the same efficacy that is reached in oxic cell, a combination of radiotherapy and chemotherapy has been demonstrated to be very successful [124]. By enhancing the DNA damage with radiosensitizing agents that can be delivered into the tumor, the given radiation dose can be lowered and the side effects for the patient minimized [125]. 5-Halogenated deoxyuridines are one type of radiosensitizers that can be incorporated into the DNA without disturbing the natural gene expression of the body cells, because they have the same chemical structure as normal nucleosides. Their integration into the DNA is even enhanced in cancer cells, since they have a higher metabolism and replication rate. For some radiosensitizer molecules like ^{5Br}U and ^{8Br}A the cell functions are not even influenced and the radiosensitizers are only toxic in combination with ionizing radiation [39].

In the present work the radiosensitizer ^{5Br}U was incorporated into different DNA sequences and investigated with respect to its enhancement of SSBs in comparison to non-modified DNA sequences. A list of the investigated DNA sequences is given in the Materials and methods section (4). ^{5Br}U is one of the most studied base analog and is known to enhance the sensitivity of cancer cells against ionizing radiation. It was demonstrated e.g. *in vitro* with ^{60}Co as a radiation source [126] that the enhancement of the DNA damage increases linearly with the number of ^{5Br}U molecules. The radiosensitizing properties of ^{5Br}U can already be observed with UV light and are presumably based on two different mechanism [127–129] that lead to the uracil-5-yl radical formation, which is the precursor of a SSB. The first mechanism is based on a photolysis of the C-Br bond in the radiosensitizer molecule. By the absorption of a UV photon (266 nm to 254 nm / 4.66 eV to 4.88 eV), ^{5Br}U is promoted into an excited state ($\pi\pi^*$), where it can decay *via* two competitive pathways [130]. In the first pathway the C-Br bond stretches and an additional bending of the Br atom from the ring occurs, which results in a change of the $\pi\pi^*$ to a $\pi\sigma^*$ orbital and a localization of a π orbital on the bromine. This way a radical ion pair is formed at large C-Br distances resulting in a homolytic cleavage of the bond to form the uracil-5-yl radical [130] as illustrated in figure 10. The second relaxation pathway is unreactive and the decay occurs *via* a conical intersection into the electronic ground state as observed for the nucleobases as well [130]. In the second mechanism to form the uracil-5-yl radical, the UV photon absorptions (302 nm) triggers a preliminary charge transfer from the adjacent nucleobase at the 5' side to ^{5Br}U to form a radical ion pair. Sugiyama *et al.* [131] proposed the adjacent nucleobase to be an A nucleobases for this mechanism to occur. Herein, the anion is localized at the radiosensitizer molecule and the cation radical at the adjacent nucleobase at the 5'side. The radical ion pair formation is followed by an abstraction of the bromine and the uracil-5-yl radical formation [131] (fig.10). The uracil-5-yl radical reacts further and captures a proton from the sugar unit of the adjacent

nucleotide at the 5'side. The released radical at the sugar unit reacts further to a cleavage in the DNA backbone i.e. to a SSB (fig.10). The reaction of the uracil-5-yl radical to form a SSB is further explained in a second mechanism below (fig.11).

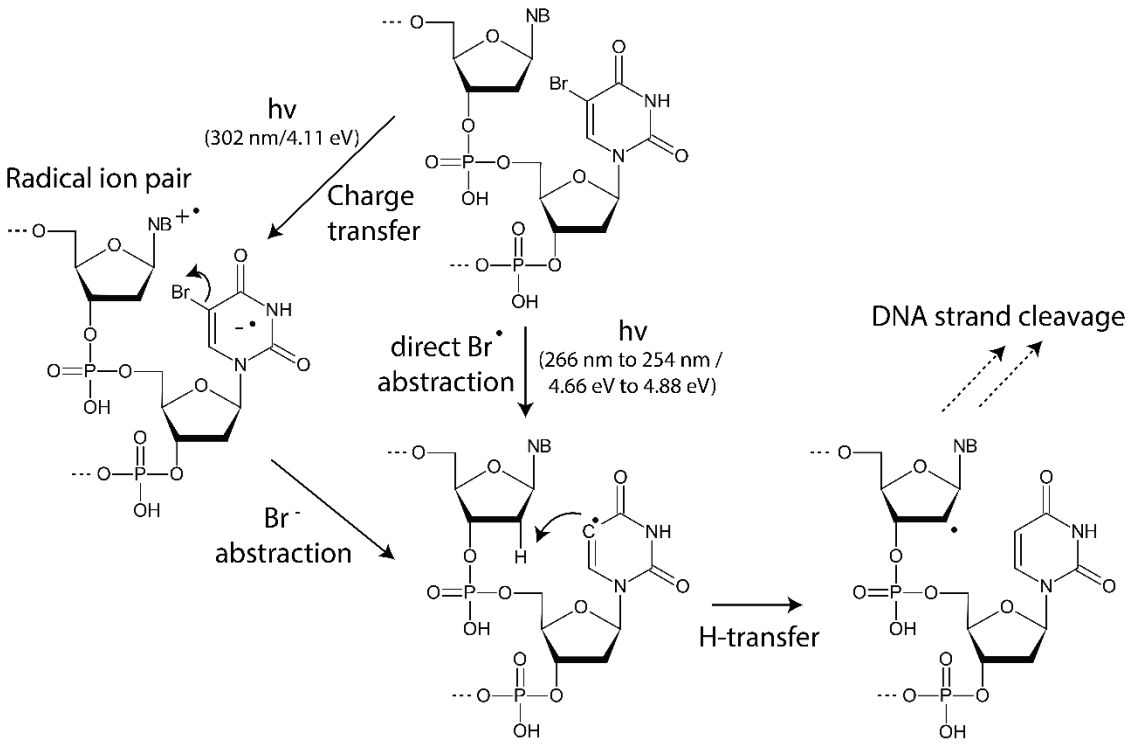

Fig. 10 Scheme of the formation of a SSB in a DNA sequence containing ^{5Br}U induced by UV light; NB = nucleobase; adapted from ref. [127–131].

Another mechanism of a possible reaction pathway of ^{5Br}U relevant for its function as a radiosensitizer was proposed by Watanabe *et al.* [73]. The formation of a SSB occurs *via* generation of a 2-deoxyribonolactone that is thermally not stable and has a life time of 32-54 h at 37 °C [132]. The formation of the ribonolactone could only be observed, if the ^{5Br}U is adjacent to T at the 3' side and an A at the 5' side. The mechanism is therefore highly DNA sequence dependent and displayed in detail in figure 11.

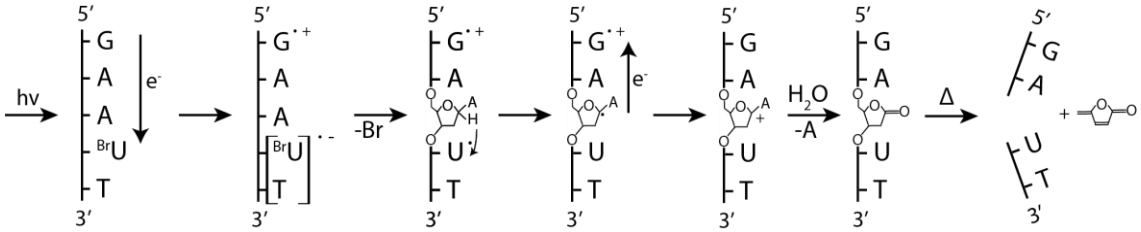

Fig. 11 Photoreaction at 300 nm of ^{5Br}U in DNA activated from G as an e^- donor leading to a SSB in the DNA sequence 5'-d(GAA^{5Br}UT); adapted from ref. [73].

Photon radiation of 300 nm/4.13 eV initiates the electron transport from a G nucleobase in a certain distance serving as an electron donor to the ^{5Br}U serving as the electron acceptor. The attachment of the electron at the ^{5Br}U containing nucleobase leads to the formation of the radical anion ^{5Br}UT$^{\bullet -}$. A uracil-5-yl radical is generated by abstraction

of the Br^- anion. This radical captures the H-atom from the neighboring adenosine at the 5'side to form a stable uracil nucleobase. The 5' side neighboring adenosine has now a radical character and releases the additional electron to be transferred back to the G nucleobase, which was serving as an electron donor. The charge of the 5' side neighboring adenosine is now positive and by adding a water molecule, the nucleobase A is released and a 2-deoxyribonolactone is formed. This molecule is not stable and will degrade already at room temperature to form a SSB in the DNA sequence. Watanabe *et al.* [73] investigated strand break yields in dsDNA in dependency of the distance of G to the radiosensitizer ^{5Br}U by using A/T base pairs as a bridge by varying the number of A/T base pairs between 0 and 5 in the dsDNA. When no A/T bridges exist in the DNA sequence, no formation of the ribonolactone was found. It was suggested that the electron back transfer was too fast in comparison to the radical formation at the ^{5Br}U reaction side [133]. The highest amount of ribonolactone was found with two bridging A/T base pairs. Here, the electron back transport seems to be lower than the radical formation. This behavior changes again with the increasing number of A/T bridges. These experiments show a clear distance dependency of the ribonolactone formation.

The radiosensitizer ^{5Br}U acts as an electron trap in the above described experiments, because it has an enhanced electron capture probability. A large positive EA_a value indicates a high stability of the anion with respect to the neutral molecule. The EA_a of ^{5Br}U is enhanced in comparison to the EA_a of the nucleobases, because the substitution of an H atom with a Br atom of the nucleobase increases this value (5-position at pyrimidines, 8-position at purines). Generally, pyrimidine bases are more prone to electron attachment than purine bases. The EA_as of the nucleobases and their brominated equivalents are listed in the following table 6.

Tab. 6 Gas phase adiabatic electron affinities (EA_as) of native and brominated nucleobases (NB) in eV; pyrimidines are substituted with Br at the 5-position and purines at the 8-position.

	U	**T**	**C**	**A**	**G**
Native NBs	0.024[a]	-0.14-0.2[b]	-0.56-0.06[b]	-1.47-0.12[b]	-1.79-(-0.01)[b]
Brominated NBs	0.49[a]	/	0.27[a]	0.01[a]	0.02[a]

[a]Rak et al. [35], [b]Gu et al. [134].

^{5Br}U possesses the highest EA_a value with 0.49 eV [35] among the modified and non-modified nucleobases. It shows also strong anionic resonances in the lower electron energy regime, which are very pronounced below 3 eV [135, 33]. The TNI $^{5Br}U^{\#-}$ can be formed through electron attachment, but is very instable and releases Br^- quite fast to form the uracil-5-yl radical (U·) (eq.6).

$$(6) \quad {}^{5Br}U + e^- \rightarrow {}^{5Br}U^{\#-} \rightarrow U\cdot + Br^- \qquad DEA$$

The uracil-5-yl radical is highly reactive to capture an H-atom from the sugar unit of the neighboring nucleoside to form uracil [73,136] as described above for the photoinduced reaction. A scheme of the latest proposal of a reaction of ^{5Br}U in a DNA sequence after electron attachment to form a SSB from Rak *et al.* [35] and Wang *et al.* [137] is displayed in figure 12.

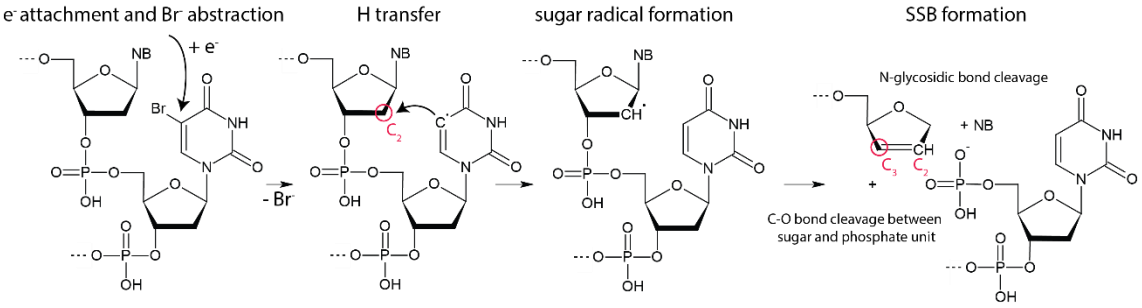

Fig. 12 Scheme of the formation of a SSB in a DNA sequence containing ^{5Br}U; NB = nucleobase; adapted from ref. [35,137].

In figure 12 it can be seen that an electron attachment to the brominated nucleobase of ^{5Br}U occurs first. This process initiates the abstraction of a Br^- anion to form a uracil-5-yl radical at the nucleobase. This radical is now capturing an H-atom of the neighboring nucleoside from the favored C_2 position of the sugar unit [137] to generate a stable uracil nucleobase. At the C_2 position a new radical is formed. An H transfer from the sugar unit, which is directly attached to^{5Br}U, on the other hand is very unlikely due to steric hindering and consequently high thermodynamic barriers. The exact mechanism of the following reaction is not known yet, but the glycosidic bond between the nucleobase and the sugar unit is cleaved to release the nucleobase. Additionally, a double bond between the C_2 and C_3 position in the sugar unit is formed and the C-O bond between the sugar unit and the phosphate unit of the DNA backbone cleaved. This way, a SSB is formed.

Keller *et al.* [118] investigated the effect of ^{5Br}U incorporated in a 13mer DNA sequence on the cross section for SSBs at an electron impact energy of 18 eV in comparison to the non-brominated DNA sequence. The results of the cross sections for SSBs are displayed in table 7.

Tab. 7 Cross sections for SSBs and order of DNA damage of electron impact experiments using the DNA origami technique, LEEs at 18 eV.

	DNA type	LEE in eV	Cross section for SSBs in 10^{-15} cm²	Trend	
ssDNA	5‘-d(TT(XTX)$_3$TT),	18			[a]
	X = A		(60 ± 9)	TT(ATA)$_3$TT >	
	X = C		(27 ± 9)	TT(CTC)$_3$TT >	
	X = G		(22 ± 9)	TT(GTG)$_3$TT	
ssDNA	5‘-d(TT(Y^{5Br}U Y)$_3$TT),	18			[a]
	Y = A		(70 ± 2)	TT(ATA)$_3$TT >	
	Y = C		(30 ± 9)	TT(CTC)$_3$TT >	
	Y = G		(37 ± 9)	TT(GTG)$_3$TT	

[a]Keller *et al*. [118].

Comparing the cross sections for SSBs of the ^{5Br}U modified and non-modified DNA sequences in table 7, it can be seen that the enhancement factor (EF) for the G flanking ^{5Br}U is the highest, followed by the EF values of the A and C flanking ^{5Br}U, which are almost giving the same values with $EF_G = 1.66$, $EF_A = 1.18$ and $EF_C = 1.14$, respectively. Thus, a clear enhancement of the cross sections for SSBs is observed for the G flanking ^{5Br}U. A and C flanking ^{5Br}U are showing only small enhancement within the error bars of the cross sections for SSBs [118].

In this thesis ^{5Br}U was incorporated in a 13mer DNA sequence flanked by different nucleobases to study their influence on the cross sections for SSBs at 8.44 eV photon irradiation energy. This experiment cannot be directly compared to the investigations of Keller *et al*. [118], since different radiation types and energies are used here. Still, an indirect comparison will be presented in the chapter 5.3 VUV induced SSBs in DNA sequences modified with ^{5Br}U. Additionally, the cross sections for SSBs were investigated in dependency of the distance of a G nucleobase to the ^{5Br}U radiosensitizer to study, if an effect also occurs in ssDNA to be compared with the results of Watanabe *et al*. [73].

3.9 Radiosensitization with 8-bromoadenine (^{8Br}A)

A second potential radiosensitizer that can be incorporated into the DNA is ^{8Br}A. The EA_a value of ^{8Br}A in the gas phase is 0.01 eV [35] and thus higher than the non-brominated A nucleobase (-1.47-0.12 eV [134]), but not as high as the EA_a of ^{5Br}U (0.49 eV [35]) (see tab.5 above) so that it also acts as an electron trap. ^{8Br}A also shows resonances below 2 eV electron radiation [34]. By the attachment of an electron through such resonances, a TNI will be formed that decomposes by the abstraction of the Br^- anion. An adenyl radical (A·) is left for further reactions (eq.7).

$$(7) \qquad {}^{8Br}A + e^- \rightarrow {}^{8Br}A^{\#-} \rightarrow A\cdot + Br^- \qquad DEA$$

Chomicz *et al.* [138] performed a computational study of the radiosensitizer ^{8Br}A being incorporated in 2'deoxyadenosine-3',5'-diphosphate and its reaction pathways that occur by electron impact. If the electron attaches to the 8-bromo-2'-deoxyadenosine-3',5'-diphosphate molecule, the C-Br bond will be cleaved and converted into a complex consisting of the radical being localized on adenine (adenyl radical) and the Br^- anion. The dissociation of the complex is thermodynamically favored in water compared to the gas phase. If the dissociation of the complex takes place, a highly reactive adenyl radical is formed that can now react along two major pathways that are displayed in figure 13.

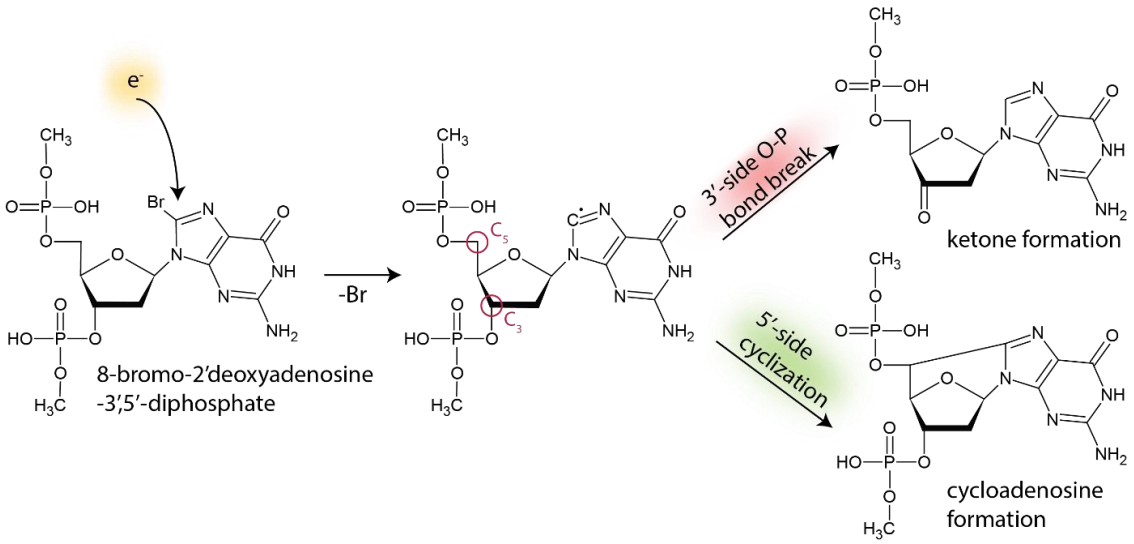

Fig. 13 Schematic reaction pathways of 8-bromo-2'-deoxyadenosine-3',5'-diphosphate through electron attachment; adapted to ref. [138].

The adenyl radical captures an H-atom from the sugar unit. From all the available possibilities, the C_3 and C_5 positions at the sugar unit are thermodynamically favored. If the H abstraction occurs at the C_3 position, a P-O bond breakage at the same side can occur. This bond cleavage corresponds to a SSB in a DNA strand. If the H abstraction occurs from the C_5 position, the sugar radical can also be stabilized by a cyclization reaction, which would form 5',8-cycloadenosine. Since the second described reaction pathway is the thermodynamically favored one, a SSB is not the most likely damage occurring here.

Schürmann *et al*. performed electron impact investigations of the radiosensitizer ^{8Br}A in the gas phase [34, 116] and in the condensed phase [116]. The gas phase experiments with LEE < 3 eV resulted in two competitive pathways that can occur after the attachment of an electron. On the one hand intense fragmentation below 2 eV LEE radiation is observed and related to the C-Br bond cleavage and a consequent formation of an adenyl radical. On the other hand, a very stable anion with an elongated C-Br bond was discovered using DFT calculations. Since the investigations were performed in the gas phase, it remains unknown, if the stable anionic state is preserved in the condensed phase. A second investigation from Schürmann *et al.* [116] was performed with ^{8Br}A molecule *via* an electron/molecule cross beam experiments in the energy regime of 0-9 eV. The Br^- fragment formation at electron impact energies below 2 eV is attributed to a shape resonance. This way, an adenyl radical can be produced that might induce a SSB as described by Chomicz *et al.* [138] (see fig.12). At higher energies more fragments appear, indicating further reaction mechanisms that might lead to different types of DNA damage. Still, the Br^- signal is the strongest one suggesting that the C-Br bond cleavage is also the main pathway for strand breakage. A third investigation of the resonant formation of SSBs incorporated in a DNA sequence in the condensed phase containing ^{8Br}A as a radiosensitizer with an electron impact energy of 0.5-9 eV by Schürmann *et al*. [116] showed that the cross section for SSBs is enhanced on average by an EF of around 2 in comparison to the non-brominated DNA sequence. From the results a clear effect of the radiosensitizer ^{8Br}A can be seen. The cross sections for SSBs are peaking at 3 and 7 eV, whereas at 7 eV a clear resonant structure could be identified. The cross sections for SSBs obtained in this study are shown in table 8.

Tab. 8 Cross sections for SSBs and order of DNA damage of electron impact experiments using the DNA origami technique, LEEs at 0.5-7 eV.

DNA type		**LEE in eV**	**Cross section for SSBs in 10^{-15} cm²**	**Trend**	
ssDNA	5‘-d(TT(ATA)$_3$TT)	0.5 3 7	(2.9 ± 0.6) (3.4 ± 0.3) (11 ± 3)		[a]
ssDNA	5‘-d(TT(^{8Br}ATA)$_3$TT)	0.5 3 7	(6.6 ± 1.9) (9.7 ± 1.6) (26.7 ± 3.8)	TT(^{8Br}ATA)$_3$T T> TT(ATA)$_3$T T	[a]

[a] Schürmann *et al. 116*

In the present work the potential radiosensitizer ^{8Br}A was studied with respect to its reactivity to photons at 8.44 eV and to LEE radiation with an energy below 3.6 eV (section 5.5).

4 Materials and methods

In this chapter the experimental details for the irradiation experiments and the tandem mass spectrometry experiment from sample preparation over the experimental set up to the data evaluation are presented. First of all, the self-assembly process of the DNA origami nanostructure, and its modification with the target DNA sequences is described. Afterwards more details are presented on the adsorption of the DNA origami nanostructures on the different substrate materials for the irradiation experiments. Then, the VUV photon irradiation and the indirect LEE experiments and their set up at the synchrotron SOLEIL facility as well as the experimental procedure are shown. The AFM imaging process of the irradiated samples and their data evaluation from the AFM images are also explained in detail. Last, the experimental set up and procedure of the gas phase photoionization tandem mass spectrometry experiment at the synchrotron SOLEIL are presented as well as the sample preparation for the experiment and the corresponding data evaluation after the experiment.

4.1 The DNA origami technique

The triangular shaped nanostructure introduced by Rothemund [37] is used in this work as a template for the target DNA sequences in the photon and electron irradiation experiments. It was chosen due to its high stability in shape and its low tendency to form clusters, since there are no blunt ends pointing out of the nanostructure. To initiate the self-assembly process to form the DNA origami nanostructure, 5 nM of the viral scaffold strand (M13mp18, tilibit nanosystems GmbH) and 200 nM of each artificial staple strand (IDT, HPLC purity) are added to a 10 x TAE-buffer (Tris(0.4 M)-acetate(0.2 M)-EDTA(0.01 M)-buffer) (Sigma-Aldrich) with 150 mM $MgCl_2$ (Sigma-Aldrich) in a total volume of 100 µL and subjected to an annealing process. The temperature program for the annealing process was conducted in a primus thermocycler (PEQLAB) and comprises four steps. First, the mixture is heated up to 80°C and cooled down to 66°C at 2°C/min. From 65°C to 25°C the solution is cooled down at 0.5°C/min and from 24°C to 8°C at 1°C/min. To remove the residues of the synthesis process, the mixture, containing now the DNA origami structures, is transferred into an Amicon Ultra 100 kDa MWCO centrifugal filter (Millipore). Two centrifugation steps are conducted with an addition of 300 µL of 1 x TAE (Tris(40 mM)-acetate(20 mM)-EDTA(10 mM)-buffer) with 15 mM $MgCl_2$ at 4629 g. Afterwards the centrifugal filter was turned around and centrifuged at 6300 g for 10 min to obtain the DNA origami nanostructures. To add the target DNA sequences for the irradiation experiments some specific staple strands have to be exchanged with extended staple strands, which consist of the staple strand sequence complemented by the target DNA sequence that is, after the synthesis, figuratively protruding from the DNA origami surface. Figure 14 illustrates the positions of the target

DNA sequences on one trapezoid of the DNA triangle. Each target DNA sequence was positioned three times on the complete DNA origami nanostructure; once on each geometrically equivalent trapezoid. The whole map of the triangular DNA origami structure is shown in figure A.1 in the appendix.

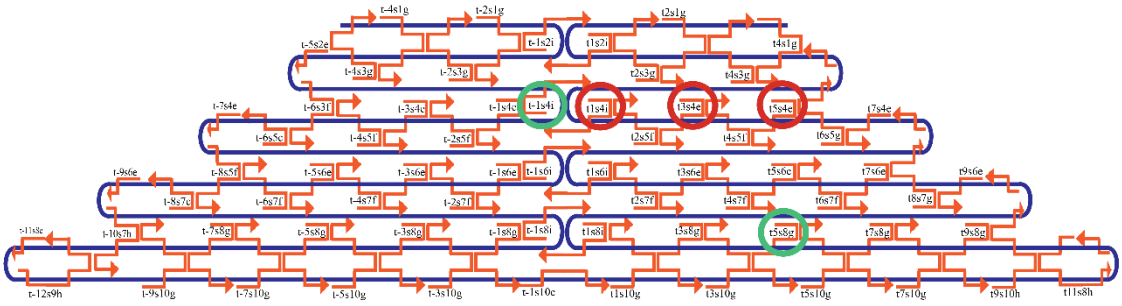

Fig. 14 Schematic map of one of the three trapezoids of the triangular DNA origami nanostructure with the denotations and positions of the staple strands (red) in the scaffold DNA strand (blue) after the self-assembly process; positioning of the target DNA sequences marked in green or dark red, respectively (Tab.9).

Two target DNA sequences were placed on one DNA origami nanostructure. In the green design only two positions are possible. In the dark red design three options to position the target DNA sequence are available, but only two different options were used for each design. The different target DNA sequences are listed in table 9 below. In this thesis 19 different DNA sequences were analyzed that varied in their nucleobase composition (no. 1-4, 18), the length of the DNA sequence (no. 1, 5-8) and the content of incorporated radiosensitizer ^{5Br}U (no. 9-17) and ^{8Br}A (no. 19), respectively. All DNA sequences were irradiated with 8.44 eV VUV photon radiation and a part of the DNA sequences with < 3.6 eV LEE radiation (no. 1-4, 18-19). The sample preparation, the general radiation procedure and the data analysis are described in detail in the next sections.

Tab. 9 List of investigated target DNA sequences with their position on the DNA origami nanostructure, the corresponding design and the irradiation type.

No.	DNA sequence	Position	Design	Radiation type
1	5'-d(A_{12})	t-1s4i, t-1s14i, t-1s24i	green	VUV, LEE
2	5'-d(C_{12})	t5s8g, t5s18g, t5s28g	green	VUV, LEE
3	5'-d(G_{12})	t-1s4i, t-1s14i, t-1s24i	green	VUV, LEE
4	5'-d(T_{12})	t5s8g, t5s18g, -5s28g	green	VUV, LEE
5	5'-d(A_4)	t-1s4i, t-1s14i, t-1s24i	green	VUV
6	5'-d(A_8)	t5s8g, t5s18g, t5s28g	green	VUV
7	5'-d(A_{16})	t-1s4i, t-1s14i, t-1s24i	green	VUV
8	5'-d(A_{20})	t5s8g, t5s18g, t5s28g	green	VUV
9	5'-d(TT($C^{5Br}UC)_3$TT)	t1s4i, t1s14i, t1s24i	red	VUV
10	5'-d(TT($G^{5Br}UG)_3$TT)	t3s4e, t3s14e, t3s24e	red	VUV
11	5'-d(TT($T^{5Br}UT)_3$TT)	t5s4e, t5s14e, t5s24e	red	VUV
12-14	5'-d(TTG$A_n{}^{5Br}$UTT) n = 0, 2, 4	t-1s4i, t-1s14i, t-1s24i	green	VUV
15-17	5'-d(TTG$A_n{}^{5Br}$UTT) n = 1, 3, 5	t5s8g, t5s18g, t5s28g	green	VUV
18	5'-d(TT(ATA)$_3$TT)	t-1s4i, t-1s14i, t-1s24i	green	VUV, LEE
19	5'-d(TT(^{8Br}ATA)$_3$TT)	t-5s8g, t-5s18g, t5s28g	green	VUV, LEE

4.2 Sample preparation

Before the irradiation experiments can start, the DNA origami nanostructures with the target DNA sequences have to be adsorbed on a substrate. Two different materials were used here. For the VUV irradiation experiments calcium fluoride (CaF_2) substrates (CaF_2(111) - CrysTec) in a size of 5 x 5 mm were applied. CaF_2 is a material, which is transparent to VUV light [139]. Consequently, no heating of the sample or generation of secondary particles from the substrate surface are expected. To have a clean surface for the DNA origami adsorption process, the 1 mm thick CaF_2 substrates were cleaved with the help of a scalpel. On the freshly cleaved surface 0.7 µL of the prepared DNA origami nanostructure solution and 15 µL of the 1 x TAE with 15 mM $MgCl_2$ buffer were added. After 2 min of residence time, the substrate was rinsed with 2 mL of a distilled water/absolute (abs.) ethanol (1:1) solution (abs. Ethanol-Sigma Aldrich) and blown dry with a stream of nitrogen.

The DNA origami nanostructures are supposed to adsorb flat and equally distributed on the substrate surface. On the CaF_2 substrate the adsorption behavior can be very different depending on the position on the surface. Due to the cleavage of the substrate, the normal F-Ca-F triple layer gets distorted and step-crossing patterns appear [140], which might lead to a different adsorption behavior. The DNA origami nanostructures can appear folded within themselves, which is on the AFM image visible as lump of DNA. Often also many

DNA origami nanostructures adsorb as a multilayer and the single structures cannot be distinguished anymore. The DNA origami nanostructure can also appear as partly flat adsorbed with only one corner folded on the structure itself. Other spots on the CaF_2 substrate show flat adsorbed DNA origami nanostructures and a homogenous submonolayer distribution. On most of the surface spots a mixture of the different adsorption behaviors can be seen. To improve the adsorption quality of the DNA origami nanostructures, 5 x 5 mm sized silicon (Si) substrates (p-Si(100) - CrysTec) were chosen in addition to CaF_2. The surface of the Si substrates was covered by a protective varnish that could be easily removed by rinsing it with abs. ethanol. To clean the surface even further, an oxygen plasma cleaning for 5 min was applied (ZEPTO - diener electronics). The surface charge of the Si substrate is negative. Hence a higher buffer concentration of 10 x TAE with 150 mM $MgCl_2$ and a longer residence time of 1 h was applied. The volumes of the used buffer and DNA origami nanostructure solution and the washing steps remained the same. The differences in the adsorption procedure are summarized in table 10 below.

Tab. 10 DNA origami nanostructure adsorption conditions for the two different materials.

Substrate material	**Buffer**	**Residence time**
CaF_2(111)	1 x TAE with 15 mM $MgCl_2$	2 min
p-Si(100)	10 x TAE with 150 mM $MgCl_2$	1 h

Si as a material for the substrate is not transparent to VUV light. Secondary electrons can be generated by VUV radiation giving rise to additional damage of the target DNA sequences on the DNA origami nanostructures. This is further discussed in chapter 4.4.

4.3 Vacuum ultraviolet (VUV) irradiation set up and fluence calculation

The VUV photon irradiation experiments were performed at the DISCO/APEX beamline of the synchrotron facility SOLEIL near Paris in France [141]. The radiation source at the synchrotron facility SOLEIL are accelerated electrons, which are generated from hot cathodes. The electrons are firstly accelerated to 100 MeV by a linear accelerator and then introduced into a storage ring to be accelerated even faster to a speed of 2.75 GeV. At the beamline DISCO/APEX a dipole generates the synchrotron radiation, which is filtered by a monochromator and coupled into the beamline. Herein, the monochromatic VUV light is filtered again by a magnesium fluoride (MgF_2) window, which is mounted on a window valve and makes the VUV light accessible with a photon energy range from 5 to 20 eV. In the beamline a differential pumping system creates an ultra-high vacuum (UHV), since the VUV light would otherwise be absorbed by the oxygen in the atmosphere. Before the VUV light is coupled into the irradiation set up, a photon shutter is installed as a switch to block the photon radiation, if needed. The shutter can be manually activated by a transistor-transistor logic (TTL) signal. When the shutter is open, the VUV photon radiation can enter the argon (Ar) filled steel chamber, where the irradiation of the

samples occurs. A continuous stream of Ar through the irradiation chamber has to be ensured to block the oxygen from the air, which might enter the chamber, when the sample holder is placed from the top of the irradiation chamber. The sample holder itself can be manipulated in the z-axis to change the position, where the photon beam hits the vertically arranged sample array. Up to 10 samples can be placed here. To detect the fluence (number of photons per surface area) of the irradiation process, a calibrated photodiode (AXUV 100, International Radiation Detectors) is placed on the axis of the VUV beam [142,143]. The whole VUV irradiation set up is illustrated in figure 15 below.

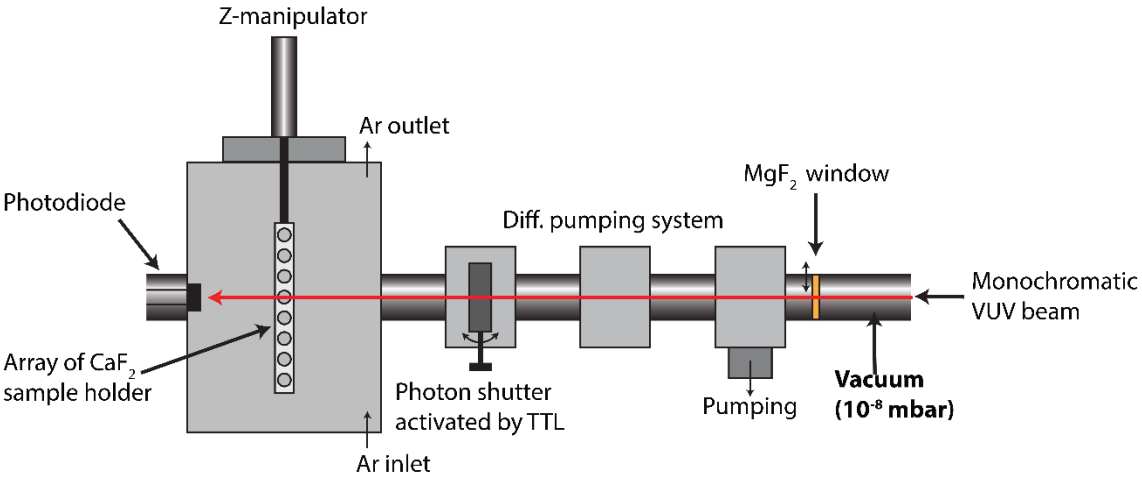

Fig. 15 Scheme of the VUV photon irradiation set up at the synchrotron facility SOLEIL [25].

To guarantee that the VUV photon beam illuminates only one sample at a time, a beam profile was measured with a photodiode as displayed in figure 16. It can be seen that the VUV beam illuminates the sample completely from the right to left side, but not at the top and at the bottom. This was considered for the later AFM imaging. The beam shows an oscillating intensity profile along one direction, which arises from the filtering and focusing of the original generated beam at the DISCO/APEX beamline. Since some spots on the substrates are exposed to higher fluence and others to lower fluence, a large number of AFM images were taken to evaluate the data properly. This will be explained in further detail in the next section.

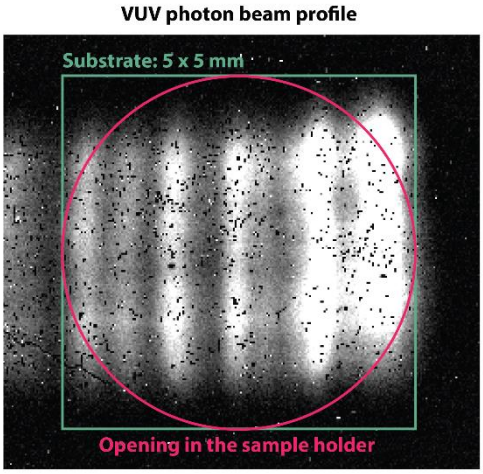

Fig. 16 VUV photon beam profile at an energy of 8.44 eV; substrate size (5 x 5 mm) marked with a green square and VUV photon beam illuminated area (diameter: 5 mm) determined by the opening in the sample holder marked with a red circle.

For every irradiation experiment the time of the irradiation (t), the energy of the photon beam (E), the bias measured at the photodiode (U) and the responsivity of the photodiode (R_{Diode}) at the specific irradiation energy was determined. The bias measured at the photodiode (U) was enhanced by an amplifier with the resistance (R) of $10^8\,\Omega$, which is used to calculate the current (I) of the photodiode (eq.8).

$$I[A] = \frac{U[V]}{R[\Omega]} = \frac{U[V]}{10^8[\Omega]} \tag{8}$$

The responsivity of the photodiode (R_{Diode}) at the specific irradiation energy is calculated by the current (I) of the photodiode, the power of the photodiode (P) and the energy of one photon (E_{Ph}) (eq.9). P in turn is calculated from the number of photons (n_{Ph}) per time (t) and the energy of one photon (E_{Ph}) (eq.10).

$$R_{Diode}\left[\frac{W}{A \cdot J}\right] = \frac{P[W]}{I[A] \cdot E_{Ph}[J]} = \frac{P\left[\frac{J}{s}\right]}{I[A] \cdot E_{Ph}[J]}\,, \tag{9}$$

$$P[W] = \frac{E_{Ph}[J]}{t[s]} = \frac{n_{Ph} \cdot E_{Ph}[J]}{t[s]}\,. \tag{10}$$

This enables the calculation of the responsivity of the photodiode (R_{Diode}) (eq.11) and the number of photons (n_{Ph}) that hit the sample within one irradiation period (eq.12).

$$R_{Diode}\left[\frac{Ph}{As}\right] = \frac{n_{Ph} \cdot E_{Ph}[J]}{t[s] \cdot I[A] \cdot E_{Ph}\,[J]}\,, \tag{11}$$

$$n_{Ph} = R_{Diode}\left[\frac{Ph}{As}\right] \cdot I[A] \cdot t[s]\,. \tag{12}$$

The responsivity of the photodiode (R_{Diode}) at 8.44 eV is a value ($5.06 \cdot 10^{-18}\,\frac{Ph}{As}$) given by the manufacturer of the photodiode. Hence, the number of photons (n_{Ph}) that hit the sample within this irradiation period can be directly calculated from the experiments with the irradiation time (t) and current (I) of the photodiode.

For the data evaluation it is necessary to know the fluence (F) of the irradiation process. It is determined by the number of photons (n_{Ph}) that hit the irradiated surface area (A). Since the irradiation area is circular here, it can be calculated from the radius (r) of the opening in the sample holder, which is 0.25 cm in these irradiation experiments. The calculations are given by the equation 13 and 14, respectively.

$$F[cm^{-2}] = \frac{n_{Ph}}{A[cm^2]}\,, \tag{13}$$

$$A[cm^2] = \pi r^2\,. \tag{14}$$

All photon irradiation experiments were conducted with CaF_2 as a substrate material. To induce an additional indirect LEE irradiation on the samples, Si as a substrate material was applied. This is further explained in the next section.

4.4 Contribution of secondary electrons

A part of the VUV irradiation experiments at an energy of 8.44 eV was performed with p-Si(100) as substrate material, which is not transparent to VUV light. The work function of Si is 4.8 eV [144], which is calculated by the difference of the vacuum level energy and the Fermi energy. Hence, with a photon energy of 8.44 eV, it can be expected to generate LEEs with an energy roughly below 3.6 eV from the substrate surface; calculated by the subtraction of the photon energy by the work function. These additional secondary electrons contribute to the DNA damage caused in the target DNA sequences incorporated in DNA origami nanostructures and is further referred to as indirect LEE radiation.

Indirect LEE impact studies on plasmid DNA exploiting the indirect LEE radiation were already performed by Liu *et al*. [145]. LEEs from the substrate surface were generated through 240-400 nm/5.2-3.1 eV UV radiation. As a substrate material n-Si was applied and the indirect LEE irradiation resulted in a significant amount of SSBs in the plasmid DNA. In the present work the influence of the indirect LEE radiation on different target DNA sequences is tested and compared to results obtained under VUV irradiation with VUV transparent substrates.

4.5 Strand break detection and data analysis

During the photon and electron irradiation process, many different types of DNA damage are induced. The target DNA sequences, which are figuratively protruding from the DNA origami nanostructure template, experience also base losses besides the SSBs and other possible damages that cannot be detected within this exact experimental approach. To detect the SSBs, the target DNA sequences are terminally labelled with a biotin molecule. After the irradiation process, the intact target DNA sequences still have this modification as visualized in figure 17a. By adding a solution of 15 µL of 50 nM streptavidin in 1xTAE buffer with 15 mM $MgCl_2$, the biotin labels will bind to the protein streptavidin. This protein has, depending on its configuration, roughly a size of (4.5 x 4.5 x 5) nm and can be easily imaged with AFM. This way, the number of visible streptavidin spots on the DNA origami nanostructure is representative for the number of intact target DNA sequences. Only if no streptavidin can be seen at the specific position, a SSB occurred. In figure 17b different amounts of SSBs for two different DNA sequences can be seen. One DNA sequence is positioned on the three center positions and the second DNA sequence is positioned on the three side positions. In the first image of figure 17b all DNA sequences are intact, since three spots on the center positions and three spots on the side positions of the triangular DNA origami nanostructure are clearly visible. In the second image only four spots can be seen on the DNA origami nanostructure. The two missing spots on one of the three trapezoids are indicating two SSBs, one in each target DNA sequence used in this sample. In the third image only two spots are visible. The center position is not occupied at all. Consequently, all three target DNA sequences experienced

a SSB here. On the side position two spots can be identified. Only one SSB occurred in this target DNA sequence. This way, the number of SSBs for every target DNA sequence was determined. About six samples were irradiated with different irradiation times for each of the 19 target DNA sequences and around 15 - 20 AFM images taken for each sample. To get good statistics 800 – 1500 spots were analyzed for each sample. In total, up to 600 000 single target DNA sequences were investigated.

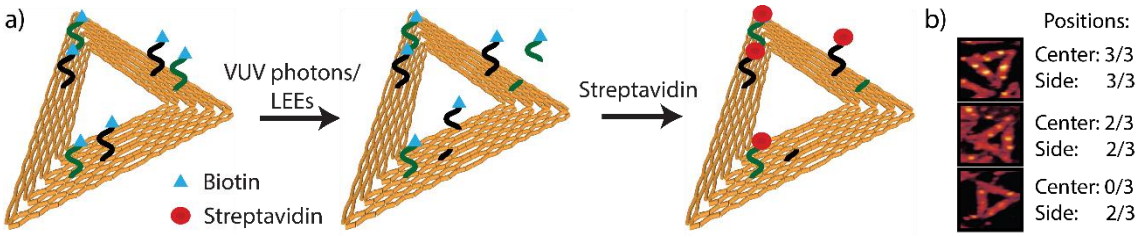

Fig. 17 a) General scheme of the irradiation process and strand break detection procedure, b) examples of AFM images of irradiated DNA nanostructures occupied with 1-6 Streptavidin; the central and side position can be analyzed separately to determine the number of SSBs for two different DNA sequences within one irradiation experiment.

The number of SSBs (n_{SSB}) of every sample from one series of measurements is analyzed. It is always given with its standard error σ_n. This is calculated from the standard deviation of the number of SSBs σ from the different AFM images applied for the data analysis divided by the square root of the number of AFM images (N) (eq. 15).

$$\sigma_n = \frac{\sigma}{\sqrt{N}} \tag{15}$$

n_{SSB} is then plotted versus the fluence of the irradiation process (fig.18). The graph is fitted linearly then and from the slope of the graph the cross section for SSBs (σ_{SSB}) is evaluated and always given with the standard deviation as an error bar. This is also expressed by equation 16.

$$\sigma_{SSB}[cm^{-2}] = \frac{n_{SSBs}}{F[cm^2]}\,. \tag{16}$$

This way, the cross section for SSBs can be obtained in dependency of the DNA sequence, the radiation type and the radiation energy.

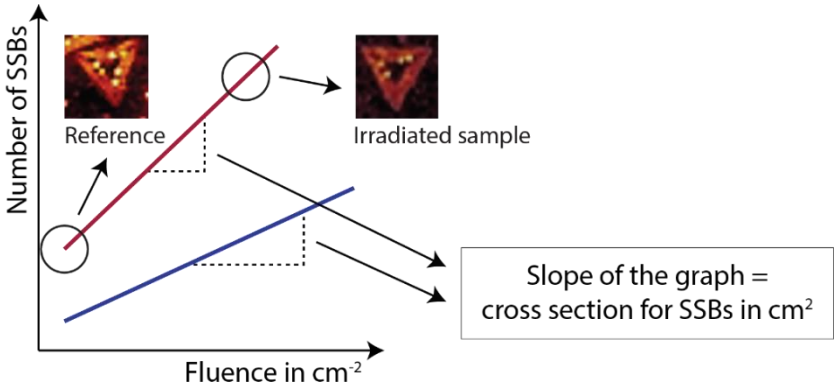

Fig. 18 Schematic plot of the number of single strand breaks as a function of the fluence of the irradiation process; the slope of the graph corresponds to the cross section for SSBs; one image of a reference and one of an irradiated sample are given here.

4.6 Atomic force microscopy (AFM)

AFM imaging is a technique to visualize surface structures in the small nanometer range and is applied in the present work to analyze the single strand breakage of the target DNA sequences incorporated in the DNA origami nanostructures. The probe, which is scanning the sample surface line-wise, is a cantilever with a sharp tip. Approaching the surface, the cantilever is bent by attractive and repulsive forces of the surface (fig.19). Van-der-Waals forces and capillary action are examples for attractive forces and the coulomb repulsion for the repulsive force. The bending of the cantilever is detected by a laser that is focused on the cantilever surface. The reflection of the laser from the cantilever surface is changing with the bending of the cantilever, which is detected by a 4-segment photodiode to be finally translated into an image of the nanostructured surface. The resolution of the image is determined by the tip size of the cantilever. The smaller the tip size, the better the resolution. Generally, the tip has a diameter of < 10 nm to reach a resolution of a few nanometers [146].

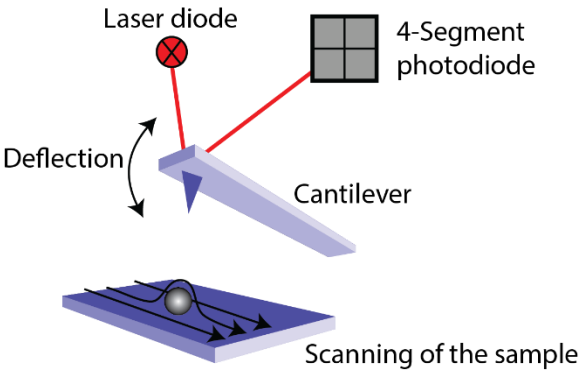

Fig. 19 Scheme of the AFM measurement principle; during the line scan of the surface structure, the cantilever reacts with bending on obstacles, which is detected by a laser being first focused on the cantilever and then reflected to a 4-segment photodiode; changes of the signal are translated into a topography image.

Depending on the investigated material different measuring modes are possible. DNA is a very soft material. Hence, the tapping mode was applied. In the tapping mode the

cantilever is stimulated by a piezo crystal to oscillate at its resonance frequency. Due to attractive and repulsive forces, the amplitude and phase of the oscillation changes according to the surface topography. A control circuit is applied to correct these changes for every image pixel. These corrections of the amplitude are translated into a topography image. In figure 20 examples for the DNA origami nanostructures are displayed, one image on CaF_2 and one on Si.

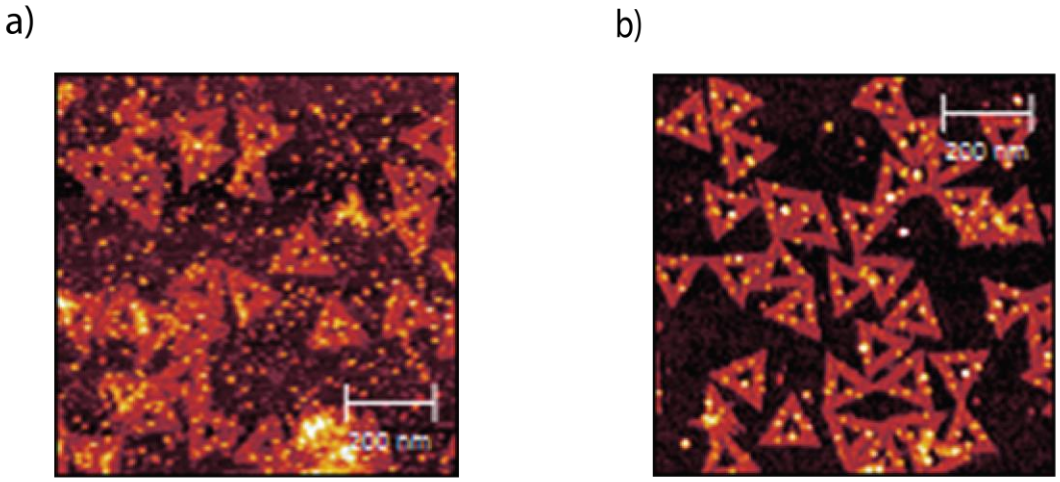

Fig. 20 Triangular shaped DNA origami nanostructures with streptavidin attached to the target DNA sequences adsorbed on a) CaF_2 and b) Si.

In this thesis AFM imaging was performed with an Agilent 5500 AFM by Keysight (former Agilent Technologies) in the soft tapping mode with the cantilever Tap 150 Al-G (Budget Sensor) that has a spring constant of 5 N/m and a resonance frequency of around 150 kHz. Typical imaging parameters are an image size of (3.5 x 3.5) µm, a resolution of 512 pixels, a scanning speed of 1.64 s/line and a P- and I-gain of 1300, respectively. The raw AFM data were processed with the program Gwyddion 2.45.

4.7 Photoionization tandem mass spectrometry sample preparation

The gas phase tandem mass spectrometry experiments were also performed at the DISCO/APEX beamline in the synchrotron facility SOLEIL [141]. In this experiment the IE of the different cationic charge states of 13 different target DNA sequences (Eurogentec, gold standard) were determined to draw conclusions on the IE of the initial target DNA sequence. In table 11 the investigated DNA sequences are listed.

Tab. 11 List of investigated target DNA sequences with their irradiation type and distinguishing feature.

No.	DNA sequence	Radiation type	Differentiator
1	5'-d(A_{12})	VUV	Type of Nucleobase / DNA sequence length
2	5'-d(C_{12})	VUV	Type of Nucleobase
3	5'-d(T_{12})	VUV	Type of Nucleobase
4	5'-d(TT$(ATA)_3$TT)	VUV	Type of Nucleobase
5	5'-d(TT$(CTC)_3$TT)	VUV	Type of Nucleobase
6	5'-d(TT$(GTG)_3$TT)	VUV	Type of Nucleobase
7	5'-d(A_4)	VUV	DNA sequence length
8	5'-d(A_8)	VUV	DNA sequence length
9	5'-d(A_{16})	VUV	DNA sequence length
10	5'-d(A_{20})	VUV	DNA sequence length
11-13	5'-d(TTGA_n^{5Br}UTT) n = 1-3	VUV	^{5Br}U radiosensitizer

To prepare the DNA sequences for the electrospray ionization (ESI) in the MS^2 experiment, they had at first to be centrifuged with a 2000 Da Vivacon 2 centrifuge filter (Sartorius stedim) four to six times at 6100 g for 30 min each to minimize the amount of sodium ions (Na^+) in the solution. In each centrifugation step 1 mL of a 0.1 M ammonium acetate (NH_4OAc) solution was added. Before the filtration the DNA sequences had a concentration of 100 µM. After the filtration the concentration is roughly doubled. For the final scan in the MS^2 experiments a volume of around 1.5 mL of the target solution, which contained 150-300 µL of the target DNA sequence solution, 750 µL methanol (MeOH) and the NH_4OAc buffer with a concentration of 0.1 M in total, was prepared. The MeOH is needed to support the solvent evaporation in the applied ESI source.

4.8 Photoionization tandem mass spectrometry set up

The experimental set up of the tandem mass spectrometry consists of two main parts, a commercially available LTQ mass spectrometer (Thermo) and a differential pumping stage, which provides the VUV photon beam (fig. 21).

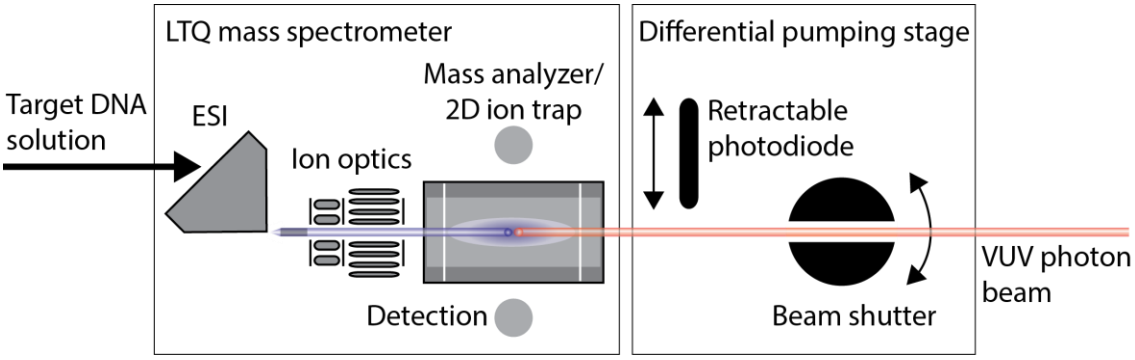

Fig. 21 Schematic set up of the photoionization gas phase tandem mass spectrometry experiment at the synchrotron SOLEIL [147].

At first the target DNA solution is sprayed in the ESI source of the LTQ mass spectrometer in the positive mode. ESI is a very mild ionization method that leads to the formation of quasimolecular ions by the addition of a proton to the molecule (M) in the positive mode resulting in $[M + H]^+$. Often also quasimolecular ions with adducts from the matrix of the solution such as $[M + Na]^+$ appear. To obtain a molecular cation stream from the ESI source, a positive voltage and a high temperature is applied on the metallic capillary containing the DNA sequence solution. Typical values for the voltage and the temperature at the ESI source are 3.5 kV and 270 °C, respectively. The vaporization of the fine aerosol is further supported by a stream of an inert gas, which is nitrogen (N_2) here. If the drop size of the sprayed aerosol becomes smaller than the Rayleigh limit, which is the maximum charge in a droplet defined by the drop size and its surface tension, the droplet collapses into smaller drops due to the coulomb repulsion of the ions. The formation of the final free ions is explained in two main theories. The charge residue model assumes that droplets in a final size of below 1 nm remain, which are containing only one charged ion [148]. The ion evaporation model on the contrary asserts that already from bigger droplets free ions are released into the gas phase [149]. However, the free ions are accelerated to a counter electrode to be directed into the ion optics of the mass spectrometer. The ion optics consists of a quadrupole and an octapole. Both are used to separate the masses of the ions, focus the ions and guide them to the mass analyzer. Here, the mass per charge ratio (m/z) is detected and can be plotted against the signal intensity as shown in figure 22 (MS 1).

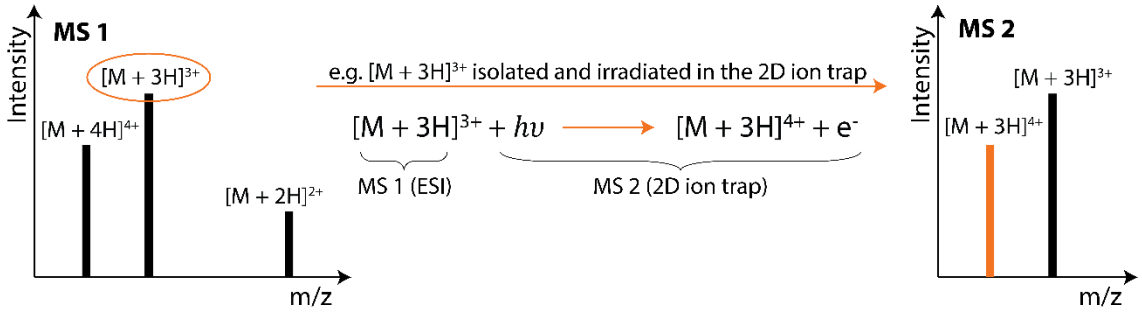

Fig. 22 Plot of the signal intensity against the mass per charge ratio (m/z) for the MS 1 and MS 2 spectra; example of the reaction of a precursor cation $[M + 3H]^{3+}$ with photon radiation isolated in the 2D ion trap, which results in the rejection of an electron and the formation of a photoinduced cation $[M + 3H]^{4+}$.

In the MS 1 spectra of the mass analyzer all available positively charged ions of the target DNA sequence can be seen. One of the positively charged ions, also referred to as precursor ions, can be selected and accumulated in the 2D ion trap. Herein, the irradiation with the VUV photon beam takes place. To control the irradiation time and energy a shutter and a retractable photodiode are connected upstream in the differential pumping stage (fig. 21). During the irradiation process of the precursor cation in the 2D ion trap, the energy of the VUV photon beam is increased stepwise by 0.2 eV starting at an energy of 8 eV and finishing at an energy of 16 eV. When the VUV beam hits the precursor cation (e.g. $[M + 3H]^{3+}$) and exceeds its IE, an electron will be removed from the molecule and a photoinduced cation ($[M + 3H]^{4+}$) generated, which has one positive charge more than the precursor cation (fig. 22). The signal intensity of the photoinduced cation is recorded in dependency of the rising photon energy. This plot is displayed in figure 23.

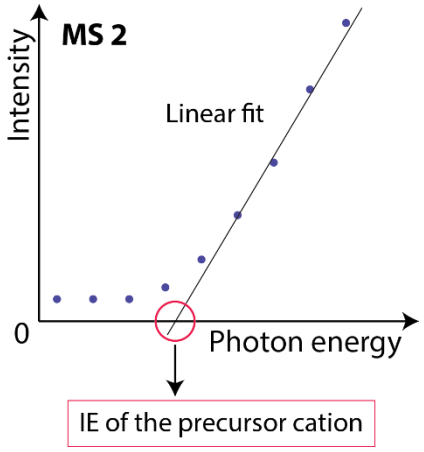

Fig. 23 Intensity of the photoinduced cation with increasing photon energy (MS 2); linear fit of the increasing part of the graph and extrapolation to intensity 0; intersection corresponds to IE of the precursor cation.

The signal intensity of the photoinduced cation describes a smooth curve before it starts to rise linearly (MS 2). Since the ssDNA sequence exists in many different conformers, which have a slightly different IE, an average signal of all conformers is seen in the MS 2 spectra. To obtain the IE of the photoinduced cation, the steeply increasing part of the curve has to be fitted linearly. The intersection of the fit with the photon energy at the x-axis determines the IE. This procedure is conducted for all precursor cations that are available at the MS 1 in the mass analyzer.

5. Results and discussion of the VUV and LEE irradiation experiments

In this chapter the results of the VUV and LEE irradiation experiments are presented and discussed in the framework of the data reported by other groups on this topic. The cross sections for SSBs are displayed in dependency on the type of the nucleobase, the DNA sequence length and on the modification with the radiosensitizers ^{5Br}U and ^{8Br}A. Additionally, enhancement factors for the SSB cross sections for modified DNA sequences in comparison to non-modified DNA sequences are given.

5.1 VUV and LEE induced SSBs in various DNA sequences

Four DNA sequences with a length of 12 nucleotides were investigated with respect to SSB cross sections upon 8.44 eV VUV photon irradiation and < 3.6 eV indirect LEE irradiation. The target DNA sequences considered in this section contain only one type of nucleobase (A, C, G or T). An overview over the samples and the results is given in table 12 below. The irradiation experiments were conducted on CaF_2 and Si as substrate materials. In section 5.1.1 and 5.1.2 the cross sections for SSBs obtained on CaF_2 and on Si, respectively are presented and discussed in the context of the results obtained by other research groups. Additionally, in chapter 5.1.2 all cross sections for SSBs of the four target DNA sequences on the two substrate materials are plotted in direct comparison. Moreover, the differences in cross section for SSBs obtained on CaF_2 and Si are displayed.

Tab. 12 Overview of the cross sections for SSBs for the different DNA sequences adsorbed on two different substrates and exposed to VUV photons.

DNA sequence	Cross section for SSBs in 10^{-16} cm²	Substrate	Radiation
5'-d(A_{12})	(2.1 ± 0.3)	CaF_2	VUV
5'-d(C_{12})	(1.7 ± 0.1)	CaF_2	VUV
5'-d(G_{12})	(2.3 ± 0.2)	CaF_2	VUV
5'-d(T_{12})	(2.1 ± 0.2)	CaF_2	VUV
5'-d(A_{12})	(4.2 ± 0.7)	Si	VUV and indirect LEE
5'-d(C_{12})	(3.6 ± 0.7)	Si	VUV and indirect LEE
5'-d(G_{12})	(2.8 ± 0.4)	Si	VUV and indirect LEE
5'-d(T_{12})	(6.9 ± 1.6)	Si	VUV and indirect LEE

5.1.1 VUV induced SSBs

The four different target DNA sequences incorporated in the DNA origami nanostructures were adsorbed on CaF_2 as a substrate and irradiated with 8.44 eV photon radiation. Figure 24 displays the relative number of SSBs plotted versus the fluence of the irradiation process. In the lower fluence regime the curve is rising nearly linearly to saturate then resulting in a plateau. The lower fluence regime is fitted linearly to obtain the cross section for SSBs from the slope of the graph. The DNA sequence 5'-d(C_{12}) shows the lowest cross section for SSBs with $\sigma = (1.7 \pm 0.1) \cdot 10^{-16}$ cm² and 5'-d(G_{12}) the highest cross section for SSBs with $\sigma = (2.3 \pm 0.2) \cdot 10^{-16}$ cm².

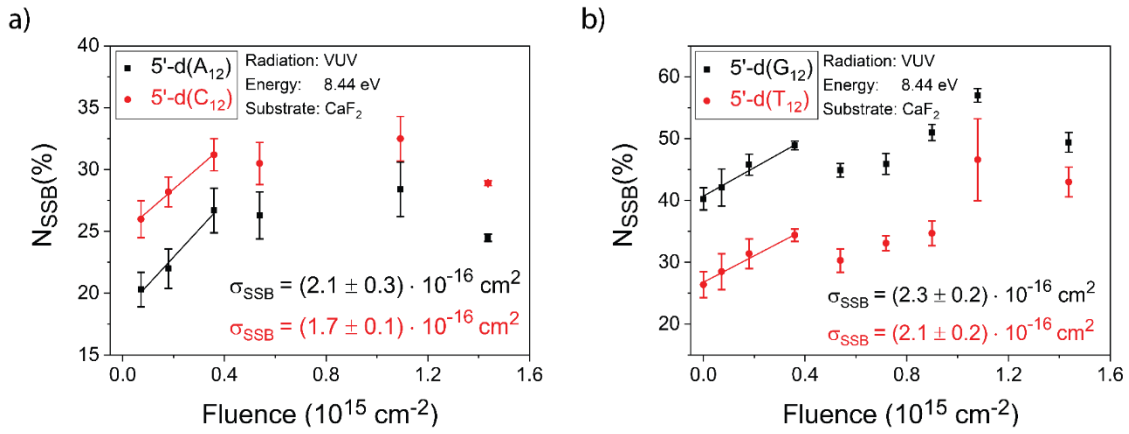

Fig. 24 Plot of the relative number of SSBs against the fluence of the VUV radiation at 8.44 eV to determine the cross sections for SSBs with a) the DNA sequences 5'-d(A_{12}) and 5'-d(C_{12}) and b) the DNA sequences 5'-d(G_{12}) and 5'-d(T_{12}), both irradiated on CaF_2.

All cross sections for SSBs obtained on CaF_2 are differing only slightly and mainly within their error bars. No clear dependency on the type of nucleobase at the VUV photon irradiation energy of 8.44 eV is observed. The initial step for a SSB formation could be the photoexcitation or photoionization. The photoexcitation process in DNA is known to be efficient already at lower energies (4.7 eV), but the corresponding excited state also decays efficiently in a non-radiative pathway [1]. At slightly higher energies SSBs are already induced, but in a small amount as demonstrated in previous work [25]. Two intermixed DNA sequences were irradiated with 6.5 eV, 7.29 eV, 8.44 eV, 8.94 eV photons [25]. At 6.5 eV irradiation energy SSBs were observed with a cross section of $\sigma = (1.2 \pm 0.3) \cdot 10^{-16}$ cm².

The photoionization process is a threshold process, which is initiated at the IE of the DNA sequence. The SSB cross section would increase, starting from an irradiation energy that corresponds to the IE of the DNA sequence. In previous work it was shown that the cross section for SSBs increases strongly from a photon energy of 7.29 eV on and with it the effective formation of SSBs [25]. The higher the irradiation energy in comparison to the IE of the DNA sequence, the higher will be the strand breakage yield. Kumar *et al.* [150] and Gallandi and Körzdörfer [151] performed computational studies on DNA sequences of a different length, which show that the IE of the DNA sequence decreases with the sequence

length. Kumar *et al*. [150] e.g. reported a decrease of the IE when going from the single nucleobase A (8.44 eV [2]) to the length of eight stacked A nucleobases by 1 eV. Thus, the applied irradiation energy of 8.44 eV should be high enough to induce SSBs *via* both processes, the photoionization and the photoexcitation.

The photon energy of 8.44 eV was chosen because it corresponds to the IE of the nucleobase A [2]. Since the nucleobases are the part of the DNA with the lowest IEs [2,28], it was proposed that they are ionized preferentially. The SSB could then occur by a charge transfer of the resulting positive charge in the nucleobase to the DNA backbone followed by a cleavage of the phosphodiester bond between the sugar and the phosphor unit (section 3.3). Since the nucleobases have different IEs in a range of 8.24 eV for G to 9.5 eV for T [2], it was expected that a similar trend is observed in the corresponding cross sections for SSBs for the four target DNA sequences, which are only differing in the type of nucleobase. Within the presented data only the DNA sequence 5'-d(G_{12}) shows a slightly increased cross section for SSBs in comparison to the other DNA sequences. This might be due to the IE of the nucleobase G being lower than the applied photon irradiation energy, whereas the IEs of the other nucleobases are at or above the photon impact energy of 8.44 eV. This could lead to a higher ionization efficiency and with it to higher SSB cross sections.

The cross sections for SSBs obtained in previous work on the intermixed DNA sequences 5'-d($TT(ATA)_3TT$) and 5'-d($TT(CTC)_3TT$) are $\sigma = (2.8 \pm 0.2) \cdot 10^{-16}$ cm² and $\sigma = (2.2 \pm 0.4) \cdot 10^{-16}$ cm², respectively [25] at the same irradiation energy as used here. The results of both experiments are in the same order of magnitude and thus, in a very good agreement. VUV impact experiments conducted with plasmid DNA instead of ssDNA result in SSB cross sections, which vary by several orders of magnitude, always depending on the initial irradiation energy of the photon impact experiments. At a photon irradiation energy of 0.79 eV below the photon irradiation energy used in this work, the cross section for SSBs is one order of magnitude lower [97]. At 1.3 eV above the irradiation energy applied in this work, the cross section for SSBs is already two orders of magnitude higher [96]. This demonstrates the sensitivity of the DNA to the VUV energy range. Unfortunately, the cross sections for SSBs obtained for the plasmid DNA and the ssDNA cannot be compared directly, since both systems vary in the sample preparation and the SSB cross sections of plasmid DNA are known to depend highly on the used buffer and the substrate temperature [41,42].

5.1.2 Si substrate effect on the VUV induced SSB cross sections

The results of the irradiation experiment with 8.44 eV photon radiation on the Si substrate are shown in figure 25. The correlation of the number of SSBs, the fluence of the irradiation process and the obtained cross sections for SSBs are presented. Here, a significant trend in the sensitivity of the different DNA sequences is observed. The obtained cross sections for SSBs are induced by both the direct VUV photon radiation and LEEs released from the Si substrate. The DNA sequence 5'-d(T_{12}) has the highest cross section for SSBs with $\sigma = (6.9 \pm 1.6) \cdot 10^{-16}$ cm². This is followed by the DNA sequence 5'-d(C_{12}) and DNA sequence 5'-d(A_{12}) with $\sigma = (4.2 \pm 0.7) \cdot 10^{-16}$ cm² and $\sigma = (3.6 \pm 0.7) \cdot 10^{-16}$ cm², respectively. The lowest cross section for SSBs has the DNA sequence 5'-d(G_{12}) with $\sigma = (2.8 \pm 0.4) \cdot 10^{-16}$ cm². The trend for the cross sections for SSBs can be summarized by $T_{12} > A_{12} > C_{12} > G_{12}$. It has to be mentioned that the presented SSB cross sections consider both, VUV and LEE induced SSBs, but are only calculated to the fluence of the VUV irradiation process.

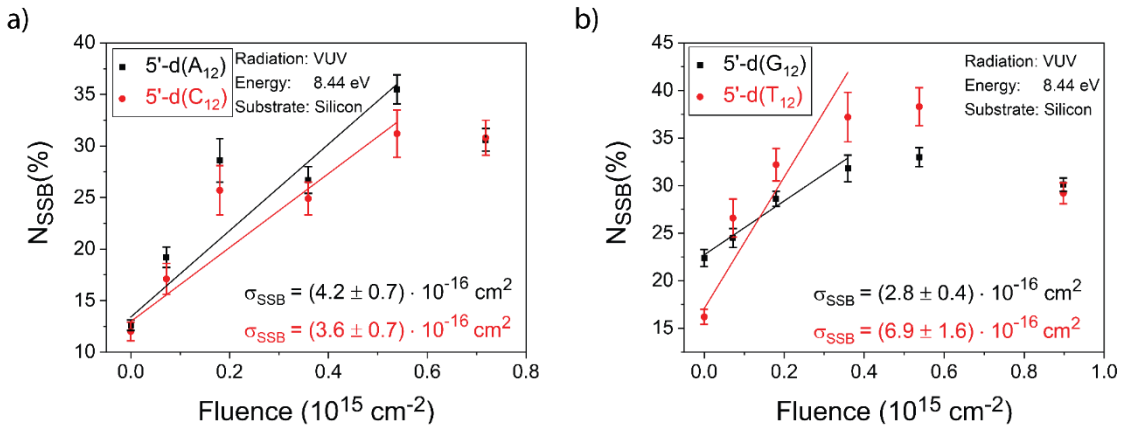

Fig. 25 Plot of the relative number of SSBs against the fluence of the VUV radiation at 8.44 eV to determine the cross sections for SSBs with a) the DNA sequences 5'-d(A_{12}) and 5'-d(C_{12}) and b) the DNA sequences 5'-d(G_{12}) and 5'-d(T_{12}), both irradiated on Si.

A direct comparison of the cross sections for SSBs of the four different target DNA sequences obtained on CaF_2 and Si is shown in figure 26a. The cross sections for SSBs obtained on Si are significantly higher than those obtained on CaF_2. This is attributed to the influence of secondary electrons released from the Si substrate. In figure 26b the differences between the cross sections obtained on CaF_2 and Si are displayed. This difference of the cross sections for SSBs can be considered as the contribution of secondarily generated LEEs from the Si surface. In figure 26b it can be seen that the DNA sequence 5'-d(G_{12}) is the least influenced by the secondary LEEs. The cross section for SSBs has barely increased. The DNA sequences 5'-d(C_{12}) and 5'-d(A_{12}) show more response to the additional indirect LEE radiation. Both cross sections for SSBs are increased by nearly the same amount. The DNA sequence 5'-d(T_{12}) clearly shows the highest response to the secondarily generated LEEs. The trend of the cross sections for SSBs due to secondary LEEs determined on Si can be summarized as follows

$T_{12} > A_{12} \geq C_{12} > G_{12}$. Since the fluence of the indirect LEE radiation is unknown, the given cross sections do not represent absolute values.

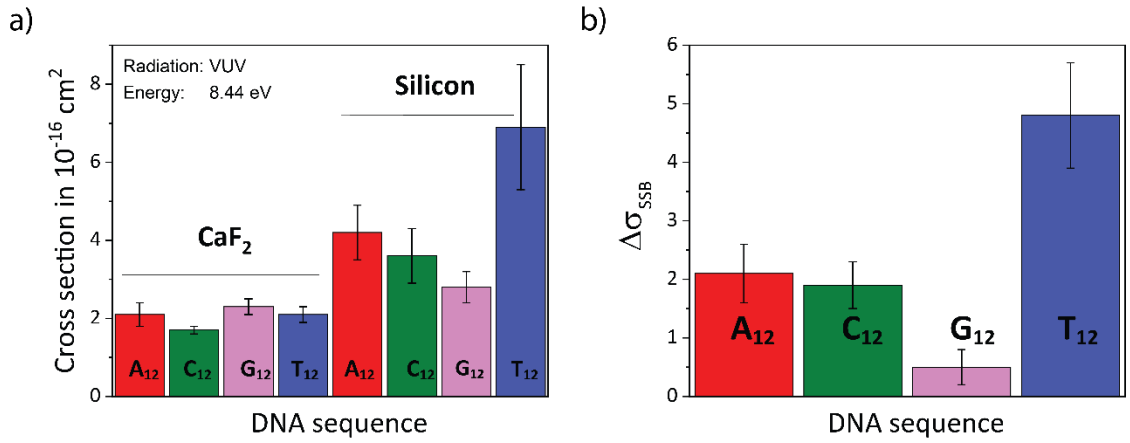

Fig. 26 a) Comparison of cross sections for SSBs for the different DNA sequences irradiated with 8.44 eV VUV irradiation on different substrates, b) comparison of the differences in cross section for SSBs of the DNA sequences irradiated on the two different substrates (subtraction of the cross section for SSBs obtained on Si by the cross section for SSBs obtained on CaF_2).

Several research groups investigated anionic resonances induced by LEEs and cross sections for SSBs from different DNA systems. It was demonstrated by Martin *et al.* [108], Panajotovic *et al.* [115] and Schürmann *et al.* [116] that anionic resonances occur in the experimentally applied electron energy region, where SSBs can be induced very effectively (i.e. below 12 eV). Anionic resonances were determined in electron impact experiments with DNA in the condensed phase at around 1 eV [115] and 2 eV [108,116], respectively. Martin *et al.* [108] and Panajotovic *et al.* [115] used plasmid DNA for their experiments that makes the comparability of the obtained SSB cross sections difficult, since the DNA system and the sample preparation conditions are very different. Schürmann *et al.* [116] in contrast used the intermixed target DNA sequences 5‘-d(TT(ATA)$_3$TT) incorporated in DNA origami nanostructures in electron impact experiments to determine cross sections for SSBs. As mentioned before, the exact fluence of the LEE radiation from the Si substrate in this work is unknown, so that a direct comparison of cross section values cannot be done either. The general trend of the DNA strand breakage in contrast can be compared with the results determined by Kenny Ebel (Vogel *et al.* [117]) , who exposed the same target DNA sequences to of 8.8 eV electron energy. The cross sections for SSBs follow the same trend ($T_{12} > A_{12} > C_{12} > G_{12}$) as observed at < 3.6 eV electron energy. The main process contributing to the strand break is DEA. At an electron energy of below 3.6 eV shape resonances and at 8.8 eV rather core-excited resonances are expected. This indicates that even if different anionic resonances mediate the strand break process, the sensitivity trend of the strand break with respect to the DNA sequence remains the same. At the electron irradiation energy of 8.8 eV also ionization events might play a role, since the energy exceeds the IEs of some

nucleobases. Thus, a release of an electron from the HOMO becomes possible. Another investigation of intermixed DNA sequences at an electron impact energy of 18 eV demonstrated also a similar sequence dependency [38]. The C and the G containing DNA sequences are showing almost the same cross section for SSBs, whereas the cross sections for SSBs of the A containing sequence is roughly doubled in comparison to the two other DNA sequences. At this irradiation energy the electron induced ionization plays already a major role and the DEA process becomes less pronounced, since less anionic resonances occur, which influences the cross sections for SSBs and therefore also the resulting nucleobase dependency. Since very similar trends of the sensitivity of the DNA sequences at three different LEE energies are observed, it can be assumed that the mechanisms behind the strand break formation could be quite similar as well. Maybe the ND is a more pronounced mechanism than considered in the current literature. ND is based on a short living electron attachment, where the scattered electron transfers energy into the molecule and promotes it into an excited state. The decay of the DNA molecule could in turn result in a dissociation reaction forming a scission in the DNA backbone, i.e. creating a SSB.

5.1.3 Influence of LEEs on the DNA origami nanostructure

As is described in detail above secondary electrons are generated from the substrate, when Si instead of CaF_2 is used as a substrate in the VUV irradiation experiments. These electrons are supposed to have an energy below 3.6 eV [145,152]. Electrons of this low energy have the ability to attach to the DNA and to induce the DEA process very effectively [108,116]. Not only the target DNA sequence suffered from the indirect LEE radiation, the DNA origami nanostructures themselves show a strong response as well. In figure 27 the structural changes of the DNA origami nanostructure are displayed. With the increasing VUV radiation and the increasing amount of secondarily generated electrons, the triangular structure gets more and more distorted. Often the bonds between the single trapezoids breaks first, since only three staple strands bind them together. This behavior of the DNA origami nanostructures is not observed with VUV irradiation on CaF_2 as a substrate. This clearly indicates the high ability of the LEEs with an energy below 3.6 eV to induce DNA damage and especially strand breakage in the DNA.

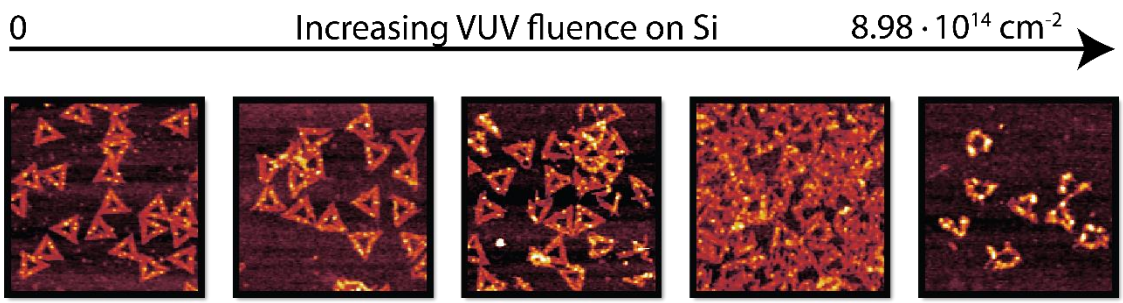

Fig. 27 The structural damage of the DNA origami nanostructures with target DNA sequences at increasing VUV fluence on Si as a substrate material.

5.1.4 Summary of the dependency VUV and LEE induced DNA strand breaks

To sum up, cross sections for SSBs for various target DNA sequences (5'-d(X_{12}), X = A, C, G and T) are presented. These DNA sequences were irradiated with VUV photons at 8.44 eV on CaF_2 and Si as substrate materials. The cross sections for SSBs determined on CaF_2 demonstrate that SSBs are induced, but indicate no significant dependency on the type of the nucleobase at this irradiation energy. These results are in a good agreement with previous work on intermixed DNA sequence using the same experimental conditions [25], since they show very similar values for the cross sections for SSBs. The DNA sequences irradiated on Si as a substrate experienced an additional indirect LEE radiation with an energy below 3.6 eV from the substrate surface. The cross sections for SSBs obtained on Si are higher than on CaF_2 and show a significant trend with respect to the type of nucleobase used ($T_{12} > A_{12} > C_{12} > G_{12}$). Anionic resonance, which depend on the type of nucleobase, occur in this low electron energy regime and lead effectively to DEA in the DNA molecule. The same trend is also observed in LEE irradiation experiments performed by Kenny Ebel (Vogel *et al.* [117]) at 8.8 eV and at 18 eV from Keller *et al.* [38]. In the latter case an additional contribution from electron induced ionization reaction must be considered as well.

5.2 VUV induced SSBs in DNA sequences of various lengths

In this section five DNA sequences differing only in the strand length were investigated with respect to their sensitivity towards 8.44 eV VUV photon radiation. All DNA sequences contain only A as a nucleobase and have a length of 4, 8, 12, 16 and 20 nucleotides. It was expected that the cross sections for SSBs would increase with the geometrical cross section of the DNA sequences, since a higher geometrical cross section could increase the probability of absorbing a photon. In figure 28a and b the number of SSBs is correlated to the fluence of the irradiation process and the cross sections for SSBs for the different DNA sequences are determined. The corresponding graph for the DNA sequence 5'-d(A_{12}) is displayed in figure 24 in section 5.1.1. A direct comparison of the cross sections for SSBs with the geometrical cross section in dependency of the DNA sequence length is given in figure 28c.

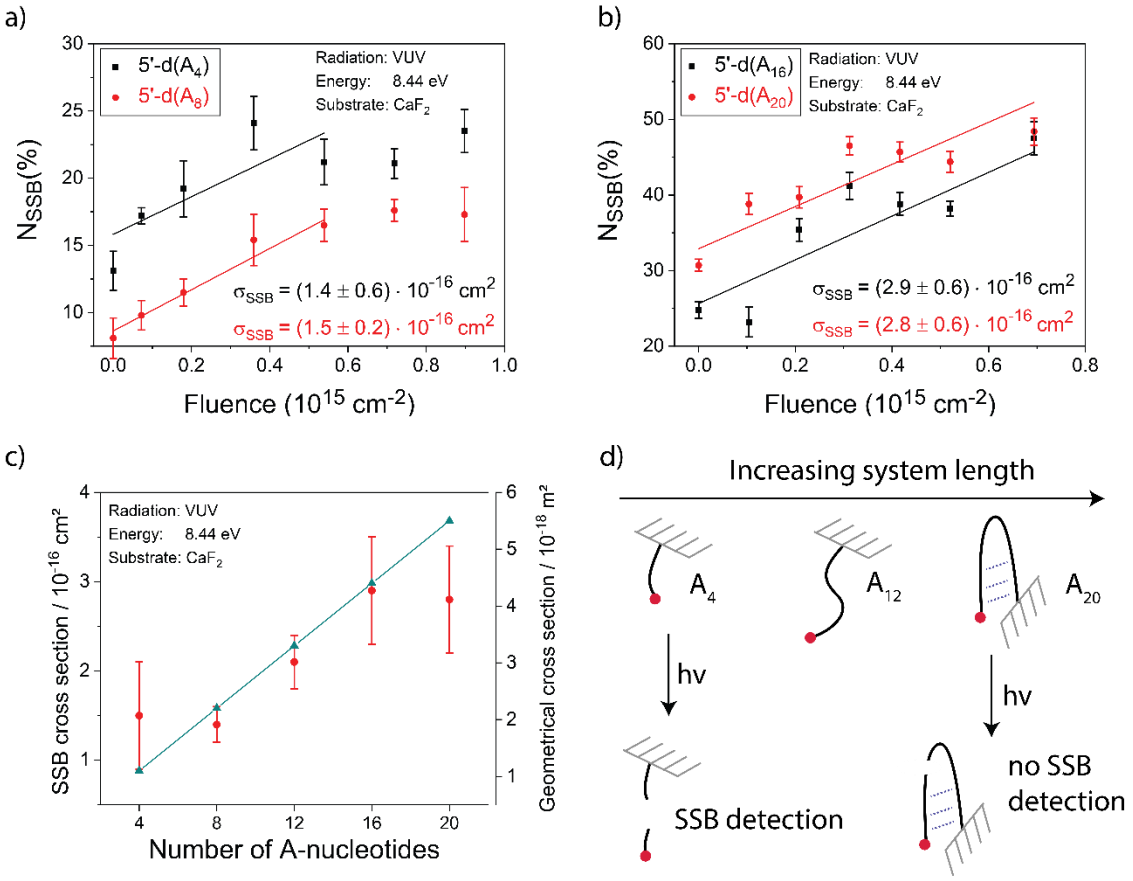

Fig. 28 Plot of the relative number of SSBs against the fluence of the VUV radiation at 8.44 eV to determine the cross sections for SSBs with a) the DNA sequences 5'-d(A_4) and 5'-d(A_8) and, b) DNA sequences 5'-d(A_{16}) and 5'-d(A_{20}), both irradiated on CaF_2; c) cross sections for SSBs (red) and the estimated geometrical cross section (turquoise) for the DNA sequences 5'-d(A_n) n = 4, 8, 12, 16, 20 plotted against the number of nucleotides, d) scheme of the conformational change of a DNA strand with increasing length and SSB formation. DNA origami platform is depicted as a pattern in grey, the biotin label a spot in red and the hydrogen bonding as a dotted line in blue.

The DNA sequences 5'-d(A_4) and 5'-d(A_8) have nearly the same cross section for SSBs with $\sigma = (1.4 \pm 0.6) \cdot 10^{-16}$ cm² and $\sigma = (1.5 \pm 0.2) \cdot 10^{-16}$ cm², respectively. They differ only within their error bars. The expected increase of the cross section for SSBs cannot be observed, whereas the standard error for the DNA sequence 5'-d(A_4) is too high to make a clear statement. When the DNA sequences 5'-d(A_8), 5'-d(A_{12}) and 5'-d(A_{16}) are compared, the cross sections for SSBs of the DNA sequence 5'-d(A_8) increased to $\sigma = (2.3 \pm 0.2) \cdot 10^{-16}$ cm² and 5'-d(A_{12}) even further to $\sigma = (2.9 \pm 0.6) \cdot 10^{-16}$ cm². The cross section for SSBs increases almost linearly within this DNA strand length regime. In figure 28c a direct comparison of the SSB cross section to the geometrical cross section is given, which was estimated with the assumption of a linear shape of the DNA sequence. The slope of the increasing geometrical cross section and the slope of the cross section for SSBs are in good agreement. This confirms the assumption that a higher geometrical cross section exposed to the radiation increases the probability of the SSB formation.

Comparing the DNA sequences 5'-d(A_{16}) and 5'-d(A_{20}), the cross section for SSBs rather decreases slightly from $\sigma = (2.9 \pm 0.6) \cdot 10^{-16}$ cm² to $\sigma = (2.8 \pm 0.6) \cdot 10^{-16}$ cm². In this case the SSB cross section does not follow the geometrical cross section any more. This change in behavior might be due to conformational changes in the DNA. If the DNA sequence reaches a certain length, the coulomb repulsion of the DNA backbone might not be enough anymore to establish a linear structure. The DNA strand will start to coil and might also create hydrogen bonds within the DNA sequence, which would increase the stability of the ssDNA strand. If enough additional hydrogen bonds would be formed, the first SSB in the DNA sequence might not be detected, since the cleaved part of the DNA sequence would stay attached and with it the biotin label. The biotin label would bind the protein streptavidin in the sample preparation procedure and be detected as an intact DNA strand *via* AFM imaging. Consequently, the cross section for SSBs would decrease. This procedure is schematically displayed in figure 28d.

In conclusion, several DNA sequences only varying in their length were investigated with respect to their sensitivity towards 8.44 eV photon radiation. For the length of 8, 12 and 16 nucleotides a clear correlation with the geometrical cross section was observed. The increasing surface area, increases the cross section for SSBs in nearly the same way, when a linear shape of the DNA sequence was assumed. At a length of 20 nucleotide a slight decrease of the cross section can be seen. This might occur due to conformational changes in the DNA leading to a higher stability of the DNA sequence and resulting in a decreased detection ability of the SSBs. The cross sections for SSBs of the different DNA sequences are summarized along with the geometrical cross section in the table below.

Tab. 13 Overview of the cross sections for SSBs of the different DNA sequences adsorbed on CaF_2 of thin film VUV photon impact experiments.

DNA sequence	Cross section for SSBs in 10^{-16} cm²	Geometrical cross section in 10^{-18} m²	Substrate	Radiation
5'-d(A_4)	(1.4 ± 0.6)	2.2	CaF_2	VUV
5'-d(A_8)	(1.5 ± 0.2)	4.4	CaF_2	VUV
5'-d(A_{12})	(2.3 ± 0.2)	6.6	CaF_2	VUV
5'-d(A_{16})	(2.9 ± 0.6)	8.8	CaF_2	VUV
5'-d(A_{20})	(2.8 ± 0.6)	11	CaF_2	VUV

5.3 VUV induced SSBs in DNA sequences modified with ^{5Br}U

In this section the influence of the radiosensitizer ^{5Br}U on the cross sections for SSBs induced by 8.44 eV VUV photon radiation is investigated. Three different DNA sequences containing ^{5Br}U were chosen to study whether the flanking nucleobases have an effect on the reactivity of the radiosensitizer. C, G and T as flanking nucleobases (X) in the DNA sequence 5'-d(TT(X^{5Br}UX)$_3$TT) were tested. In figure 29a the number of SSBs for the three DNA sequences is plotted versus the fluence of the irradiation process. The cross sections for SSBs for the different DNA sequences are also determined. In figure 29b the molecular structure of a DNA nucleotide, where a nucleobase is substituted by the radiosensitizer ^{5Br}U, is displayed. A direct comparison of the cross sections for SSBs to those determined for non-modified DNA sequences is given in the end of this section (fig.30).

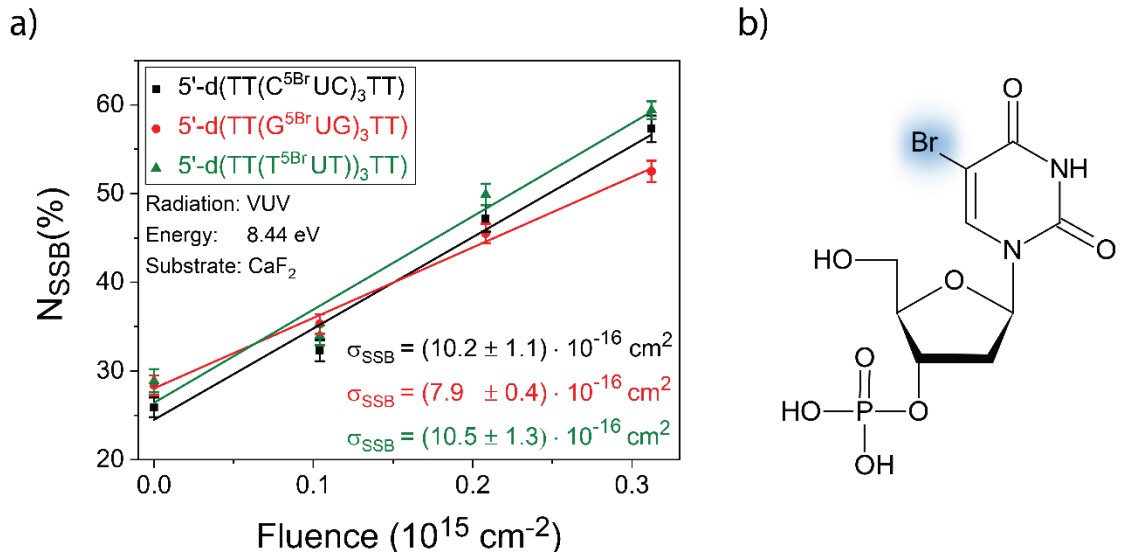

Fig. 29 a) Plot of the relative number of SSBs against the fluence of the VUV radiation at 8.44 eV to determine the cross sections for SSBs for the DNA sequences 5'-d(TT(C^{5Br}UC)$_3$TT), 5'-d(TT(G^{5Br}UG)$_3$TT) and 5'-d(TT(T^{5Br}UT)$_3$TT), all irradiated on CaF$_2$; b) molecular structure of a nucleotide labelled with ^{5Br}U.

Comparing the cross sections for SSBs of the ^{5Br}U modified DNA sequences among each other, it can be seen that the DNA sequences 5'-d(TT(C^{5Br}UC)$_3$TT) and 5'-d(TT(T^{5Br}UT)$_3$TT) show the highest response to the VUV radiation with cross sections for SSBs of $\sigma = (10.2 \pm 1.1) \cdot 10^{-16}$ cm² and $\sigma = (10.5 \pm 1.3) \cdot 10^{-16}$ cm², respectively. The DNA sequence 5'-d(TT(G^{5Br}UG)$_3$TT) shows a significantly lower cross section for SSBs with $\sigma = (7.9 \pm 0.4) \cdot 10^{-16}$ cm². Still, all DNA sequences show a clear enhancement of the SSB formation in comparison to the results presented so far.

In chapter 3.8 two different mechanisms of the strand break formation in DNA caused by UV radiation in the photosensitizer ^{5Br}U incorporated in a DNA sequence were introduced. In the first mechanism the uracil-5-yl radical is formed upon photolysis and of the C-Br bond cleavage after the excitation of the ^{5Br}U molecule [130]. In the second

mechanism an initial electron transfer occurs from a nucleobase at the 5' side to ^{5Br}U resulting in a radical ion pair [131]. A bromine abstraction releases then the uracil-5-yl radical to react further [127–129]. Watanabe *et al.* [73] observed that this preliminary electron transfer can be induced by G nucleobases that are separated by one up to several A spacers from the ^{5Br}U molecule. However, the formed uracil-5-yl radical reacts further *via* an H abstraction from the adjacent nucleobase. This nucleobase is cleaved from the DNA sequence to form a lactone at the remained sugar unit, which in turn decomposes thermally leading eventually to a strand break in the DNA sequence.

This raises the question, whether ^{5Br}U is initially activated by a preliminary electron transfer or a direct photolysis at the applied irradiation energy of 8.44 eV. The results of the present work demonstrate that the SSB cross sections obtained with ^{5Br}U are sequence dependent. The lowest SSB cross section was determined for 5'-d(TT(G^{5Br}UG)$_3$TT), where the radiosensitizer is flanked by G nucleobases. A preliminary charge transfer was observed by Watanabe *et al.* [73], if G was separated from ^{5Br}U by at least one A spacer at the 5' side. With G adjacent to ^{5Br}U almost no strand breakage was observed. This was justified with a high electron back transfer rate [73,153] and could also explain the lower SSB cross section obtained in the present work for the G containing DNA sequence. Additionally, in the DNA sequence used in the present work two G nucleobases are positioned next to each other, which is known to further decrease their IE [119] and to function this way as an even better electron trap such as observed for telomere DNA sequences containing a GGG stack [23,119]. Still, the mechanisms of strand break formation over a lactone formation was only observed by Watanabe *et al.* [73], when ^{5Br}U was adjacent to an A at the 5' side. This is not the case for the DNA sequences applied in the present work. But still a strong enhancement of the strand breakage is observed. This indicates that the photolysis of ^{5Br}U would rather initiate the strand breakage. The strand break mechanism that might occur, could be similar to the one reported by Rak *et al.* [35] and Wang *et al.* [137] for initial electron attachment followed by uracil-5-yl radical formation. The uracil-5-yl radical, which is in the present work rather formed through photolysis, might also capture a proton from the neighboring sugar unit (C_2-position), which would lead to a radical formation at this sugar unit resulting in glycosidic bond cleavage in the DNA backbone, i.e. in a SSB. The differences in SSB cross section could also occur through the GG-stack acting as an electron trap, since Kobyłecka *et al.* [130] demonstrated that a radical ion pair is formed before the homolytic cleavage occurs, which might decrease the uracil-5-yl radical formation.

Another mechanism that might occur under ionizing radiation is the ejection of an electron from the nucleobases and a subsequent electron attachment. The formation of the TNI would result in a uracil-5-yl radical at the nucleobase that then reacts further to form a SSB [35,137]. This process is rather unlikely to contribute significantly to the observed SSB cross sections, since the irradiation energy used here is just around the IE of the DNA sequence, at which only a small number of ionizations occur [154]. Moreover, it was

demonstrated by Keller *et al.* [118] that only a small enhancement of the cross sections for SSBs can be obtained with 18 eV electrons.

To illustrate the SSB enhancement of the brominated DNA sequences in comparison to the non-modified DNA sequences upon 8.44 eV photon radiation, an EF value can be calculated. For this, the SSB cross section of the modified DNA sequences was divided by the SSB cross section of the non-modified DNA sequences (eq. 17).

$$(17) \quad EF = \frac{\sigma_{SSB}\,(modified\ DNA\ sequence)}{\sigma_{SSB}\,(non\text{-}modified\ DNA\ sequence)}$$

For comparison, the non-modified DNA sequences 5'-d(X_{12}) wit X = A, C, G, T displayed in section 5.1.1 were chosen and related to the modified DNA sequences 5'-d(TT($X^{5BrU}X$)$_3$TT) with X = C, G, T. The strongest enhancement is observed for the DNA sequence 5'-d(TT($C^{5BrU}C$)$_3$TT) in comparison to the DNA sequence 5'-d(C_{12}) with an EF of 6.0. The DNA sequence 5'-d(TT($T^{5BrU}T$)$_3$TT) shows a little less enhancement with an EF of 5.0 in comparison to the non-modified DNA sequence 5'-d(T_{12}). The DNA sequence 5'-d(TT($G^{5BrU}G$)$_3$TT) shows the lowest enhancement of the cross section for SSBs with an EF of 3.4 in comparison to the DNA sequence 5'-d(G_{12}). The EF trend can be summarized as $C^{5BrU}C > T^{5BrU}T > G^{5BrU}G$. In figure 30 the cross sections for SSBs of modified and non-modified sequences are compared and displayed with their corresponding EFs.

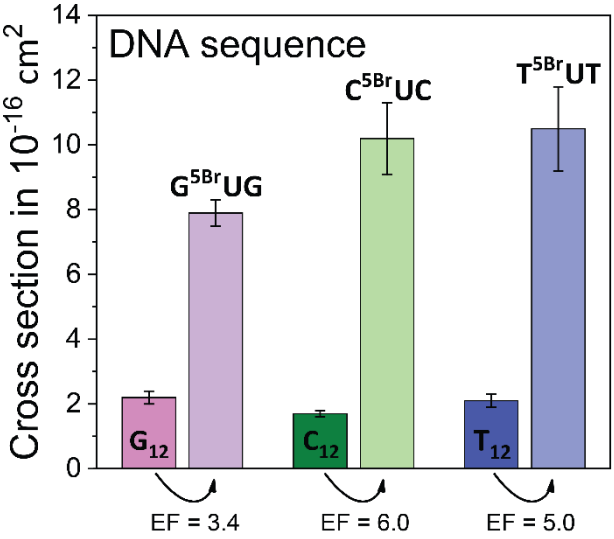

Fig. 30 Comparison of cross sections for SSBs of the modified and non-modified DNA sequences and determination of the corresponding EFs; all DNA sequences were irradiated on CaF_2 with 8.44 eV VUV photon radiation.

In summary, the strand break formation in the DNA sequences modified with the radiosensitizer ^{5BrU}U is induced very effectively by VUV radiation. The most likely mechanisms for the strand break process is a homolytic cleavage of the C-Br bond that results in a highly reactive uracil-5-yl radical to react further. Still, a sequence dependence is clearly visible leading to an EF trend of $C^{5BrU}C > T^{5BrU}T > G^{5BrU}G$. Since a radical

ion pair is formed after UV excitation but before the C-Br bond is cleaved [130], the GG-stack in the 5'-d(TT($G^{5BrU}G)_3$TT) sequence might act as electron trap due to its low IE [119]. This way, the SSB cross section could be decreased. The cross sections for SSBs of the six different DNA sequences are summarized again the table below.

Tab. 14 Overview of the cross sections for SSBs for the different non-modified and brominated DNA sequences upon VUV irradiation.

DNA sequence	Cross section for SSBs in 10^{-16} cm²	Substrate	Radiation
5'-d(G_{12})	(2.3 ± 0.2)	CaF_2	VUV
5'-d(TT($G^{5BrU}G)_3$TT)	(7.9 ± 0.4)	CaF_2	VUV
5'-d(C_{12})	(1.7 ± 0.1)	CaF_2	VUV
5'-d(TT($C^{5BrU}C)_3$TT)	(10.2 ± 1.1)	CaF_2	VUV
5'-d(T_{12})	(2.1 ± 0.2)	CaF_2	VUV
5'-d(TT($T^{5BrU}T)_3$TT)	(10.5 ± 1.3)	CaF_2	VUV

5.4 Activation of ^{5BrU} in dependency of the distance to G

In this section six different DNA sequence containing the radiosensitizer ^{5BrU} were investigated with respect to their cross section for SSBs induced by 8.44 eV VUV photon radiation. In the DNA sequence 5'-d(TTG$A_n{}^{5BrU}$TT) the number of A spacers (n) was varied between 0 and 5. Here, the radiosensitizer ^{5BrU} was flanked by the nucleobase A, so that the mechanism proposed by Watanabe *et al.* [73] might occur. Accordingly, an initial electron transfer from the G nucleobase to ^{5BrU} occurs under photon absorption to form a uracil-5-yl radical, which reacts further under abstraction of an adenine nucleobase to form a lactone. The lactone in turn is thermally not stable [132] and reacts further resulting in a strand break. Watanabe *et al.* [73] investigated the same DNA sequences in dsDNA instead of ssDNA as in the present work. The highest strand break yield occurred for n = 2 and 3. For a higher or lower number of A, a decreasing strand break yield was observed. No strand break yield was reported, when G was placed right next to ^{5BrU}. A similar behavior was expected for the DNA sequences investigated in the present work, since the irradiation energy used by Watanabe *et al.* [73] (302 nm/4.1 eV photon irradiation) was only slightly lower than the photon energy applied here. In figure 31a-c the number of SSBs is correlated to the fluence of the irradiation process and the cross sections for SSBs determined from the slope of the graph. In figure 31d all cross sections for SSBs are compared in dependency of the distance between the nucleobase G and the radiosensitizer ^{5BrU}, i.e. the number of A spacers.

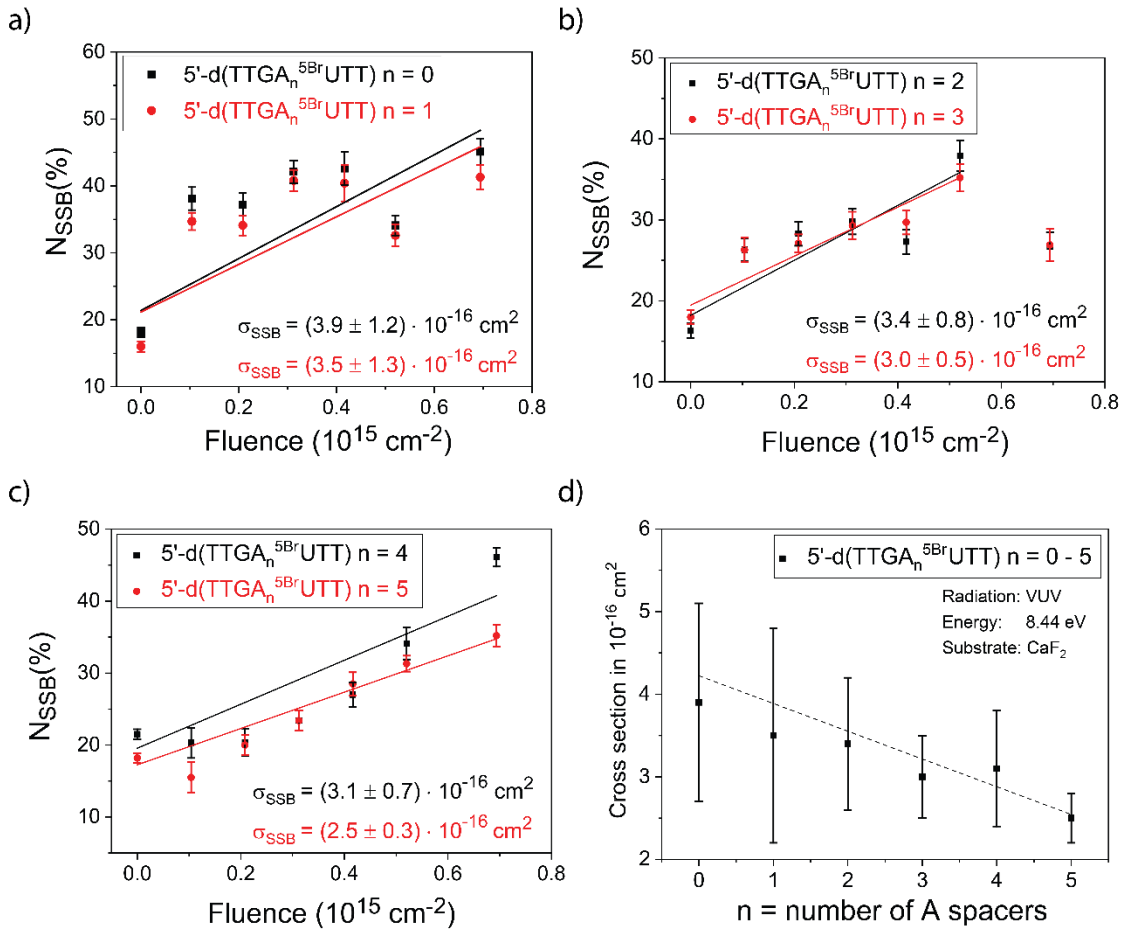

Fig. 31 Plot of the relative number of SSBs against the fluence of the VUV radiation at 8.44 eV to determine the cross sections for SSBs with the DNA sequences 5'-d(TTGA$_n$^{5Br}UTT) with a) n = 0, 1 b) n = 2, 3 and c) n = 4, 5, all irradiated on CaF$_2$; d) comparison of cross sections for SSBs of the six DNA sequences in dependency of the nucleotides containing A as a nucleobase serving as a spacer between the G as an e$^-$ donor and ^{5Br}U as an e$^-$ acceptor, dotted line is showing the trend.

Comparing the cross sections for SSBs for various distances between the radiosensitizer ^{5Br}U and the nucleobase G a clear decreasing trend is illustrated by the blue dotted line in figure 31d. For the DNA sequences 5'-d(TTGA$_n$^{5Br}UTT) with n = 0 and 1 the highest cross sections for SSBs are observed with $\sigma = (3.9 \pm 1.2) \cdot 10^{-16}$ cm² and $\sigma = (3.5 \pm 1.3) \cdot 10^{-16}$ cm². Reaching the maximum distance with the A spacer of n = 5 the cross section for SSBs is already reduced to a value of $\sigma = (2.5 \pm 0.3) \cdot 10^{-16}$ cm², which is almost on the level of SSB cross sections for non-modified DNA sequences, but irradiated under the same experimental conditions (section 5.1). In comparison to the investigations of Watanabe *et al.* [73], who found no strand breakage for n = 0 and a low amount for n = 1, a clear strand break formation is observed in the present work. The lack of strand breaks was reasoned with a very fast electron back transfer, even faster than radical formation at the ^{5Br}U radiosensitizer [153]. A reason for that could be that Watanabe *et al.* [73] used dsDNA for their experiments, which provides higher conformational stability and thus more efficient charge transfer in a dry state than the ssDNA used here.

On the other hand a higher photon energy is used in the present work, which could be efficient enough to induce direct excitation in ^{5Br}U, which is accompanied with a homolytic C-Br bond cleavage [130].

In total three mechanisms to create a strand break in a ssDNA sequence are identified in the present work. In non-modified DNA sequences SSBs are initialized *via* photoexcitation resulting in a neutral dissociation. Furthermore, ionization reactions can occur, when the IE of the DNA sequence is exceeded. Accordingly, a positive charge will be induced most likely at a nucleobase. An electron could then migrate from the DNA backbone to the nucleobase, releasing a positive charge in the DNA backbone, which can result in the cleavage of the C-O bond between the sugar and phosphate unit, i.e. in a SSB. Most probably both (photoexcitation and photoionization) occur, but contribute in a different extend to the strand breakage. In the brominated DNA sequences higher cross sections for SSBs are observed, which indicate that further SSB mechanisms exist. Two mechanisms were identified, which contribute to the SSBs, but have a different effectivity to induce SSBs. In the DNA sequences 5'-d(TT($X^{5Br}UX)_3$TT) X = C, G, T the strand break process is probably induced by a direct excitation of ^{5Br}U resulting in the photolysis of the C-Br bond and a subsequent uracil-5-yl radical formation. The uracil-5-yl radical can react further by an H abstraction from the adjacent sugar unit at the 5' side to form a sugar radical. This can in turn react further to form an SSB as described by Rak *et al.* [35] and Wang *et al.* [137] for electron induced SSBs in ^{5Br}U containing DNA sequences (section 3.6). In the DNA sequences 5'-d(TTG$A_n{}^{5Br}$UTT), n = 0 - 5 the SSB is assumed to occur *via* an excitation of the G nucleobase followed by a charge transfer to ^{5Br}U as described in the beginning of this section [73]. To estimate now the different contributions of the two strand break mechanisms in the brominated DNA sequences, which are discussed above (charge transfer vs. direct photolysis) for the applied photon energy of 8.44 eV, different SSB cross section for the DNA sequences are compared in the following. First, the DNA sequence 5'-d(TTG$A_n{}^{5Br}$UTT), n = 5 ($\sigma = (2.5 \pm 0.3) \cdot 10^{-16}$ cm²) is compared to the non-brominated DNA sequence 5'-d(A_{12}) ($\sigma = (2.1 \pm 0.3) \cdot 10^{-16}$ cm²). Since both SSB cross sections are nearly the same and differ only within their error bars, it seems that neither a photolysis of the ^{5Br}U molecule nor a charge transfer reaction from the G nucleobase to ^{5Br}U take place, which could initialize the uracil-5-yl radical formation to react further to a SSB. Instead, only strand breakage initialized by photoexcitation and -ionization of the non-modified nucleobases seem to occur. A high number of A nucleobases being placed at the 5' side to ^{5Br}U seem to block the C-Br photolysis deactivation pathway and decrease the charge transfer probability from G to ^{5Br}U. This phenomenon is apparently highly sequence dependent, since the SSB cross sections of the DNA sequences 5'-d(TTG$A_n{}^{5Br}$UTT) increase with the decrease of the number of A spacers (n = 1 - 5) to a SSB cross section of $\sigma = (3.5 \pm 1.3) \cdot 10^{-16}$ cm² for n = 1. If the photolysis deactivation pathway is really blocked for n = 5, it could also be the case for n = 1, which indicates that only the charge transfer mechanism from G to ^{5Br}U is responsible for the SSB induced by ^{5Br}U. If the photolysis of C-Br is not blocked, this mechanism would mainly contribute to the strand breakage as observed for the DNA sequence 5'-d(TT($T^{5Br}UT)_3$TT) with

$\sigma = (10.5 \pm 1.3) \cdot 10^{-16}$ cm². Here, it was already demonstrated that the high SSB cross section can only be caused by photolysis, since the IE of T is even higher than the IE of ^{5Br}U and this way, no charge transfer from T to ^{5Br}U can occur. This is rather not the case for 5'-d(TTGA$_n$^{5Br}UTT) with n = 1, since a strong sequence distance dependency of G to ^{5Br}U for the strand breakage is observed. If no A spacer between G at the 5' side of ^{5Br}U in the DNA sequence 5'-d(TTGA$_n$^{5Br}UTT) with n = 0 is placed, the SSB cross section is almost equally high as the one obtained for 5'-d(TT(T^{5Br}UT)$_3$TT), considering the higher number of ^{5Br}U molecule in 5'-d(TT(T^{5Br}UT)$_3$TT), which indicates that mainly the photolysis of C-Br is active and responsible for the SSBs. In conclusion, the crucial nucleobase determining, whether a photolysis of C-Br or an initial charge transfer lead to the formation of the uracil-5-yl radical, seem to be A at the 5'side of ^{5Br}U. If the A is positioned there, no direct C-Br occurs and with an increasing number of A the charge transfer as an initial step to form uracil-5-yl radical gets blocked as well, which fully deactivates the function of ^{5Br}U as a radiosensitizer.

In summary, a study of a set of DNA sequences 5'-d(TTGA$_n$^{5Br}UTT) with n = 0 - 5 containing ^{5Br}U as a radiosensitizer was presented. The cross section for SSBs was determined in dependency of the distance of ^{5Br}U to the electron donor G (tab.15) and compared to the SSB cross sections obtained for the DNA sequences 5'-d(TT(X^{5Br}UX)$_3$TT) X = C, G, T. The highest strand break formation was found for G flanking ^{5Br}U. The mechanism for the DNA strand breakage might be similar to those obtained for the DNA sequences 5'-d(TT(X^{5Br}UX)$_3$TT) X = C, G, T, which are probably induced by a direct excitation of ^{5Br}U and a subsequent homolytic cleavage of the C-Br bond. The further reaction to form an SSB might be an H abstraction of the sugar unit at the 5' side, which results in the formation of a new radical that reacts further to form an SSB [35,137]. On the other hand, the SSB cross sections for 5'-d(TTGA$_n$^{5Br}UTT) with n = 1 - 5 are decreasing almost linearly with the increasing number of A spacers. Since the strand breakage is clearly distance dependent, the SSB mechanism, which is initialized by a charge transfer [73] might be the dominating one here. At n = 5 both mechanisms seem to be deactivated, since the SSB cross section is nearly the same as those of the non-modified DNA sequences.

Tab. 15 Overview of the cross sections for SSBs for the different DNA sequences modified with ^{5Br}U upon VUV irradiation.

DNA sequence	**Cross section for SSBs in 10^{-16} cm²**	**Substrate**	**Radiation**
5'-d(TTG^{5Br}UTT)	(3.9 ± 1.2)	CaF_2	VUV
5'-d(TTGA^{5Br}UTT)	(3.5 ± 1.3)	CaF_2	VUV
5'-d(TTGAA^{5Br}UTT)	(3.4 ± 0.8)	CaF_2	VUV
5'-d(TTGAAA^{5Br}UTT)	(3.0 ± 0.5)	CaF_2	VUV
5'-d(TTGAAAA^{5Br}UTT)	(3.1 ± 0.7)	CaF_2	VUV
5'-d(TTGAAAAA^{5Br}UTT)	(2.5 ± 0.3)	CaF_2	VUV

5.5 VUV induced SSBs in DNA sequences modified with ^{8Br}A

In this section the influence of the radiosensitizer ^{8Br}A on the cross sections for SSBs induced by VUV photon radiation is investigated. Two structurally identical DNA sequences 5'-d(TT(XTA)$_3$TT) with X = A or ^{8Br}A were investigated. This way, the effect of the reactivity of the radiosensitizer can be observed in direct comparison to a non-modified DNA sequence. Moreover, the two DNA sequences were irradiated on CaF_2 and Si as substrate material to study the influence of the 8.44 eV VUV photons and the indirect LEE irradiation (< 3.6 eV) on the SSB formation. In figure 32a and b the number of SSBs of the two DNA sequences on CaF_2 and Si is plotted against the fluence of the irradiation process. The cross sections for SSBs for the different DNA sequences are also determined and a direct comparison is illustrated in figure 32c. Additionally, the molecular structure of a DNA nucleotide, where the normal nucleobase is substituted by the radiosensitizer ^{8Br}A, is shown.

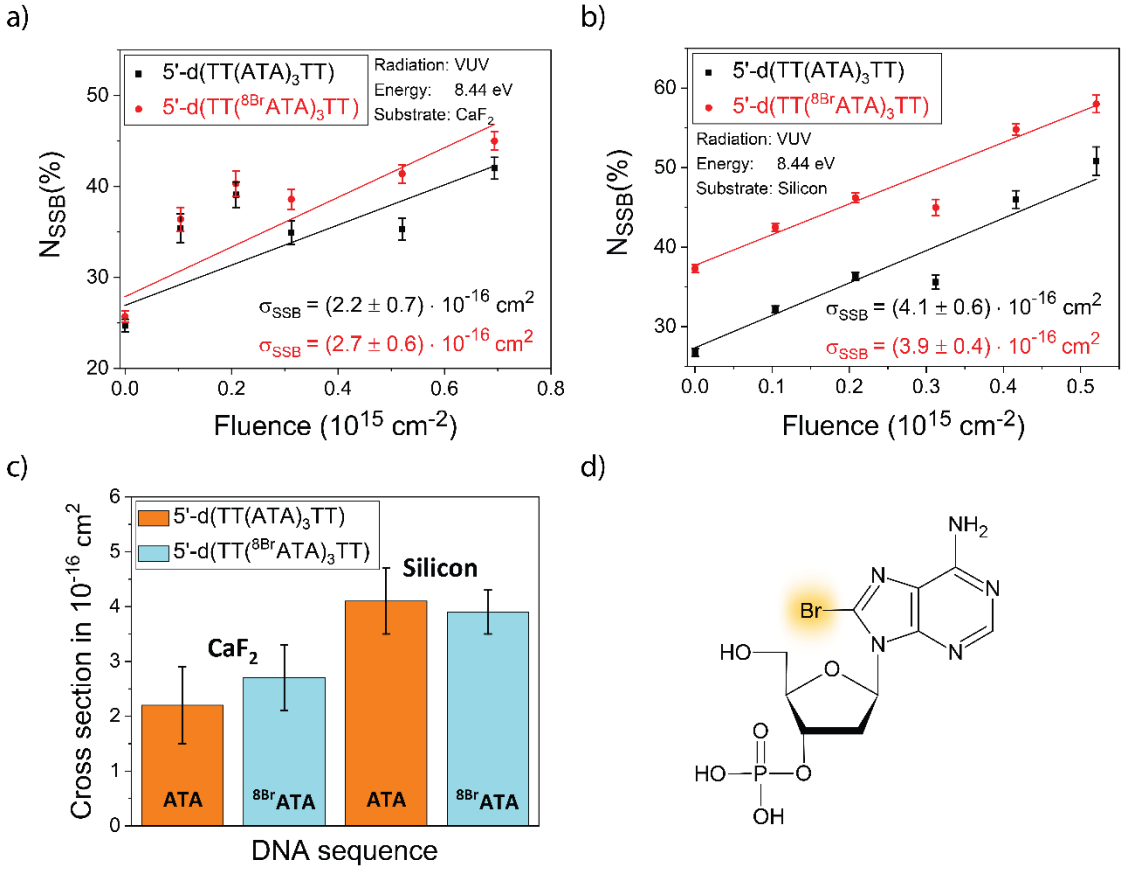

Fig. 32 Plot of the relative number of SSBs against the fluence of the VUV radiation at 8.44 eV to determine the cross sections for SSBs with a) the DNA sequences 5'-d(TT(ATA)$_3$TT) and 5'-d(TT(^{8Br}ATA)$_3$TT) irradiated a) on CaF_2 and b) on Si; c) comparison of cross sections for SSBs of the two DNA sequences on the two different substrates; d) molecular structure of a nucleotide labelled with ^{8Br}A.

Comparing the cross sections for SSBs obtained on CaF_2 as a substrate, it can be seen that the DNA sequence containing the radiosensitizer ^{8Br}A shows a higher value than the non-modified DNA sequence with $\sigma = (2.7 \pm 0.6) \cdot 10^{-16}$ cm² and $\sigma = (2.2 \pm 0.7) \cdot 10^{-16}$ cm²,

respectively. Since both cross sections for SSBs are only differing within their standard errors, no clear enhancement of the photon induced SSB formation can be claimed. Comparing the cross sections for SSBs obtained on CaF_2 to those obtained on Si as a substrate, it can be seen that both, the modified and the non-modified DNA sequence show nearly the same cross sections for SSBs with $\sigma = (3.9 \pm 0.4) \cdot 10^{-16}$ cm² and $\sigma = (4.1 \pm 0.6) \cdot 10^{-16}$ cm², respectively. The additional indirect LEE irradiation from the Si substrate surface resulted again in increased cross sections for SSBs. The contribution of strand breaks induced by secondary LEEs is in the same range as for the mono nucleobase DNA sequences described in chapter 5.1.2 and the trend of sequence sensitivity can be summarized as follows: $T_{12} > A_{12} \geq TT(ATA)_3TT \geq C_{12} > G_{12}$.

No enhancement of the cross section for SSB caused by the incorporated ^{8Br}A can be observed. Neither the 8.44 eV photon radiation nor the secondarily generated LEEs (< 3.6 eV) can activate the radiosensitizer within the experimental conditions used in the present work. So far, no other studies of the interaction of ^{8Br}A with UV or VUV light are known. Intuitively, it could be assumed that ^{8Br}A has similar properties as ^{5Br}U, since the bromine is attached to a nucleobase in both cases. With ^{5Br}U a homolytic C-Br bond cleavage occurs under UV excitation [73,128,130], which apparently does not occur for ^{8Br}A at this VUV irradiation energy. A few studies exist, which consider electron interactions with ^{8Br}A. Chomicz *et al.* [138] studied ^{8Br}A incorporated in 8-bromo-2'-deoxyadenosine-3',5'-diphosphate computationally and asserted two main reaction pathways that are occurring on electron impact (chapter 3.6). Only one of them leads to a SSB in a DNA strand and the other one stabilizes the molecule even more, since a cross link between the nucleobase and the backbone is formed. It was also observed that the formation of the adenyl radical *via* the DEA process rather occurs in water than in the gas phase. Since the DNA system used in the present work is in a dry state, and thus, closer to the system in the gas phase isolated from water molecules, it is not astonishing that ^{8Br}A doesn't show any activity through the secondarily generated electron. Still, Schürmann *et al.* [116] could find an increase of the cross section for SSBs upon electron impact below 4 eV for the same DNA sequences such as the ones displayed in this section. The EFs for the cross sections of SSBs for LEEs range from 2.3 for 0.5 eV to 1.3 for 2 eV up to 2.8 for 3 eV electron energy. However, it has also to be mentioned that in the low-energy regime applied by Schürmann *et al.* [116] the cross sections for SSBs, which were used for the EF determination differ only within their error bars.

In summary, the reactivity of the radiosensitizer ^{8Br}A towards 8.44 eV photon radiation and secondarily generated electrons with an energy of < 3.6 eV was investigated. The radiosensitizer was incorporated in an intermixed DNA sequence and experimentally investigated in direct comparison to a non-modified DNA sequence of the same nucleotide composition. It was observed that neither the VUV nor the LEEs in this energy range could activate the radiosensitizing properties of ^{8Br}A. Since computational investigations suggested ^{8Br}A being more active in an aqueous environment [138], this result was not too surprising. This is even feasible in the light of the investigation by

Schürmann *et al*. [116], who were also applying the DNA origami technique and could find an enhancement of the cross section for SSBs, but with high errors.

Tab. 16 Overview of the cross sections for SSBs of the different DNA sequences modified with ^{8Br}A irradiated on two different substrates of thin film VUV photon impact experiments.

DNA sequence	Cross section for SSBs in 10^{-16} cm²	Substrate	Radiation
5'-d(TT(ATA)$_3$TT)	(2.2 ± 0.7)	CaF_2	VUV
5'-d(TT(^{8Br}ATA)$_3$TT)	(2.7 ± 0.6)	CaF_2	VUV
5'-d(TT(ATA)$_3$TT)	(4.1 ± 0.6)	Si	VUV and indirect LEE
5'-d(TT(^{8Br}ATA)$_3$TT)	(3.9 ± 0.4)	Si	VUV and indirect LEE

5.6 Errors sources

Every cross section for SSBs is given here with a standard error value. This error value represents statistic and systematic errors arising from the experimental irradiation set up and artefacts arising from the data evaluation procedure. In the next two sections both are explained in detail.

5.6.1 The irradiation set up

The substrate with the adsorbed target DNA sequences incorporated in the DNA origami nanostructures is mounted in the sample holder of the irradiation set up as a vertical array. The irradiation of the sample is carried out through the circular opening of the sample holder in front of each sample. The VUV beam does not illuminate the sample completely, instead small areas at the top and at the bottom of the sample are not illuminated (fig.33). As long as the adjustment of the sample with the beam in one axis is performed correctly, the illuminated area is known and can be considered in the AFM imaging process. Unfortunately, the screw thread to fix the sample position in the y-axis distorted it a little, which could result in a slightly shifted sample position. Then, the illuminated area on the sample would shift to the top or the bottom and release a corresponding larger non-illuminated area, which is unknown and cannot be considered in the AFM imaging process. The influence of this error on the cross sections for SSBs cannot exactly be determined, since the shift is not known. It leads to a stronger variation of the number of SSBs and thus to a higher standard error in the cross sections for SSBs. One examples can be seen in the trend of number of SSBs correlated to the fluence of the irradiation process in figure 34b. One sample shows a lowered number of SSBs, which is most probably due to an up or down shift of the sample position in the VUV beam.

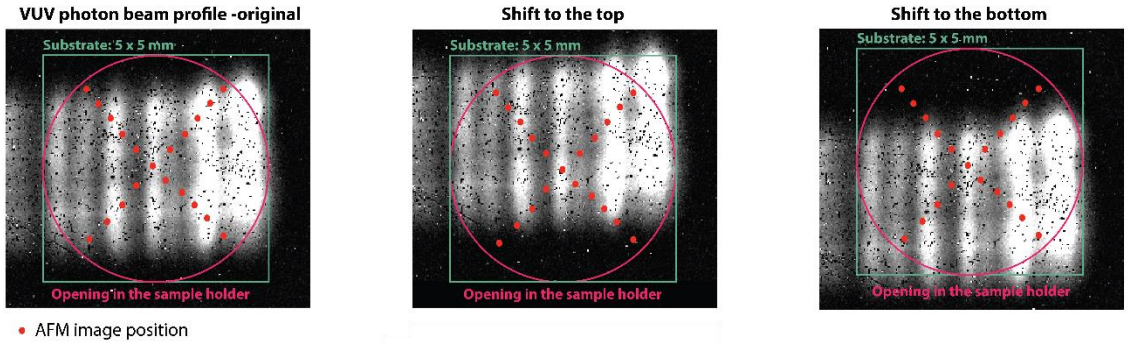

Fig. 33 Beam profile of the 8.44 eV photon beam at the synchrotron facility SOLEIL with a schematic view on the substrate and sample holder position; from left to right: original position of the illuminated area, shift to the top, shift to the bottom.

A second systematic error in the sample holder adjustment affects also the total number of SSBs and is clearly visible the correlation of the number of SSBs versus the fluence of the irradiation process. The section of the sample holder, where the samples are mounted is fixed to the sample holder by one screw and can be shifted in a certain angle with respect to the rest of the sample holder (fig.34a). If the sample array is not perfectly vertically aligned with the sample holder, the sample itself is shifted to the right or to the left (fig.34b). The deeper the sample position in the sample array, the stronger will be the shift and the unilluminated area. This can be clearly seen in the diagrams as a bow in the fluence dependence of N_{SSB} (fig.24a/b).

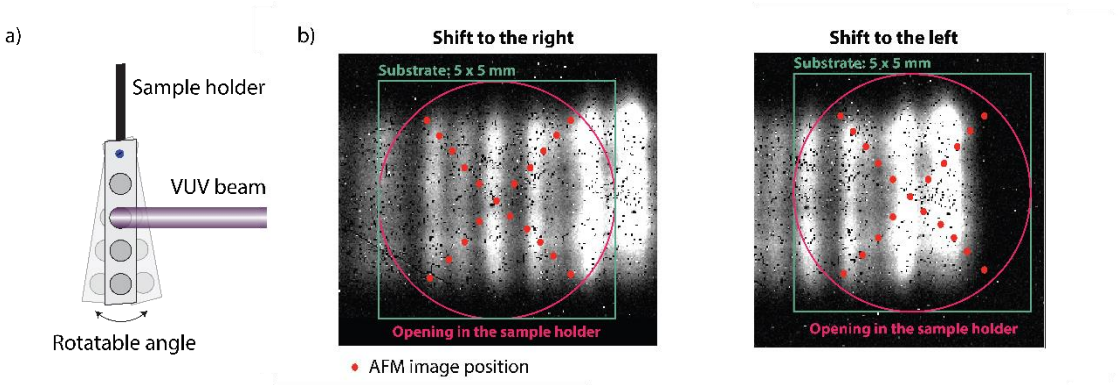

Fig. 34 a) Scheme of the illuminated sample holder with a shift of the sample array, b) beam profile of the 8.44 eV photon beam at the synchrotron facility SOLEIL with a schematic view on the substrate and sample holder position with shifted sample holder position (right or left, respectively).

A third systematic error arises from the photodiode that is measuring the photon fluence. During the irradiation process, carbon impurities in the Ar gas such as CO_2 or CH_4 are cracked and deposit as a layer on the photodiode, thereby changing its absorption properties. With the proceeding irradiation experiments, the carbonization increased as well. This way the detected fluence is underestimated, which would lead to increased SSB cross sections. Since this issue is known, the fluence is measured in the beginning of the experiments and the change of the fluence is monitored during the experiment. If

necessary, corresponding corrections are taken into account for SSB cross section calculation.

5.6.2 Data evaluation process

Another issue is the surface structure of the CaF_2 substrate. To obtain a fresh and clean surface, the 0.5 mm thick substrate was cleaved with the help of a scalpel. Since CaF_2(111) consists of layers horizontal to substrate surface, the cleaving procedure yields an even and flat surface. Since the cleavage almost never happens only within one layer of the material, a stepped surface structure is released after the cleavage. Depending on the surface layer, the adsorption quality of the DNA origami nanostructures differs as already described in section 4.2. If now certain surface area is occupied with poorly adsorbed DNA origami nanostructures, they can barely be included into the data analyses. Since the VUV beam exhibits periodically changing intensities as it is shown in figures 33 and 34, a strong deviation from the real cross section for SSBs can be introduced here. To still assure a good data quality, a high number of AFM images for each sample was taken and analyzed. The cleaved CaF_2 surface gives the highest fraction in the standard error of the cross sections for SSBs, since the error source in the irradiation set up can be minimized by a careful handling of the instrument.

6 Photoionization tandem mass spectrometry

The initial step for photoinduced SSBs can be either photoexcitation or photoionization. One important parameter in this context is the IE of the DNA sequence. Since the photoionization is a threshold process, it affects the reaction mechanism above the IE of the molecule. Therefore, it is expected that the SSB cross sections increase clearly, when the IE of the DNA sequence is reached. With the help of photoionization tandem mass spectrometry, the IE of the DNA sequence can be explored further. In this chapter the results of the gas phase photoionization tandem mass spectrometry experiment are presented. Several charge states of the precursor cation were accessible by the positive ESI mode in the mass analyzer. All precursor cations were accumulated in the ion trap to be irradiated with the VUV photon beam, whose energy was scanned from 8 to 16 eV. The target DNA sequences investigated with this experimental technique vary in their length and nucleobase composition, and are partly modified with the radiosensitizer ^{5Br}U. Two ways of data evaluation are presented for the target DNA sequences differing in the DNA sequences length. These results are additionally compared with theoretical data provided by Lukas Gallandi and Prof. Thomas Körzdörfer, Department of Theoretical Chemistry of the University of Potsdam.

6.1 Dependency of the IE on the DNA sequence length

In this section the influence of the DNA sequences length on the IE of the precursor cations ($[M + nH]^{n+}$) of five different DNA sequences 5'-d(A_n) with n = 4, 8, 12, 16, 20 were investigated. Depending on the DNA sequence two to four different charge states of the precursor cations could be obtained in the MS 1 with the positive ESI mode at the LTQ mass spectrometer. Each charge state of the precursor cation was accumulated in the ion trap to generate an additional photoinduced cation through VUV photon radiation. From the intensity trend of the photoinduced cation, the IE of each precursor cation can be determined. The IEs of the precursor cations of the different DNA sequences are shown in figure 35 below and in table 17 at the end of this section.

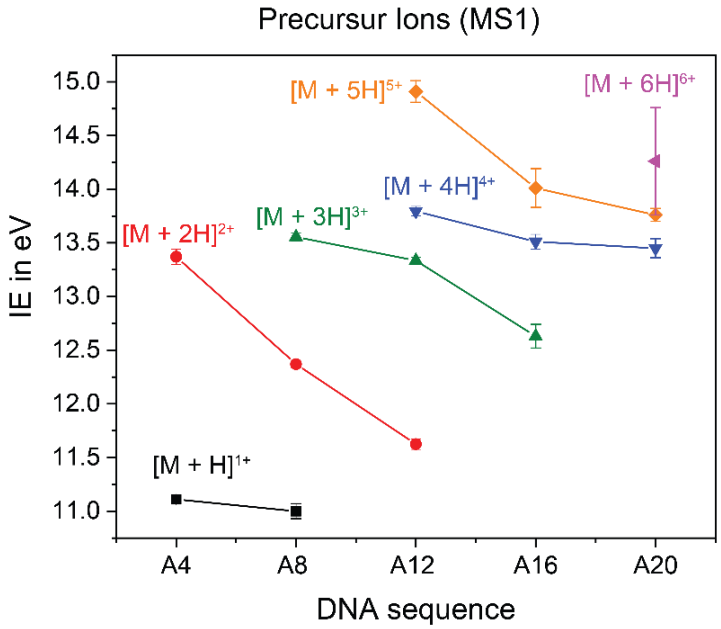

Fig. 35 Correlation of the IEs of the precursor cations ($[M + nH]^{n+}$), n = 1-6 to the length of the initial DNA sequence 5'-d(A_n) with n = 4, 8, 12, 16, 20; the precursor cation with the charge state +1 is displayed in black, +2 in red, +3 in green, +4 in blue, +5 in orange and +6 in pink; the lines only guide the eye.

In figure 35 the different IEs of the precursor cations in the MS 1 are presented. Generally, it can be seen that the IE value increases with the increasing positive charge of the precursor cation. The higher the charge of the precursor cation, the more energy has to be applied to eject further electrons from the molecule. The reason for that is the increasing Coulombic interaction between the ejected electron and the increased charged ion core.

Within one charge state the IE of the precursor cations also decreases with the increasing DNA sequences length. The longer the DNA sequence, the larger the distance between the charges, which in turn lowers the potential energy of the system. This general trend is also reflected in the computational studies of Kumar *et al.* [150] and Gallandi and Körzdörfer [151] on oligonucleotides and nucleobases. Decreasing IE values for the neutral DNA sequences 5'-d(A_n) with n = 1 – 8 with increasing DNA sequence length was observed by Kumar *et al.* [150] by DFT calculations. The DNA sequence 5'-d(A) was calculated to have an IE of 8.32 eV and the IE value decreases exponentially as the DNA sequence becomes longer until the IE value reaches a saturation at 7.45 eV with 5'-d(A_8). Gallandi and Körzdörfer [151] used delta self-consistent-field (ΔSCF) calculations to determine the IE values for the DNA sequences 5'-d(A_n) with n = 1 – 4, 6. The IE values show also a decreasing trend with 9.21 eV for 5'-d(A) to around 6.94 eV for 5'-d(A_6). It was already demonstrated for N-methylated stacked nucleobases by Sugiyama *et al.* [155] that the interactions between two HOMOs of the two adjacent nucleobases in the neutral DNA sequence create an energy splitting, which results in an energy gap with a new HOMO of a lower energy and a molecular orbital (HOMO-1) of higher energy. Since Koopmans' Theorem is applied here, this results in lowered IE values of the stacked system. The

distribution of the HOMO within the stacked nucleobases depends strongly on the stacking interaction. The smaller the distance between the nucleobases, the better the stacking interaction and the better the distribution of delocalized electron density of the HOMO and HOMO-1 orbitals on both nucleobases, which results in an energy decrease of both molecular orbitals. The HOMO energy of the stacked nucleobases is also dependent on the twist angle between the stacked nucleobases. Herein, no clear trend can be identified. For the planar geometry as well as for different twist angles a lowering of the HOMO energy was observed. A similar behavior might be observed for the energy level of the cationic state of a stacked DNA system.

Calculating the IE of the neutral system instead with the energy difference of the neutral and the cationic system, no IE change would be observed, if the HOMO and the cationic state would decrease their energy by the same amount. But the IE values were observed to decrease with the increasing length of the DNA strand [150,155]. If the stacking interactions extend to more than two nucleobases, it seems to result in even lower IE values. To obtain such a decreased IE, the energy level of the cationic state has to be lowered by a higher amount than the HOMO of the neutral system. Kumar *et al.* [150] reported the spin density of the radical cations of the DNA sequences 5'-d(A_n) with n = 1 – 8 to be distributed over up to four nucleobases. This might be an indication that the stacking interaction is very strong and hence a decreased IE value of the neutral system results, which agrees with the aforementioned assumption and with the presented results.

Tab. 17 Table of the IEs in eV of the precursor cations of the DNA sequences 5'-d(A_n) with n = 4, 8, 12, 16, 20 with their standard deviation.

DNA sequence / precursor ion	$[M + H]^{1+}$	$[M + 2H]^{2+}$	$[M + 3H]^{3+}$	$[M + 4H]^{4+}$	$[M + 5H]^{5+}$	$[M + 6H]^{6+}$
5'-d(A_4)	11.11 ± 0.02	13.37 ± 0.07				
5'-d(A_8)	11.00 ± 0.07	12.37 ± 0.04	13.56 ± 0.04			
5'-d(A_{12})		11.63 ± 0.11	13.34 ± 0.03	13.80 ± 0.05	14.91 ± 0.10	
5'-d(A_{16})			12.63 ± 0.11	13.51 ± 0.07	14.01 ± 0.18	
5'-d(A_{20})				13.45 ± 0.09	13.76 ± 0.06	14.26 ± 0.50

Moreover, it has to be mentioned that the IE values of the precursor cations determined with the tandem mass spectrometry experiment are overestimated by around 0.2 eV. Additional higher energetic photons of the VUV beam influenced the measurement of the

intensity trend of the photoinduced cation, which is used to obtain the IE of the precursor cation. This is explained in detail in section 6.4. In the following it will be discussed whether and how the IEs of the different charge states of the precursor cations can be applied to obtain the IE value for the respective neutral DNA sequence. The measured signal intensities of the precursor cations plotted versus the photon energy to determine their IE are shown in the appendix A.2-8. If data from 2015 and 2016 are shown, the average value was used for further data evaluation. In the next two sections (6.1.1 and 6.1.2) two possible evaluation procedures are presented and compared to IE data provided by Kumar *et al.* [150] and Gallandi and Körzdörfer [151].

6.1.1 IE evaluation procedure 1

The first evaluation procedure to obtain the IEs of the neutral DNA sequence was adapted from the work of Budnik and coworkers [156,157], who investigated the IE of different polypeptides with the help of photoionization tandem mass spectrometry. With ESI as an ionization source, charge states of the precursor cations of the polypeptides from +1 to +5 were obtained and plotted against their ionization energies showing a nearly linear behavior. Therefore, a linear correlation between the charge state of the precursor cations and their IE values was assumed by Budnik *et al.* [156,157], but no model provided. To obtain the IE of the neutral polypeptide, the IEs of the precursor cations were fitted linearly and extrapolated to the charge state zero. This way, the IE of the neutral polypeptide is obtained. The procedure is schematically shown in figure 36.

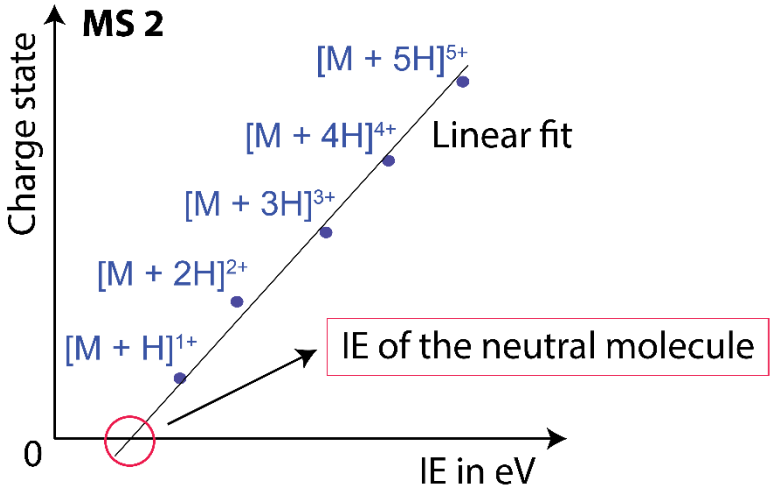

Fig. 36 Scheme of the correlation of the charge states +1 to +5 of the precursor ions ($[M + nH]^{n+}$, n = 1-5) to their IEs, the linear fit of the charge states is extrapolated to the charge zero to obtain the IE of the neutral molecule; adapted from ref. [156,157].

This method was used for the DNA sequences 5'-d(A_n) with n = 4, 8, 12, 16 and 20, since the IEs of the precursor cations of different charge states within one DNA sequence showed a nearly linear behavior as well. One example of a linear fit and the consequent

extrapolation to the charge zero is shown in figure 37a for the DNA sequences 5'-d(A_{16}). The IE data for all neutral polyadenine DNA sequences are displayed in figure 37b.

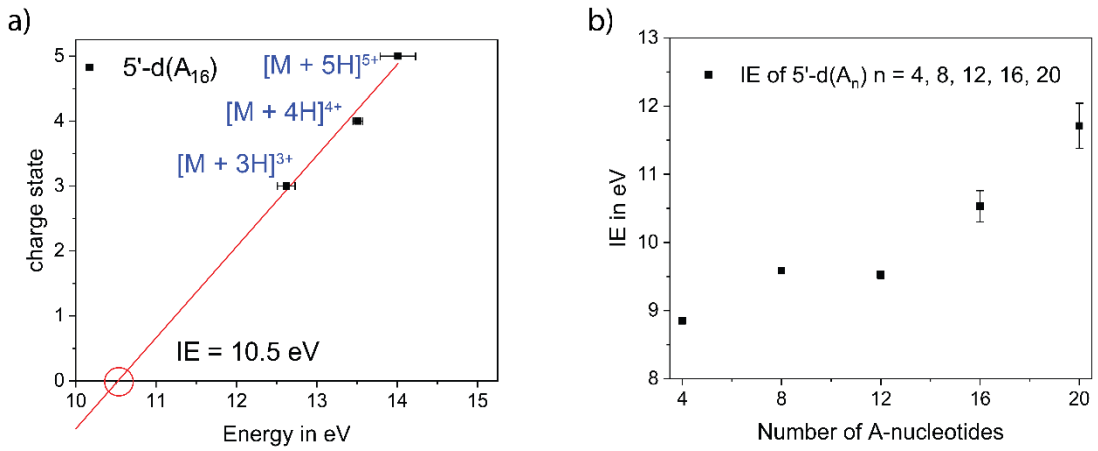

Fig. 37 a) Correlation of the charge states +3, +4 and +5 of the DNA sequence 5'-d(A_{16}) to their IE; data points are fitted linearly and extrapolated to the charge zero to obtain the IE of the neutral DNA molecule, b) IEs obtained for the DNA sequences 5'-d(A_n) with n = 4, 8, 12, 16, 20 to the number of A nucleotides in the DNA sequence.

The correlation of the charge states 3+ to 5+ to their IE is shown exemplarily in figure 37a for the DNA sequence 5'-d(A_{16}). The charge states are fitted linearly and extrapolated to the charge zero to obtain the IE of the neutral DNA molecule. In figure 37b the IEs of all neutral DNA sequences 5'-d(A_n), n = 4, 8, 12, 16 and 20 are compared. Accordingly, the IE is increasing with the length of the DNA strand. This is in strong contrast to the results of Kumar *et al.* [150] and Gallandi and Körzdörfer [151]. Both are reporting a decreasing IE with increasing length of the DNA sequence (see above). This demonstrates, that the IE values for the neutral DNA sequences obtained with the evaluation method adapted from Budnik *et al.* [156,157] are clearly overestimated. Hence, the correlation of the charge states to their IEs seems to be linear, but results in misleading IE data for the neutral system. Consequently, this evaluation method cannot be used for oligonucleotides. One reason might be a too small number of data points available in the present experiments. Only two to four charge states for each DNA sequence were accessible in the MS 1 spectra. This might not be enough to reproduce a linear behavior as assumed by Budnik *et al.* [156,157]. The error might even increase, if the length of the DNA system is increased, since only higher charge states are produced in this case. If only high charge states are available, the extrapolation to zero creates a larger error.

Another study to obtain IE values experimentally *via* tandem mass spectrometry was performed by Giuliani *et al.* [158] on the protein ubiquitin. In their investigations the charge states +4 to +9 of the precursor cations were accessible in the mass analyzer through ESI to determine the IE of the neutral protein. Also in this study no linear correlation of the IE of the precursor cation and its charge state could be applied. The IE values show an increasing trend with the increasing charge states, which is interrupted by nearly constant IE values at the charges states +5 to +7 forming a plateau in the graph. This plateau can

be attributed to a folding step within the protein. To still obtain the IE of the neutral ubiquitin molecule, simulations were performed, which consider the folding state of the protein at different charges states.

In the case of the DNA sequences 5'-d(A_n) with n = 8 and 12, the IE values seem to form a plateau as well (fig. 36b), since their IE value with 9.6 eV and 9.2 eV, respectively are very similar. The IE of the DNA sequence 5'-d(A_n) with n = 16 and 20 in turn increases again strongly to 10.5 eV and 11.7 eV, respectively. At a strand length of 12 nucleotides conformational changes in the ssDNA strand could take place that might change the stacking interaction between the nucleobases, which in turn could lead to an increase of the IE. Still, the IE values obtained in this way do not agree with theoretical predictions. Consequently, a second evaluation method was attempted to determine the IE of the neutral target DNA sequence (section 6.1.2).

6.1.2 IE evaluation procedure 2

In the second evaluation procedure the IE values of the precursor cations of one charge state were used to extrapolate the IE values of the missing charge states of the different DNA sequences. If more precursor cations with their IEs are available, the correlation of the charge states with the IEs could be improved and with it, the extrapolation to the charge zero to obtain the IE of the neutral DNA sequence (fig.36). The precursor cation $[M + 2H]^{2+}$ e.g. was only available for the DNA sequences 5'-d(A_n) with n = 4, 8 and 12. The missing IE values for the +2 charge states for the DNA sequences 5'-d(A_n) with n = 16 and 20 were extrapolated from a linear fit through the IE values obtained for the charge state +2 of the DNA sequences 5'-d(A_n) with n = 4, 8 and 12 (fig.38). A linear correlation was assumed, since no distinct function is evident and a linear correlation is reasonable within the error bars of the experiment. This evaluation methods was done for the charge states +3, +4 and +5 as well, since here already three IE values of the precursor cations are available. The precursor cations $[M + H]^+$ and $[M + 6H]^{6+}$ have not been treated this way, since for $[M + H]^+$ only two IE values from the DNA sequences 5'-d(A_n) with n = 4 and 8 and for $[M + 6H]^{6+}$ only one IE value from the DNA sequences 5'-d(A_n) with n = 20 were obtained in the tandem mass spectrometry experiment. All experimental IE values and all extrapolated IE values of the charge state of the precursor cations are shown in figure 38a/b below and are summarized in table 18 at the end of this section.

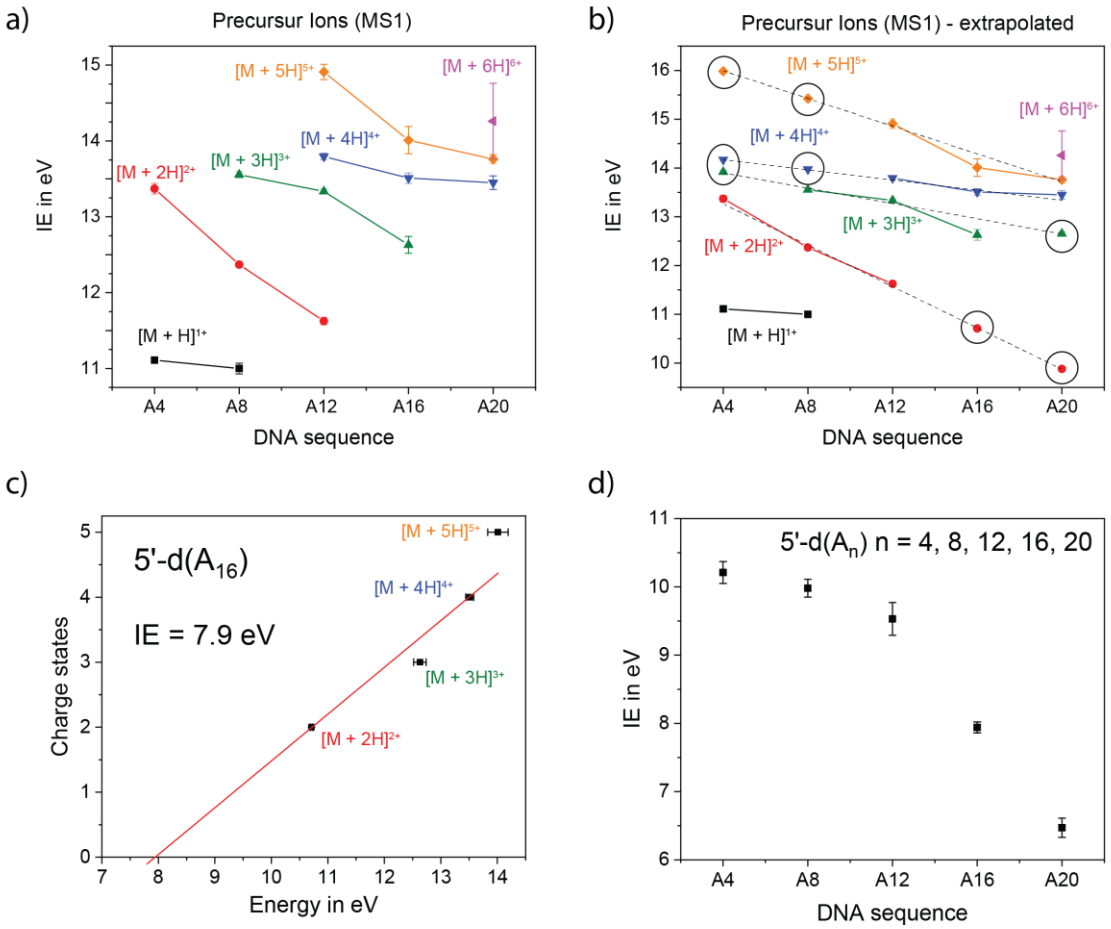

Fig. 38 a) Correlation of the IEs of the precursor cations of different charge states ($[M + nH]^{+n}$) to the DNA sequence 5'-d(A_n), differing in its length with n = 4, 8, 12, 16, 20, (same data as in fig. 35) b) the values presented in a) are extended by extrapolation for the charge states +2 (red), +3 (green), +4 (blue) and +5 (orange); the linear fit is displayed with a dotted black line and the additional IE values marked with a black circle, c) plot of the charge states of the precursor cations of the DNA sequence 5'-d(A_{16}) against their IEs; extrapolation to the charge zero, i.e. the neutral molecule to obtain the IE of the neutral DNA sequence (red line), d) plot of the IEs of the different DNA sequences 5'-d(A_n) with n = 4, 8, 12, 16, 20 against their length.

In figure 38c the charge states of the precursor cations of the DNA sequence 5'-d(A_{16}) are plotted versus their IE and the linear fit extrapolated to the charge state zero to obtain the IE of the neutral DNA sequence. 5'-d(A_{16}) was chosen as an example. In the diagram it can be seen that the trend of the IEs of the precursor cations is not linear anymore. It rather shows an exponential behavior. If the IEs of the precursor ions would be fitted exponentially, the IE of the neutral molecule would be far below zero. Since no other distinct function is apparent, a linear fit seemed to be the most reasonable. The same procedure was applied to the other DNA sequences 5'-d(A_n) with n = 4, 8, 12 and 20, and the obtained IEs of the neutral sequences are displayed in figure 38d. The IEs are showing now a decreasing trend, which is more realistic, but the IE values for the DNA sequences 5'-d(A_n) with n = 4, 8, 12 and 16 are still overestimated in comparison to the IE data

obtained by Kumar *et al.* [150]. Nevertheless, the differences between the IE values for the sequences with n = 12, 16 and 20 are very large resulting in an underestimation of the IE value of the DNA sequence 5'-d(A_{20}). In conclusion, this evaluation method results in a correct trend, but is still not sufficient to provide IE data of the neutral DNA sequences.

Tab. 18 Table of the IEs in eV of the precursor cations of the DNA sequences 5'-d(A_n) with n = 4, 8, 12, 16, 20 with their standard deviation; the extrapolated IE values are shown in blue.

DNA sequence / precursor ion	$[M + H]^{1+}$	$[M + 2H]^{2+}$	$[M + 3H]^{3+}$	$[M + 4H]^{4+}$	$[M + 5H]^{5+}$	$[M + 6H]^{6+}$
5'-d(A_4)	11.11 ± 0.02	13.37 ± 0.07	13.9 ± 0.04	14.2 ± 0.02	16.0 ± 0.02	
5'-d(A_8)	11.00 ± 0.07	12.37 ± 0.04	13.56 ± 0.04	14.0 ± 0.02	15.4 ± 0.02	
5'-d(A_{12})		11.63 ± 0.11	13.34 ± 0.03	13.80 ± 0.05	14.91 ± 0.10	
5'-d(A_{16})		10.7 ± 0.02	12.63 ± 0.11	13.51 ± 0.07	14.01 ± 0.18	
5'-d(A_{20})		9.9 ± 0.02	12.7 ± 0.04	13.45 ± 0.09	13.76 ± 0.06	14.26 ± 0.50

To check, whether the IEs of the precursor cations of the DNA sequences follow a linear trend with respect to their charge state, computed IEs were provided by Lukas Gallandi and Prof. Thomas Körzdörfer, Department for Theoretical Chemistry at Potsdam University. These data are presented in the next section and compared to the results of the present work.

6.1.3 Comparison with theoretical data

In this section the IEs of the different precursor cations of the DNA sequences 5'-d(A_4), which were obtained experimentally in the framework of this thesis, are compared with theoretical data provided by Gallandi and Körzdörfer [151]. They performed ΔSCF calculations with the B3LYP [159] and LC-ωPBE (ω = 0.4 1/a_0) [160] functionals to obtain the vertical IE (IE_v) of the neutral DNA system 5'-d(A_4) and the different precursor cations. In both methods, the IEs were calculated from the difference between the total energies of the neutral and charged system. The geometry predictions were conducted at two temperatures; 0 K and 300 K. At 0 K the geometry of the ssDNA strand remains in a helical structure. At 300 K fluctuations in the molecular structure occur and therefore an arbitrary geometry was used. For both temperatures, 0 K and 300 K, three structures with

different number of explicitly considered atoms were used. The first structure only consists of the nucleobases without backbone (A4-structure). In the second structure, the sugar units are attached to the nucleobases (A4s-structure). The final third structure consists of the full DNA including the sugar-phosphate backbone (A4sp-structure). Each of the six geometries is treated by the ΔSCF method with B3LYP. The geometrical optimization was performed with Gaussian09 [161] at 0 K and with Gabedit 2.4.8 [162] at 300 K with a molecular dynamic (MD) simulation and the Berendsen thermostat. Consequently, six different structures were investigated with respect to their influence on the IE value of the neutral DNA system. For the structures A4 an A4s additionally the IE values of the different precursor cations were calculated. The structures are displayed in the appendix (A.17-19). The results of the calculations are presented figure 39.

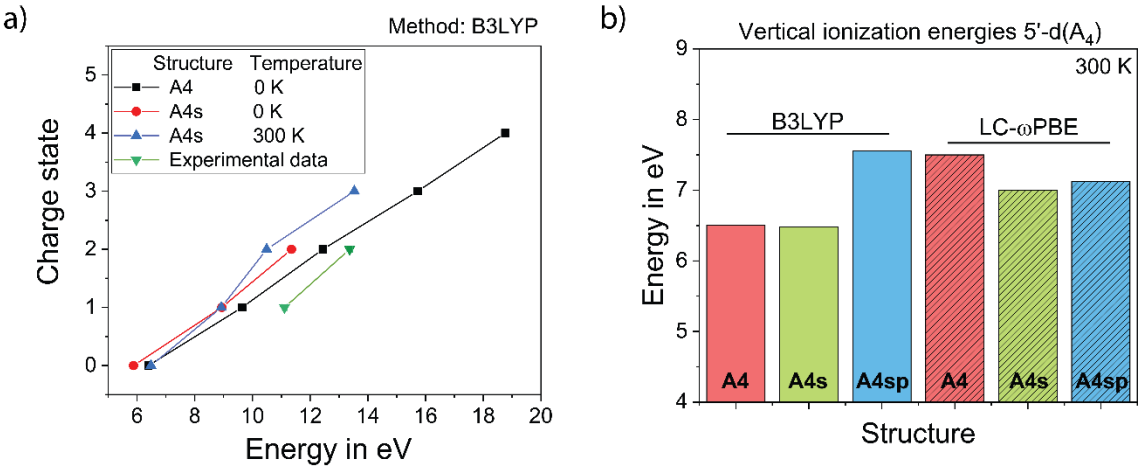

Fig. 39 a) Correlation of the charge states and the corresponding IE of the DNA sequence 5'-d(A_4) using experimental and theoretical data (IE_v); calculations were conducted by the ΔSCF@B3LYP method at the temperatures 0 K and 300 K for the structures A4 and A4s, b) IE_vs of the neutral DNA sequence 5'-d(A_4) calculated for the structures A4, A4s and A4sp at 300 K with the ΔSCF@B3LYP and ΔSCF@LC-ωPBE (ω=0.4 1/a_0) methods; a, b) data provided by Gallandi and Körzdörfer [151].

In figure 39a the results for the ΔSCF@B3LYP calculations at 0 K and 300 K are presented. The IEs of the precursor cations of the A4-structure ($[M + H]^+$, $[M + 2H]^{2+}$) and of the A4s-structure ($[M + H]^+$ to $[M + 4H]^{4+}$) were calculated as well as the IE for the neutral system at the temperature of 0 K. It can be seen that the IE is increasing almost linearly with the increasing charge state. The IEs for the A4s structure in that case are lower than to the IEs for the A4 structure. The addition of the sugar unit to the nucleobase might allow for an even better delocalization of the electron density in the stacked nucleobases to the sugar unit for the HOMOs of the neutral DNA sequences as well as for its cationic state, which could result in even lower energy levels. If the energy level of the cationic state is lowered more than the HOMOs of the neutral DNA sequence, the IE value would be decreased as well.

Since the tandem mass spectrometry experiments were performed at room temperature, another calculation of the IE values of the precursor cations ($[M + H]^+$ to $[M + 3H]^{3+}$) and the IE for the neutral system for the A4s-structure at the temperature of 300 K was performed. Herein, an arbitrary geometry was used, which allows less stacking interaction between the nucleobases resulting in higher IE values. Still, the experimentally determined IE value of the precursor cations are still 1-2 eV higher than the calculated values. It might be that the geometry of the real structure in the experimental set up possesses an even less stacked geometry than the one used for the calculation, which would lead to even increased IE values. The IEs at 300 K are increasing with the charge state, but not as linear as at 0 K. The higher temperature leads to conformational changes within the structure, which could influence its final IE value. From the theoretical data shown here it can be concluded that a linear fit of the IEs to the charge states would result in an incorrect IE of the neutral system, and can thus not be applied on the experimental data.

Since the calculated IE values (ΔSCF@B3LYP) of the precursor cations lie energetically lower than the experimental data, additional calculations of the IE values of the DNA sequences 5'-d(A_4) at 300 K with the ΔSCF@B3LYP method on the A4sp-structure and with ΔSCF@LC-ωPBE method on the A4, A4s and A4sp-structure were performed. Herein, only neutral IEs were calculated to see, which influence the chosen structure and method has on the IE of the DNA sequence. In figure 39b the results of these calculation are presented. The IEs for the A4 and A4s structures calculated with ΔSCF@B3LYP are around 6.50 and 6.48 eV, respectively and increase by around 1 eV, when the phosphate unit is added to the structure (A4sp). The IE of the A4 structure obtained by ΔSCF@LC-ωPBE in contrast is has a value of 7.50 eV and is thus 1 eV higher than the one calculated with the method applied before. The IEs of the A4s and A4sp structures on the other hand decrease to 7.00 and 7.12 eV, respectively. Generally, the B3LYP method is known to underestimate IE values of stacked nucleobases [163], but is fast to obtain more results in a shorter time. The LC-ωPBE method is slower, but is better suited to describe a stacked nucleobase system and the obtained IE values are more reliable. For the A4 structure and A4s structure, for which the IE values of the precursor cations were already calculated, the IE value for the neutral system is around 1 eV and 0.7 eV higher, respectively, when calculated with the LC-ωPBE method. Since the IE values are calculated from the difference of the total energies of the neutral and the charged system and the IE of the neutral DNA sequence is higher with the LC-ωPBE method than with the B3LYP method, two possible reasons could explain the changes. On the one hand, the IE value of the HOMO of the neutral system is lowered. On the other hand the IE of the cationic system could be increased, which would lead to IE values closer to the experimentally obtained IE values for the precursor cations.

In summary, the IE values of the precursor cations seem to be reflected the best by the calculations at 300 K, since this temperature allows fluctuations of the DNA, which can result in less stacking interaction between the nucleobases. Poor stacking interactions

would barely lead to a change in the IEs of the full DNA sequence in comparison to the single nucleobases. A similar influence might occur for the energy of the cationic state of the DNA strand. At 300 K a geometry with less stacking interaction was chosen and higher IEs were obtained in comparison to the IE determined at 0 K. Additionally, the trend of the IEs at 300 K is less linear than at 0 K (fig. 38a). Allowing conformational changes seem to influence the different IEs of the precursor cations to a different extent, which might depend on the charge distribution within the complete DNA sequence. These calculations confirm that a simple linear fit can lead easily to wrong IE values and cannot be applied for the ssDNA system. Additionally, it was shown, that the calculated IE values of the cationic system might be underestimated, since it is calculated with the B3LYP method. Calculation with the LC-ωPBE method lead to higher IE values in the neutral DNA sequence, which might be due to higher energies of the cationic state of the DNA sequence.

6.1.4 Summary

The IE of the DNA sequences 5'-d(A_n) with n = 4, 8, 12, 16, 20 were investigated with the tandem mass spectrometry experiment. The IEs of the precursor cations could be determined and a general trend identified. On the one hand the IE values are increasing with the higher charge state, since the Coulomb interaction between the ion core and the ejected electron increases as well. On the other hand, the IE values decrease with increasing DNA strand length, because the longer the DNA sequence, the larger the distance between the charges, which in turn decreases the potential energy of the system.

Two procedures were tested on their suitability to identify the IE of the neutral DNA system. In the first procedure the charge states of the precursor cations of one DNA sequences were correlated to the corresponding IE values to obtain the IE of the neutral system by extrapolation to the charge zero. This procedure results in strongly increasing IE values for the neutral DNA sequence with increasing DNA sequence length. In the second procedure, all IE values of precursor cations with the same charge state are correlated the DNA strand length and extrapolated to obtain the IE values of the missing precursor cations. In turn, all charge states of the precursor cations of one DNA sequence were correlated to the corresponding IE values to obtain the IE of the neutral system by extrapolation to the charge zero. This procedure resulted in a decreasing trend of the IE values of the neutral DNA sequences with increasing strand length. Still, the IE values obtained with both procedures are mainly overestimated in comparison to Kumar *et al.* [150] and Gallandi and Körzdörfer [151]. The second procedure gives at least a correct trend, but is not sufficient to provide feasible IE data for the neutral DNA sequences.

Finally, the experimental data were cross checked with computed IE values of the neutral DNA sequence 5'-d(A_4) and the IE values of the corresponding precursor ions. The calculated IE values are generally higher than the experimentally determined IE values. The application of an arbitrary geometry at 300 K resulted in IE values that are the closest

to the experimental data, since this geometry has less stacking interactions between the nucleobases, which is presumably closer to the situation in the experiment. The same calculations might lead to even higher IEs, if a geometry with an even more unstacked geometry is applied. Additionally, the IE values of the precursor cations with different charge states could be identified. Comparing calculations at 0 K and 300 K, an increasing trend of the IEs with the charge state can be observed, whereas the trend at 0 K is linear and at 300 K a clear deviation from a linear relationship occurs. Since 300 K are closer to the experimental condition, this trend can be assumed for the experimental data as well. Thus, the experimental data cannot be fitted linearly to obtain the IE of the neutral system, since it would lead to incorrect IE values.

6.2 Dependency of the IE on the DNA sequence

In this section the influence of the DNA sequences on the IE of the precursor cations of six different DNA sequences 5'-d(X_{12}) with X = A, C, T and 5'-d(TT(XTX)$_3$TT) with X = G, A, C were investigated. Depending on the DNA sequence two to four different charge states of the precursor cations could be obtained in the MS 1. The IEs of the precursor cations of the different DNA sequences are shown in figure 40 below and are summarized in table 19 at the end of this sections.

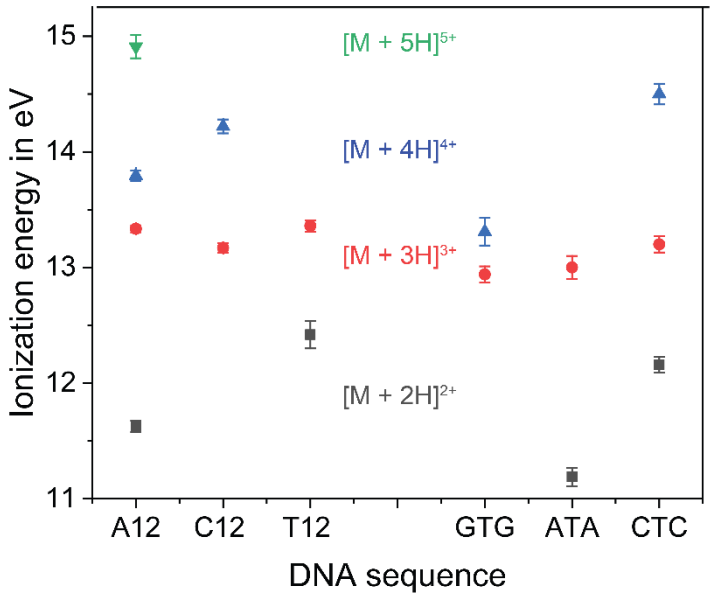

Fig. 40 Correlation of the IEs of the precursor cations of the different DNA sequence 5'-d(X_{12}) with X = A, C, T and 5'-d(TT(XTX)$_3$TT) with X = G, A, C; the precursor cation with the charge state +2 is displayed in grey, +3 in red, +4 in blue and +5 in green; the lines only guide the eye to see the trend.

In figure 40 the different IEs of the precursor cations obtained in the MS 1 are presented. The order of the DNA sequences in the x-axis corresponds to the order of the IE values of the single nucleobases G < A < C < T [2]. Regarding the mono-nucleobase DNA

sequences 5'-d(X_{12}) with X = A, C, T, a clear increasing trend of the IE values of the precursor cations $[M + 2H]^{2+}$ and $[M + 4H]^{4+}$ can be observed. Considering the intermixed DNA sequences 5'-d(TT(XTX)$_3$TT) with X = G, A, C, a similar trend regarding the content of G, A and C nucleobases can be seen. Herein, the IE values of the precursor cations with the charge states +2 and +4 are increasing. The precursor cations $[M + 3H]^{3+}$ have a similar IE for the compared DNA sequences. For both, the mono-nucleobase and the intermixed DNA sequences, the IE values increase in the same order as the IE values of the single nucleobases. The nucleobases with the lowest IE seem to be the crucial subunit, which determines the final IE of the DNA sequence and its precursor ions. It was already mentioned that Sugiyama *et al.* [155] demonstrated that in two stacked nucleobases the HOMOs of both nucleobases underlie an energy splitting. The energy splitting results in turn in a dominant localization of the HOMO on the nucleobase with the lower IE, which is then determining the IE of the stacked nucleobases. This trend seems to be similar in the longer DNA sequences investigated in the present work.

Tab. 19 Table of the IEs in eV of the precursor cations of the DNA sequences 5'-d(X_{12}) with X = A, C, T and 5'-d(TT(XTX)$_3$TT) with X = G, A, C with their standard deviation.

DNA sequence / precursor ion	**$[H + 2H]^{2+}$**	**$[H + 3H]^{3+}$**	**$[H + 4H]^{4+}$**	**$[H + 5H]^{5+}$**
5'-d(A_{12})	11.63 ± 0.05	13.34 ± 0.03	13.80 ± 0.05	14.91 ± 0.10
5'-d(C_{12})		13.17 ± 0.04	14.22 ± 0.06	
5'-d(T_{12})	12.42 ± 0.12	13.36 ± 0.05		
5'-d(TT(GTG)$_3$TT)		12.94 ± 0.07	13.31 ± 0.12	
5'-d(TT(ATA)$_3$TT)	11.19 ± 0.08	13.00 ± 0.10		
5'-d(TT(CTC)$_3$TT)	12.16 ± 0.07	13.20 ± 0.07	14.5± 0.09	

The measured signal intensities of the precursor cations plotted against the photon energy to determine their IE are shown in the appendix (A.5-6, 9-13).

6.3 Dependency of the IE on the DNA sequence modification with ^{5Br}U

In this section the influence of radiosensitizer ^{5Br}U and its distance to the nucleobase G within the DNA sequences 5'-d(TTGA$_n$^{5Br}UTT) on the IE of the precursor cations is investigated. Two different charge states of the precursor cations of each DNA sequence could be obtained in the MS 1. The IEs of the precursor cations of the different DNA sequences are shown in figure 41 below and are summarized in table 20 at the end of this sections.

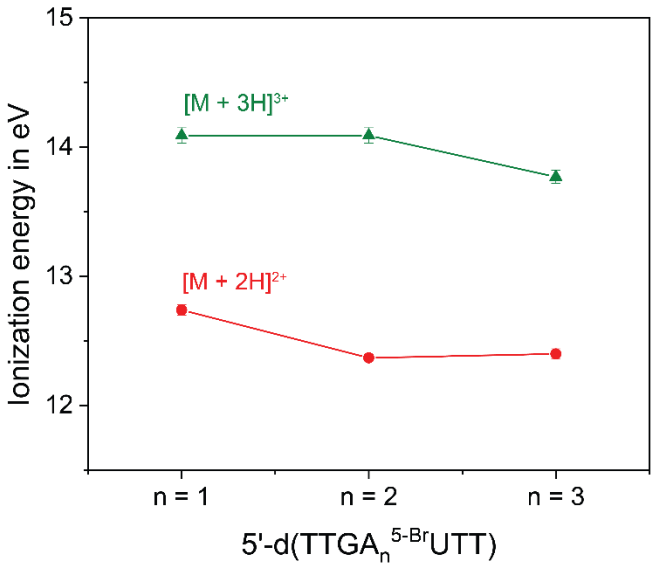

Fig. 41 Correlation of the IEs of the precursor cations of the DNA sequence 5'-d(TTGA$_n$^{5Br}UTT) with n = 1 - 3; the precursor cation with the charge state +2 is displayed in red and +3 in green; the lines only guide the eye..

In figure 41 the different IEs of the precursor cations obtained in the MS 1 are presented. Only a slightly decreasing trend for IE values of the precursor cations of the DNA sequences 5'-d(TTGA$_n$^{5Br}UTT) with n = 1 – 3 is observed with the increasing number of A spacers separating the G nucleobase from the radiosensitizer ^{5Br}U. This trend might be attributed to the increasing length of DNA sequences (7 - 9 nucleotides), since the IE values a very similar to the IE values of the non-brominated DNA sequences 5'-d(A$_n$) with n = 4 and 8 (section 6.2). The radiosensitizer ^{5Br}U itself seems not to have a big influence, since the IE values do not differ significantly from IE values determined for the other DNA sequences. The measured signal intensities of the precursor cations plotted against the photon energy to determine their IE is shown in the appendix A.14-16.

Tab. 20 Table of the IEs in eV of the precursor cations of the DNA sequences 5'-d(TTGA$_n$^{5Br}UTT) with n = 1 – 3 with their standard deviation.

DNA sequence / precursor ion	**[M + 2H]$^{2+}$**	**[M + 3H]$^{3+}$**
5'-d(TTGA^{5Br}UTT)	12.74 ± 0.04	14.09 ± 0.06
5'-d(TTGAA^{5Br}UTT)	12.37 ± 0.03	14.09 ± 0.06
5'-d(TTGAAA^{5Br}UTT)	12.40 ± 0.04	13.77 ± 0.05

6.4 Contribution of higher energy photons

In this sections the contribution of higher energy photons and their influence on the experimental IE data is presented. The experimental set up of the tandem mass spectrometry experiment is selecting higher energy photons *via* a grating that is integrated into the beamline set up (fig. 15 in section 4.3). This way higher harmonics of the selected VUV energy value are passing the set up as well to interact inadvertently with the sample. If e.g. the VUV beam possesses an irradiation energy of 8 eV, photons with an energy of 16 eV will pass as well. To filter the additional higher harmonics from the VUV beam, an Ar gas was introduced in one of the vacuum chambers of the differential pumping stage of the experimental set up. Ar absorbs photons with an energy above 16 eV, which is exactly the cut off that was desired. In figure 42a the flux of the irradiation process, i.e. the number of photons per second and per surface area is plotted versus the VUV photon energy. The flux recorded without the Ar gas filter (green graph) is double as high as the flux with a gas filter (red graph). The higher energy photons are able to eject an electron from the target DNA sequence. This way, ionizations are induced at low VUV energies (below the ionization threshold), which can be observed in the intensity trend of the photoinduced cation. The cation intensity is plotted versus the VUV photon energy as shown in figure 42b. In the lower photon energy regime (10 - 12 eV) almost no photoinduced cation is observed with a Ar gas filter (red graph), whereas a clear amount of photoinduced cations is observed in the measurement without a Ar gas filter (green graph). The relevant energy regime that is used to obtain the IE of the precursor cation in the present example of the precursor $[M + 3H]^{3+}$ of the DNA sequence 5'-d(A_{12}) is roughly 14 to 15.5 eV. Here, the graph is rising linearly. Comparing the slope of both graphs, it can be seen that the red graph is steeper than the green one resulting in an energy shift of the IE value of 0.2 eV.

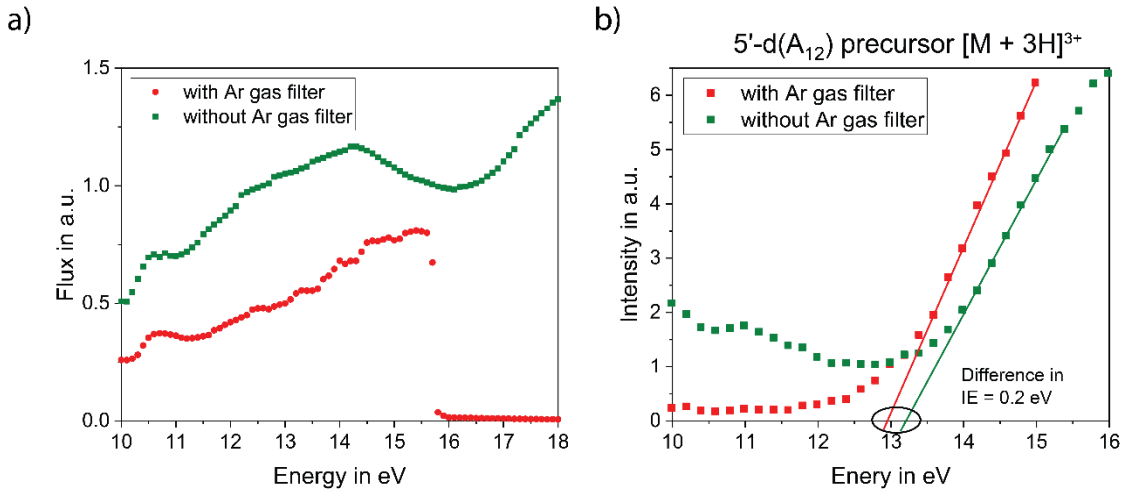

Fig. 42 a) Flux (photons per second and surface area) correlated with the VUV irradiation energy, b) correlation of the intensity of the photoinduced cation (M4+) generated from the precursor cation ($[M + 3H]^{3+}$), and the VUV photon energy; a/b) signal obtained with an Ar gas filter is shown in red and without an Ar gas filter in green.

The use of an Ar gas filter in the way described above is very demanding for the turbomolecular pumps. Therefore, within the synchrotron beamtimes carried out during the present thesis work the Ar gas filter could only be used once for the measurements shown in figure 41. Since all measured photoinduced cations were exposed to the same flux, the relative shift of the IE values of the precursor cations might be very similar, which would preserve the obtained trends of the IE values. Due to this systematic error the IEs determined in the present work are overestimated by approximately 0.2 eV.

6.5 Comparison of the IE trend to the cross sections for SSBs

In this section the trends for the cross sections for SSBs of the different DNA sequences investigated in the present wok are compared to the trend in the IE values of the precursor cations determined by photoionization tandem mass spectrometry. For the DNA sequences 5'-d(A_n) with n = 4, 8, 12, 16, 20, which are differing only in their length, it was observed that the cross section for SSBs was increasing, whereas the IE values are decreasing within the sequence length. Assuming that the IEs of the neutral DNA sequences would follow the same behavior as those of the precursor cations as also reported by Kumar *et al*. [150], the increase of the cross section for SSB with the DNA sequence length can be attributed to the decreasing IE value. The lower the IE values, and thus the lower the ionization threshold of the DNA sequence, the higher the probability of inducing a SSB *via* the ionization process, which leads to higher cross sections for SSBs. The trends of the cross sections for SSBs and the IE trend for the intermixed DNA sequences 5'-d(TT(XTX)$_3$TT) with X = G, A, C correlate in the same way. Herein, the nucleobase with the lowest IE seems to be the crucial subunit determining the IE of the DNA sequence, since the SSB cross sections are increasing in the same order like the IEs of the isolated nucleobases [2].

The mono-nucleobase DNA sequences 5'-d(X_{12}) with X = A, C, G, T do not show a pronounced difference in the cross sections for SSBs. Only the SSB cross section for 5'-d(G_{12}) is slightly increased. The IEs of the precursor cations on the other hand indicates that 5'-d(A_{12}) has a lower IE than 5'-d(C_{12}) and 5'-d(T_{12}), which seem not to influence the SSB cross section data. The computed IE study of 5'-d(A_n) with n = 1 - 8 by Kumar *et al*. [150] showed that the IE of the polyadenine stacked nucleobase system decreases exponentially by 0.87 eV from 5'-d(A) to 5'-d(A_8). Gallandi and Körzdörfer [151] reports a decrease of even 2.27 eV from 5'-d(A) to 5'-d(A_6). If a similar IE decrease would be assumed for the other mono nucleobase DNA sequences, the VUV irradiation energy of 8.44eV would exceed all IEs of the target DNA sequences from a certain length on. All mono nucleobase DNA sequences would be affected in a similar way and a similar cross section for SSBs should be expected. This might be supported by the cross sections for SSBs for the DNA sequences 5'-d(TT(ATA)$_3$TT) and 5'-d(TT(CTC)$_3$TT) [25] determined in the framework of my master thesis. Their SSB cross sections are in the same range like those of the mono nucleobase DNA sequences. Herein, the DNA sequence 5'-d(TT(ATA)$_3$TT) shows a slightly higher SSB cross section (increased by around

$0.5 \cdot 10^{-16}$ cm²). This difference indicates that even if the differences between the SSB cross sections of all mono nucleobase and intermixed DNA sequences determined with 8.44 V VUV radiation are very small, an influence of the type of nucleobase remains, which can lower the IE value like observed for the natural telomere DNA sequence (5'-d(TTAGGG)) [119].

The DNA sequences modified with the radiosensitizer ^{5Br}U show a very clear trend in the cross sections for SSBs and only a slight trend for the IE values of the precursor cations. The cross sections for SSBs increase with the decreasing number of A spacers between the nucleobase G and the radiosensitizer, which is incorporated in the DNA sequence. The IE values on the other hand decrease only marginally. Hence, the IE value cannot be the determining parameter in this investigation, which leads to the SSB cross section trend described above. A reaction of ^{5Br}U might rather be induced by a direct excitation of ^{5Br}U reaction followed by a photolysis of the C-Br bond [130], if ^{5Br}U is flanked by G, C, T or by an excitation of G followed by a charge transfer over adjacent A as a bridge (5' side) to ^{5Br}U [73]. To further investigate, which mechanisms might occur in the different DNA sequences, and how the SSB inducing mechanism differs in the modified und non-modified DNA sequences, time-resolved spectroscopy in the ps range would be a possibility. The dynamics of the photo reaction of ^{5Br}U could e.g. be observed and compared to the photoreaction of a brominated DNA sequence with different distances between G and ^{5Br}U. This way the lactone formation as described by Watanabe *et al.* [73] might be observed. This could be realized with a Nd:Yag-Laser (266 nm/4.6 eV) or a ArF-Laser (193 nm/6.3 eV). Both lasers provide photons of a lower energy than the IE of the molecule, but if the pulse length is short enough (picosecond range), a two photon absorption would lead to an ionization, which might be observed spectroscopically as well as subsequent reactions leading to key products and single strand breakage. All trends are summarized and compared in table 21 below.

Tab. 21 Comparison of the sequence dependence for the cross sections of SSBs obtained at 8.44 eV VUV radiation and of the IEs of the precursor cations, both determined for four different DNA sequences.

DNA sequences	**SSB cross section trend at 8.44 eV VUV photon energy**	**IE trend of the precursor cations**
5'-d(A_n) **n = 4, 8, 12, 16, 20**	$A_4 = A_8 < A_{12} < A_{16} \geq A_{20}$	$A_4 > A_8 > A_{12} > A_{16} \geq A_{20}$
5'-d(TT(XTX)$_3$TT) **X = G, A, C**	$TT(ATA)_3TT >$ $TT(CTC)_3TT$ [25]	$TT(GTG)_3TT <$ $TT(ATA)_3TT <$ $TT(CTC)_3TT$
5'-d(X_{12}) **X = A, C, G, T**	$G_{12} > A_{12} \geq T_{12} \geq C_{12}$	T_{12} and $C_{12} > A_{12}$
5'-d(TTG$A_n{}^{5Br}$UTT) **n = 0-5**	n = 0 > 1 > 2 > 3 > 4 > 5	n = 1 ≥ 2 ≥ 3

7. Summary and Outlook

DNA is the carrier of human genetic information and is exposed to many environmental influences every day such as the UV fraction of sunlight. The photostability of the DNA against UV light (380 nm-100 nm/3.26 eV-12.4 eV) is astonishing. Even if the DNA bases have a strong absorption at the wavelength of 300 nm-200 nm (4.13 eV-6.2 eV) with a maximum at around 260 nm/4.77 eV, their quantum yield of photoproducts remains very low [1]. If the photon energies exceed the IEs of the nucleobases (~8-9 eV) [2], the DNA can be severely damaged. The damage becomes irreparable, when two SSBs in close proximity occur in a dsDNA strand and form a DSB, so that the cell induces its own death (apoptosis). My work focuses on the investigation of SSBs for a variety of target DNA sequences induced by VUV photons in the energy range of the IEs of the DNA components. The target DNA sequences differ in their type of nucleobase, the DNA sequence length and in the modification with the radiosensitizers ^{5Br}U and ^{8Br}A. To investigate the various target DNA sequences in experimentally comparable conditions, they were incorporated in DNA origami nanostructures and adsorbed on a substrate surface (CaF_2 or Si). The DNA origami technique enables us to perform measurements on a single molecular level, which allows to obtain absolute values for the strand breakage. For the VUV photon irradiations an energy of 8.44 eV was applied, since this energy is close to the IEs [2] of the nucleobases as the part of the DNA with the lowest IEs [2,27,28]. If the primary photon energy exceeds the IE of the molecule, an electron can be ejected to consequently ionize the DNA system. Only excitation reactions will occur, if the primary photon energy is too low to induce an ionization. Both processes (photoionization and excitation) will lead to SSBs, but to a different extent. The efficiency of the excitation and ionization induced strand breaks in the target DNA sequences are represented by the cross sections for SSBs determined for every single target DNA sequence. If Si instead of CaF_2 as a substrate material was used in the VUV radiation experiments, secondary electrons with an energy below 3.6 eV were generated from the substrate. LEEs in this energy regime are known to be responsible for a high amount of DNA damage, since they are generated secondarily from ionizing radiation in cancer radiation therapy. LEEs have the ability to attach to the DNA directly and induce SSBs *via* the DEA process. Hence, in the target DNA sequences investigated on Si as a substrate even three process occur (photoexcitation and -ionization, and DEA), which are represented in the SSB cross sections determined in the VUV irradiation experiments.

To estimate, whether the photoionization already occurs at a VUV energy of 8.44 eV, photoionization tandem mass spectrometry was applied on the same target DNA sequences as used for the irradiation experiments. The target DNA sequences were ionized with ESI in the positive mode to access two to four different precursor cations in the MS 1 spectra. Each precursor cation was isolated in the ion trap to be irradiated with the VUV beam from 8 to 16 eV. When the IE of the precursor cation is reached, an

electron will be ejected and a photoinduced cation generated. From the appearance energy of the photoinduced cation, the IE of the precursor cation can be determined. This way, a trend of the IE values in dependency of the type of nucleobase, the strand length and the influence of the radiosensitizer ^{5Br}U could be identified.

The IE trends together with the SSB cross sections are key findings of this work, which are presented in the following. Regarding the mono-nucleobase DNA sequences 5'-d(X_{12}) with X = A, C, G, T irradiated with 8.44 eV VUV photons on CaF_2 as a substrate, no significant difference in the cross sections for SSBs could be found indicating no dependency of the photoexcitation and -ionization as an initial step to a SSB. The DNA sequence 5'-d(C_{12}) showed the lowest cross section for SSBs with $\sigma = (1.7 \pm 0.1) \cdot 10^{-16}$ cm² and 5'-d(G_{12}) the highest cross section for SSBs with $\sigma = (2.3 \pm 0.2) \cdot 10^{-16}$ cm². SSB cross sections for the intermixed DNA sequences 5'-d(TT(XTX)$_3$TT) with X = A, C determined in the framework of my master thesis [25] are in the same range and confirm the present results. When the same mono-nucleobase DNA sequences were irradiated on Si as a substrate material, a clear dependency of the cross sections for SSBs on the type of nucleobase with $T_{12} > A_{12} \geq C_{12} > G_{12}$ could be observed. The LEEs generated from the substrate (< 3.6 eV) induce additional SSBs *via* DEA, which are highly dependent on the type of nucleobase, since strong resonances in the DNA molecule are reported [18,108]. The IEs of the precursor cations of the mono-nucleobase and intermixed DNA sequences show a correlation to the IEs of the single nucleobases (G < A < C < T) [2], when only the nucleobase in the DNA sequences with the lowest IE is considered as the IE determining subunit. 5'-d(A_{12}) shows increased IE values in comparison to 5'-d(C_{12}) and 5'-d(T_{12}), and the intermixed DNA sequences show IEs in the order of 5'-d(TT(GTG)$_3$TT) > 5'-d(TT(ATA)$_3$TT) > 5'-d(TT(CTC)$_3$TT). This indicates that DNA sequences containing the nucleobase G might show a higher SSB cross section, since the photoionization occurs already at a lower energy, which is consistent with the findings of this work. The increased SSB cross sections for 5'-d(TT(ATA)$_3$TT) in comparison to 5'-d(TT(CTC)$_3$TT) [25] are also reflected in the IE trend determined in the present work. Now, it would be interesting to extend the irradiation experiments as well as the tandem mass spectrometry experiments to dsDNA, which is closer to the natural conditions in the cell. Since two SSBs in a close proximity have to occur to form a DBS, lower DSB cross sections would be expected. The IE of a base pair on the other hand shows decreased as well as increased values in computations [164]. Since Koopmans' Theorem is applied here [164], where orbital relaxation and electron correlation are not considered, this is just a rough approximation. Both, the IEs and the SSB cross section would therefore be interesting to be determined experimentally.

Furthermore, the mono-nucleobase DNA sequence 5'-d(A_n) was varied in its length with n = 4, 8, 12, 16 and 20. With the increasing number of nucleotides, the geometrical cross section is increasing as well. For the DNA sequences with a length of n = 8, 12 and 16 nucleotides, the cross sections for SSBs is increasing nearly in the same way as the geometrical cross section. The shortest DNA sequence 5'-d(A_4) does not show a

significant difference compared to 5'-d(A_8). For the longest DNA sequence 5'-d(A_{20}) on the other hand an interesting behavior is observed. The cross section for SSBs is slightly decreased in comparison to the DNA sequence 5'-d(A_{16}), which might be due to conformational changes in the DNA from a linear to a more coiled structure. This way, additional hydrogen bonding within the DNA sequence could hold the DNA strand together, even if a SSB occurred, so that the SSB cannot be detected and the cross section for SSBs appears to be lower. Concerning the corresponding IE values determined *via* tandem mass spectrometry it was shown that the IE values on the one hand increase with the charge state of the precursor ion, which can be attributed to the increasing Coulomb repulsion of the ejected electron to the ion core. On the other hand the IE value of the precursor ion was increasing with the length of the DNA sequence, which can be attributed to a lowering of the potential energy that is induced with an increasing charge separation. Also here, SSB cross sections are correlating with the IE values of the precursor cations. A high SSB cross section is accompanied by a low IEs of the precursor cations matching with the length of the polyadenine DNA sequence. These findings correlate additionally to the computed IE trend proposed for the neutral polyadenine systems by Kumar *et al.* [150] and Gallandi and Körzdörfer [151]. Moreover, two procedures were tested to obtain the IE of the neutral DNA sequence from a linear fit of the IE values of the precursor cations to their charge states. Both procedures resulted in overestimated IE values. The second procedure at least reflected the correct trend of a decreasing IE with an increasing length of the DNA strand. To check, whether the determined IE values of the precursor cations are reasonable, computed IEs of precursor cations as well as IE of a neutral DNA sequence were provided by Lukas Gallandi and Thomas Körzdörfer of the Department of Theoretical Chemistry, University of Potsdam. They performed ΔSCF@B3LYP calculations on a polyadenine sequence of four stacked nucleobases at 0 K and of a less stacked geometry at 300 K. The computed IEs of the precursor cations show for 300 K in comparison to 0 K a distinct deviation from a linear correlation of the IEs to their charge states. These results clearly show that a linear correlation of the IEs of the precursor cations to their charge states under the current experimental conditions lead to wrong IE values of the neutral DNA system and cannot be applied here. To further investigate the conformational changes in the ssDNA, which might be responsible for several finding in this work, ion mobility spectrometry (IMS) could be applied. The DNA molecule can be ionized by ESI as well and would be separated by its structure, while flying through a drift tube, where on the one hand an electric field and on the other hand an opposed gas stream is applied. This way coiled, linear or intermediate DNA structures at different charge states could be identified.

Intermixed DNA sequences modified with the radiosensitizers ^{5Br}U and ^{8Br}A were also investigated. Both molecules can be easily incorporated in the DNA sequence, since they are structurally very similar to the natural nucleobases. First, a DNA sequence, where ^{5Br}U is flanked by the nucleobases X = C, G, or T within the DNA sequences 5'-d(TT(X^{5Br}UX)$_3$TT), was chosen to be investigated with respect to 8.44 eV VUV radiation. This way, the influence of the adjacent nucleobase on the strand breakage was

elucidated. In the proposed strand break mechanism an excitation of ^{5Br}U occurs that decays *via* the homolytic cleavage of the C-Br bond releasing an uracil-5-yl radical, which reacts further to induce a SSB [128,130]. Very high cross sections for SSBs were obtained for the DNA sequences 5'-d(TT(X^{5Br}UX)$_3$TT) with X = T, C and G with $\sigma = (10.2 \pm 1.1) \cdot 10^{-16}$ cm², $\sigma = (10.5 \pm 1.3) \cdot 10^{-16}$ cm² and $\sigma = (7.9 \pm 0.4) \cdot 10^{-16}$ cm², respectively. These results illustrate the high sensitivity of the radiosensitizer ^{5Br}U against VUV light. In the DNA sequence 5'-d(TTGA$_n$^{5Br}UTT) with n = 0 - 5 , when A is adjacent at the 5'side to ^{5Br}U and separates this way G from the radiosensitizer, a different mechanism proposed by Watanabe *et al.* [73] emerges. The excitation of ^{5Br}U occurs with an initial charge transfer, which results in a lactone formation that is in turn thermally not stable and results in a cleavage in the DNA backbone, i.e. in a SSB. This mechanism is highly distance dependent, which is reflected by a decreasing SSB cross section with the increasing number of A spacers ($\sigma = (3.5 \pm 1.3) \cdot 10^{-16}$ cm² for n = 1 to $\sigma = (2.5 \pm 0.7) \cdot 10^{-16}$ cm² for n = 5). At n = 5 the SSB cross section is almost as low as those obtained for non-brominated DNA sequences, indicating that in this specific sequences either photolysis or a charge transfer reaction occur that would form the uracil-5-yl radical, which is a strand break precursor. The IEs of the precursor cations of the DNA sequences 5'-d(TTGA$_n$^{5Br}UTT), n = 1-3 were investigated as well. Herein no significant trend can be observed, indicating that ionization might not be the triggering step that leads to strand breakage, which agrees with excitation activated reactions described above.

The radiosensitizer ^{8Br}A on the other hand does not show a significant SSB enhancement, neither for the VUV photon radiation nor the indirect LEE radiation. ^{8Br}A was incorporated in the DNA sequence 5'-d(TT(^{8Br}ATA)$_3$TT) and investigated in direct comparison to the non-modified DNA sequence 5'-d(TT(ATA)$_3$TT). Apparently, no adenyl radical is formed *via* photolysis or DEA, which could react further to induce single strand breakage. Consequently, ^{5Br}U can be recommended as a radiosensitizer, since it shows great response to the applied VUV irradiation and is already know to be very effective in SSB generation in the UV range [73,128,131]. ^{8Br}A on the other hand shows barely any response at this irradiation energy, but might be rather active in water as a surrounding media [138] or under electron radiation of higher energies (7-8 eV) [116]. It would also be interesting to investigate the ability of the two radiosensitizers in dsDNA or even in cell line experiments, since both system are closer to the natural conditions in the cell.

Bibliography

1. Middleton, C.T. *et al.* DNA excited-state dynamics. From single bases to the double helix. *Annual review of physical chemistry* **60,** 217–239 (2009).
2. Cauët, E., Dehareng, D. & Liévin, J. Ab initio study of the ionization of the DNA bases. Ionization potentials and excited states of the cations. *The journal of physical chemistry. A* **110,** 9200–9211 (2006).
3. Alberts, B. *Molecular biology of the cell.* 4th ed. (Garland, New York, 2002).
4. Sinha, R.P. & Häder, D.-P. UV-induced DNA damage and repair. A review. *Photochem. Photobiol. Sci.* **1,** 225–236 (2002).
5. Gofman, J.W. *Radiation and human health* (1981).
6. Hecht, S.S. Cigarette smoking. Cancer risks, carcinogens, and mechanisms. *Langenbeck's archives of surgery* **391,** 603–613 (2006).
7. Schultz, T. *et al.* Efficient deactivation of a model base pair via excited-state hydrogen transfer. *Science (New York, N.Y.)* **306,** 1765–1768 (2004).
8. Grollman, A.P. & Moriya, M. Mutagenesis by 8-oxoguanine. An enemy within. *Trends in Genetics* **9,** 246–249 (1993).
9. Cadet, J., Sage, E. & Douki, T. Ultraviolet radiation-mediated damage to cellular DNA. *Mutation research* **571,** 3–17 (2005).
10. Gallandi, L. & Körzdörfer, T. Long-Range Corrected DFT Meets GW. Vibrationally Resolved Photoelectron Spectra from First Principles. *J. Chem. Theory Comput.* **11,** 5391–5400 (2015).
11. Hoeijmakers, J.H.J. DNA repair mechanisms. *Maturitas* **38,** 17–22 (2001).
12. Jeggo, P.A. & Löbrich, M. DNA double-strand breaks. Their cellular and clinical impact? *Oncogene* **26,** 7717–7719 (2007).
13. Torre, L.A. *et al.* Global cancer statistics, 2012. *CA: a cancer journal for clinicians* **65,** 87–108 (2015).
14. Miller, K.D. *et al.* Cancer treatment and survivorship statistics, 2016. *CA: a cancer journal for clinicians* **66,** 271–289 (2016).
15. Dasari, S. & Tchounwou, P.B. Cisplatin in cancer therapy. Molecular mechanisms of action. *European journal of pharmacology* **740,** 364–378 (2014).
16. Pimblott, S.M. & LaVerne, J.A. Production of low-energy electrons by ionizing radiation. *Radiation Physics and Chemistry* **76,** 1244–1247 (2007).
17. Sonntag, C. von. *Free-Radical-Induced DNA Damage and Its Repair* (Springer Berlin Heidelberg, Berlin, Heidelberg, 2006).
18. Badia Boudaïffa, Pierre Cloutier, Darel Hunting, Michael A. Huels, Léon Sanche. Resonant Formation of DNA Strand Breaks by Low-Energy (3 to 20 eV) Electrons. *Science* **287,** 1658–1660 (2000).
19. Li, X., Sevilla, M.D. & Sanche, L. Density functional theory studies of electron interaction with DNA. Can zero eV electrons induce strand breaks? *Journal of the American Chemical Society* **125,** 13668–13669 (2003).
20. Gu, J., Wang, J. & Leszczynski, J. Electron attachment-induced DNA single strand breaks. C3'-O3' sigma-bond breaking of pyrimidine nucleotides predominates. *Journal of the American Chemical Society* **128,** 9322–9323 (2006).
21. Richardson, N.A., Gu, J., Wang, S., Xie, Y. & Schaefer III, H.F. DNA nucleosides and their radical anions. Molecular structures and electron affinities. *Journal of the American Chemical Society* **126,** 4404–4411 (2004).

22. Alizadeh, E., Orlando, T.M. & Sanche, L. Biomolecular damage induced by ionizing radiation. The direct and indirect effects of low-energy electrons on DNA. *Annual review of physical chemistry* **66,** 379–398 (2015).
23. Rackwitz, J. & Bald, I. Low-Energy Electron-Induced Strand Breaks in Telomere-Derived DNA Sequences-Influence of DNA Sequence and Topology. *Chem. Eur. J.,* 1–10 (2018).
24. Rackwitz, J., Ranković, M.L., Milosavljević, A.R. & Bald, I. A novel setup for the determination of absolute cross sections for low-energy electron induced strand breaks in oligonucleotides – The effect of the radiosensitizer 5-fluorouracil*. *Eur. Phys. J. D* **71,** R287 (2017).
25. Vogel S., Rackwitz J., Schümann R., Prinz, J., Milosavljevic´ A., Réfrégiers M., Giuliani, A., Bals I., Using DNA origami nanostructures to determine absolute cross sections for UV photon-induced DNA strand breakage. *The journal of physical chemistry letters* **6,** 4589–4593 (2015).
26. Cadet, J., Douki, T. & Ravanat, J.-L. Oxidatively generated damage to cellular DNA by UVB and UVA radiation. *Photochemistry and photobiology* **91,** 140–155 (2015).
27. Ghosh, D., Golan, A., Takahashi, L.K., Krylov, A.I. & Ahmed, M. A VUV Photoionization and Ab Initio Determination of the Ionization Energy of a Gas-Phase Sugar (Deoxyribose). *The journal of physical chemistry letters* **3,** 97–101 (2012).
28. Colson, A.O., Besler, B. & Sevilla, M.D. Ab initio molecular orbital calculations on DNA radical ions. 3. Ionization potentials and ionization sites in components of the DNA sugar phosphate backbone. *J. Phys. Chem.* **97,** 8092–8097 (1993).
29. Chapman, J.D., Reuvers, A.P., Borsa, J. & Greenstock, C.L. Chemical Radioprotection and Radiosensitization of Mammalian Cells Growing in Vitro. *Radiation Research* **56,** 291 (1973).
30. Nguyen, J. *et al.* Direct observation of ultrafast-electron-transfer reactions unravels high effectiveness of reductive DNA damage. *Proceedings of the National Academy of Sciences of the United States of America* **108,** 11778–11783 (2011).
31. Gomez, C.R. Editorial. Tumor Hypoxia: Impact in Tumorigenesis, Diagnosis, Prognosis, and Therapeutics. *Frontiers in oncology* **6,** 229 (2016).
32. Godefridus J. Peters. *Deoxynucleoside Analogs In Cancer Therapy* (Humana Press, Totowa, N.J., 2006).
33. Abdoul-Carime, H. *et al.* Sensitization of 5-bromouridine by slow electrons. *Chemical Physics Letters* **393,** 442–447 (2004).
34. Schürmann, R., Tanzer, K., Dąbkowska, I., Denifl, S. & Bald, I. Stability of the Parent Anion of the Potential Radiosensitizer 8-Bromoadenine Formed by Low-Energy (<3 eV) Electron Attachment. *The journal of physical chemistry. B* **121,** 5730–5734 (2017).
35. Rak, J. *et al.* Mechanisms of Damage to DNA Labeled with Electrophilic Nucleobases Induced by Ionizing or UV Radiation. *The journal of physical chemistry. B* **119,** 8227–8238 (2015).
36. Zheng, Y. & Sanche, L. Effective and absolute cross sections for low-energy (1-30 eV) electron interactions with condensed biomolecules. *Applied Physics Reviews* **5,** 21302 (2018).
37. Rothemund, P.W.K. Folding DNA to create nanoscale shapes and patterns. *Nature* **440,** 297–302 (2006).

38. Keller, A. *et al.* Probing electron-induced bond cleavage at the single-molecule level using DNA origami templates. *ACS nano* **2012,** 4392–4399 (2012).
39. Choy, H. *Chemoradiation in cancer therapy* (Humana Press, Totowa, N.J., 2003).
40. Folkard, K. M. Prise B. Vojnovic M., B. Brocklehurst, B. D. Michael. Critical energies for ssb and dsb induction in plasmid DNA by vacuum-UV photons. An arrangement for irradiating dry or hydrated DNA with monochromatic photons. *International Journal of Radiation Biology* **76,** 763–771 (1999).
41. Śmiałek, M.A., Balog, R., Jones, N.C., Field, D. & Mason, N.J. Preparation of DNA films for studies under vacuum conditions. *Eur. Phys. J. D* **60,** 31–36 (2010).
42. Śmiałek, M.A., Jones, N.C., Balog, R., Mason, N.J. & Field, D. The influence of the substrate temperature on the preparation of DNA films for studies under vacuum conditions. *Eur. Phys. J. D* **62,** 197–203 (2011).
43. Li, Z., Cloutier, P., Sanche, L. & Wagner, J.R. Low-energy electron-induced DNA damage. Effect of base sequence in oligonucleotide trimers. *Journal of the American Chemical Society* **132,** 5422–5427 (2010).
44. Bald, I., Langer, J., Tegeder, P. & Ingólfsson, O. From isolated molecules through clusters and condensates to the building blocks of life. *International Journal of Mass Spectrometry* **277,** 4–25 (2008).
45. Kopyra, J. Low energy electron attachment to the nucleotide deoxycytidine monophosphate. Direct evidence for the molecular mechanisms of electron-induced DNA strand breaks. *Physical chemistry chemical physics : PCCP* **14,** 8287–8289 (2012).
46. Ptasińska, S. & Sanche, L. Dissociative electron attachment to hydrated single DNA strands. *Physical review. E, Statistical, nonlinear, and soft matter physics* **75,** 31915 (2007).
47. Watson, J.D. & Crick, F.H.C. Molecular structure of nucleic acids; a structure for deoxyribose nucleic acid. *Nature* **171,** 737–738 (1953).
48. Sponer, J., Riley, K.E. & Hobza, P. Nature and magnitude of aromatic stacking of nucleic acid bases. *Physical chemistry chemical physics : PCCP* **10,** 2595–2610 (2008).
49. Michelotti, N., Johnson-Buck, A., Manzo, A.J. & Walter, N.G. Beyond DNA origami. The unfolding prospects of nucleic acid nanotechnology. *Wiley interdisciplinary reviews. Nanomedicine and nanobiotechnology* **4,** 139–152 (2012).
50. Saenger, W. Water and Nucleic Acids. *Springer Advanced Texts in Chemistry, NY,* 368–384 (1984).
51. Dickerson, R.E., pp. 67–111.
52. A. Rich, A. Nordheim, A. H.-f. Wang. The Chemistry and Biology of Left-Handed Z-DNA. *Ann. Rev. Biochem.,* 791–846 (1984).
53. Zhang, H., Yu, H., Ren, J. & Qu, X. Reversible B/Z-DNA transition under the low salt condition and non-B-form polydApolydT selectivity by a cubane-like europium-L-aspartic acid complex. *Biophysical journal* **90,** 3203–3207 (2006).
54. Meyer, T., La Cruz, X. de & Orozco, M. An atomistic view to the gas phase proteome. *Structure (London, England : 1993)* **17,** 88–95 (2009).
55. Rueda, M., Kalko, S.G., Luque, F.J. & Orozco, M. The structure and dynamics of DNA in the gas phase. *Journal of the American Chemical Society* **125,** 8007–8014 (2003).

56. Colominas, C., Luque, F.J. & Orozco, M. Tautomerism and Protonation of Guanine and Cytosine. Implications in the Formation of Hydrogen-Bonded Complexes. *Journal of the American Chemical Society* **118,** 6811–6821 (1996).
57. Hoaglund, C.S., Liu, Y., Ellington, A.D., Pagel, M. & Clemmer, D.E. Gas-Phase DNA. Oligothymidine Ion Conformers. *Journal of the American Chemical Society* **119,** 9051–9052 (1997).
58. Phillips, D.R. & McCloskey, J.A. A comprehensive study of the low energy collision-induced dissociation of dinucleoside monophosphates. *International Journal of Mass Spectrometry and Ion Processes* **128,** 61–82 (1993).
59. Douglas, S.M. *et al.* Self-assembly of DNA into nanoscale three-dimensional shapes. *Nature* **459,** 414–418 (2009).
60. Beaucage, S.L. & Caruthers, M.H. Deoxynucleoside phosphoramidites—A new class of key intermediates for deoxypolynucleotide synthesis. *Tetrahedron Letters* **22,** 1859–1862 (1981).
61. Chao, J., Zhu, D., Zhang, Y., Wang, L. & Fan, C. DNA nanotechnology-enabled biosensors. *Biosensors & bioelectronics* **76,** 68–79 (2016).
62. Tan, S.J., Campolongo, M.J., Luo, D. & Cheng, W. Building plasmonic nanostructures with DNA. *Nature nanotechnology* **6,** 268–276 (2011).
63. Pei, H., Zuo, X., Zhu, D., Huang, Q. & Fan, C. Functional DNA nanostructures for theranostic applications. *Accounts of chemical research* **47,** 550–559 (2014).
64. Tasciotti, E. Smart cancer therapy with DNA origami. *Nature biotechnology* **36,** 234–235 (2018).
65. Prokhorenko, V.I., Picchiotti, A., Pola, M., Dijkstra, A.G. & Miller, R.J.D. New Insights into the Photophysics of DNA Nucleobases. *The journal of physical chemistry letters* **7,** 4445–4450 (2016).
66. Malinge, J.-M., Giraud-Panis, M.-J. & Leng, M. Interstrand cross-links of cisplatin induce striking distortions in DNA. *Journal of Inorganic Biochemistry* **77,** 23–29 (1999).
67. Gabelica, V. *Gabelica, Valérie. Nucleic Acids in the Gas Phase* (Springer, 2016).
68. Eley, D. D., Spivey, D. I. Semiconductivity of organic substances. Part 9.-Nucleic acid in the dry state. *Transactions of the Faraday Society,* 411–415 (1962).
69. Endres, R.G., Cox, D.L. & Singh, R.R.P. Colloquium. The quest for high-conductance DNA. *Rev. Mod. Phys.* **76,** 195–214 (2004).
70. Voityuk, A.A. Effects of dynamic disorder on exciton delocalization and photoinduced charge separation in DNA. *Photochemical & photobiological sciences : Official journal of the European Photochemistry Association and the European Society for Photobiology* **12,** 1303–1309 (2013).
71. Marcus, R.A. & Sutin, N. Electron transfers in chemistry and biology. *Biochimica et Biophysica Acta (BBA) - Reviews on Bioenergetics* **811,** 265–322 (1985).
72. Giese, B. & Spichty, M. Long Distance Charge Transport through DNA. Quantification and Extension of the Hopping Model. *ChemPhysChem* **1,** 195–198 (2000).
73. Watanabe, T., Tashiro, R. & Sugiyama, H. Photoreaction at 5'-(G/C)AA(Br)UT-3' sequence in duplex DNA. Efficient generation of uracil-5-yl radical by charge transfer. *Journal of the American Chemical Society* **129,** 8163–8168 (2007).

74. Cadet, J., Douki, T. & Ravanat, J.-L. Oxidatively generated damage to the guanine moiety of DNA. Mechanistic aspects and formation in cells. *Accounts of chemical research* **41,** 1075–1083 (2008).
75. Seidel, C.A.M., Schulz, A. & Sauer, M.H.M. Nucleobase-Specific Quenching of Fluorescent Dyes. 1. Nucleobase One-Electron Redox Potentials and Their Correlation with Static and Dynamic Quenching Efficiencies. *J. Phys. Chem.* **100,** 5541–5553 (1996).
76. Joseph, J. & Schuster, G.B. Emergent functionality of nucleobase radical cations in duplex DNA. Prediction of reactivity using qualitative potential energy landscapes. *Journal of the American Chemical Society* **128,** 6070–6074 (2006).
77. Ferran Prat, K. N. Houk, Christopher S. Foote. Effect of guanine stacking on the oxidation of 8-oxoguanine in B-DNA. *J. Am. Chem. Soc* **1998,** 845–846.
78. Berger, M., Anselmino, C., Mouret, J.-F. & Cadet, J. High Performance Liquid Chromatography-Electrochemical Assay for Monitoring the Formation of 8-Oxo-7,8-dihydroadenine and its Related 2′-Deoxyribonucleoside. *Journal of Liquid Chromatography* **13,** 929–940 (1990).
79. Kanvah, S. *et al.* Oxidation of DNA. Damage to nucleobases. *Accounts of chemical research* **43,** 280–287 (2010).
80. Wiczk, J., Miloch, J. & Rak, J. UV-Induced Strand Breaks in Double-Stranded DNA Labeled with 5-Bromouracil. Frank or Secondary? *The journal of physical chemistry letters* **4,** 4014–4018 (2013).
81. Rattemeyer, M., Popp, F.A. & Nagl, W. Evidence of photon emission from DNA in living systems. *Naturwissenschaften* **68,** 572–573 (1981).
82. Liss, K.-D., Bartels, A., Schreyer, A. & Clemens, H. High-Energy X-Rays. A tool for Advanced Bulk Investigations in Materials Science and Physics. *Textures and Microstructures* **35,** 219–252 (2003).
83. Deutsches Krebsforschungszentrum - Krebsinformationsdienst. Radiation therapy and nuclear medicine. Available at. Available at https://www.krebsinformationsdienst.de/behandlung/strahlentherapie-physik.php.
84. Heidelberg Ion Beam Therapy Center. Proton and heavy ion therapy. Available at https://www.heidelberg-university-hospital.com/de/erkrankungen-behandlungen/tumorerkrankungen/protonen-und-schwerionentherapie/.
85. Strohmaier, S. & Zwierzchowski, G. Comparison of (60)Co and (192)Ir sources in HDR brachytherapy. *Journal of contemporary brachytherapy* **3,** 199–208 (2011).
86. M. Wannenmacher, J. Debus & F. Wenz eds. *Strahlentherapie* (Springer, 2006).
87. Burke, D.L. *et al.* Positron Production in Multiphoton Light-by-Light Scattering. *Physical review letters* **79,** 1626–1629 (1997).
88. Brini, D., Fuschini, E., Grimellini, N.T. & Murty, D.S.R. Compton effect on the bound electrons. *Nuovo Cim* **16,** 727–736 (1960).
89. Adawi, I. Theory of the Surface Photoelectric Effect for One and Two Photons. *Phys. Rev.* **134,** A788-A798 (1964).
90. J. A. O'Donoghue, T. E. Wheldon. Targeted radiotherapy using Auger electron emitters. *Phys. Med. Biol.,* 1973–1992 (1996).
91. Trinter, F. *et al.* Evolution of interatomic Coulombic decay in the time domain. *Physical review letters* **111,** 93401 (2013).
92. Neufingerl, F. *Chemie 1. Allgemeine und anorganische Chemie* (Jugend & Volk, Wien, 2006).

93. Kang, H., Lee, K.T., Jung, B., Ko, Y.J. & Kim, S.K. Intrinsic Lifetimes of the Excited State of DNA and RNA Bases. *Journal of the American Chemical Society* **124,** 12958–12959 (2002).
94. Gomes, P.J. *et al.* Energy Thresholds of DNA Damage Induced by UV Radiation: An XPS Study. An XPS Study. *The journal of physical chemistry. B* **119,** 5404–5411 (2015).
95. Hieda, K. DNA Damage Induced by Vacuum and Soft X-ray Photons from Synchrotron Radiation. *International Journal of Radiation Biology* **66,** 561–567 (1994).
96. M. Prise, M. Folkard B. D. Michael, K.B. Vojnovic, B. Brocklehurst, A. Hopkirk, I. H. Munro. Critical energies for SSB and DSB induction in plasmid DNA by low-energy photons. Action spectra for strand-break induction in plasmid DNA irradiated in vacuum. *International Journal of Radiation Biology* **76,** 881–890 (2000).
97. Wehner, J. & Horneck, G. Effects of vacuum UV and UVC radiation on dry E. coli plasmid pUC19 I. Inactivation, lacZ− mutation induction and strand breaks. *Journal of Photochemistry and Photobiology B: Biology* **28,** 77–85 (1995).
98. González-Magaña, O. *et al.* Fragmentation of protonated oligonucleotides by energetic photons and C q+ ions. *Phys. Rev. A* **87** (2013).
99. Shin, J.-W. & Bernstein, E.R. Vacuum ultraviolet photoionization of carbohydrates and nucleotides. *The Journal of chemical physics* **140,** 44330 (2014).
100. Barrios, R., Skurski, P. & Simons, J. Mechanism for Damage to DNA by Low-Energy Electrons †. *J. Phys. Chem. B* **106,** 7991–7994 (2002).
101. Simons, J. How do low-energy (0.1-2 eV) electrons cause DNA-strand breaks? *Accounts of chemical research* **39,** 772–779 (2006).
102. Zheng, Y., Cloutier, P., Hunting, D.J., Wagner, J.R. & Sanche, L. Glycosidic bond cleavage of thymidine by low-energy electrons. *Journal of the American Chemical Society* **126,** 1002–1003 (2004).
103. Zheng, Y., Cloutier, P., Hunting, D.J., Wagner, J.R. & Sanche, L. Phosphodiester and N-glycosidic bond cleavage in DNA induced by 4-15 eV electrons. *The Journal of chemical physics* **124,** 64710 (2006).
104. Aflatooni, K., Gallup, G.A. & Burrow, P.D. Electron Attachment Energies of the DNA Bases. *The journal of physical chemistry. A* **102,** 6205–6207 (1998).
105. Ptasińska, S. *et al.* Bond-selective H- ion abstraction from thymine. *Angewandte Chemie (International ed. in English)* **44,** 1647–1650 (2005).
106. Ptasińska, S. *et al.* Bond- and site-selective loss of H- from pyrimidine bases. *Physical review letters* **95,** 93201 (2005).
107. Denifl, S. *et al.* Electron Attachment to the Gas-Phase DNA Bases Cytosine and Thymine. *The journal of physical chemistry. A* **108,** 6562–6569 (2004).
108. Martin, F. *et al.* DNA strand breaks induced by 0-4 eV electrons. The role of shape resonances. *Physical review letters* **93,** 68101 (2004).
109. Abdoul-Carime, H., Gohlke, S., Fischbach, E., Scheike, J. & Illenberger, E. Thymine excision from DNA by subexcitation electrons. *Chemical Physics Letters* **387,** 267–270 (2004).
110. Anusiewicz, I., Berdys, J., Sobczyk, M., Skurski, P. & Simons, J. Effects of Base π-Stacking on Damage to DNA by Low-Energy Electrons. *The journal of physical chemistry. A* **108,** 11381–11387 (2004).

111. Berdys, J., Anusiewicz, I., Skurski, P. & Simons, J. Theoretical Study of Damage to DNA by 0.2−1.5 eV Electrons Attached to Cytosine †. *The journal of physical chemistry. A* **108,** 2999–3005 (2004).
112. Berdys, J., Anusiewicz, I., Skurski, P. & Simons, J. Damage to model DNA fragments from very low-energy (<1 eV) electrons. *Journal of the American Chemical Society* **126,** 6441–6447 (2004).
113. Berdys, J., Skurski, P. & Simons, J. Damage to Model DNA Fragments by 0.25−1.0 eV Electrons Attached to a Thymine π* Orbital. *J. Phys. Chem. B* **108,** 5800–5805 (2004).
114. Théodore, M., Sobczyk, M. & Simons, J. Cleavage of thymine N3–H bonds by low-energy electrons attached to base π∗ orbitals. *Chemical Physics* **329,** 139–147 (2006).
115. Panajotovic, R., Martin, F., Cloutier, P., Hunting, D. & Sanche, L. Effective Cross Sections for Production of Single-Strand Breaks in Plasmid DNA by 0.1 to 4.7 eV Electrons. *Radiation Research* **165,** 452–459 (2006).
116. Schürmann, R. *et al.* Resonant Formation of Strand Breaks in Sensitized Oligonucleotides Induced by Low-Energy Electrons (0.5-9 eV). *Angewandte Chemie (International ed. in English)* **56,** 10952–10955 (2017).
117. Vogel S., Ebel K., Schürmann R., Heck C., Guiliani A., Milosavljević A. R., Bald I., Vacuum-UV and Low-Energy Electron Induced DNA Strand Breaks – Influence of the DNA Sequence and Substrate. *submitted* (2018).
118. Keller, A. *et al.* Sequence dependence of electron-induced DNA strand breakage revealed by DNA nanoarrays. *Scientific reports* **4,** 7391 (2014).
119. Cauët, E. Unique hole-trapping property of the human telomere sequence. *Journal of biomolecular structure & dynamics* **29,** 557–561.
120. Solomun, T., Seitz, H. & Sturm, H. DNA damage by low-energy electron impact. Dependence on guanine content. *The journal of physical chemistry. B* **113,** 11557–11559 (2009).
121. Park, Y., Polska, K., Rak, J., Wagner, J.R. & Sanche, L. Fundamental mechanisms of DNA radiosensitization. Damage induced by low-energy electrons in brominated oligonucleotide trimers. *The journal of physical chemistry. B* **116,** 9676–9682 (2012).
122. Daşu, A. & Denekamp, J. New insights into factors influencing the clinically relevant oxygen enhancement ratio. *Radiotherapy and Oncology* **46,** 269–277 (1998).
123. Burrows, C.J. & Muller, J.G. Oxidative Nucleobase Modifications Leading to Strand Scission. *Chem. Rev.* **98,** 1109–1152 (1998).
124. Wardman, P. Chemical radiosensitizers for use in radiotherapy. *Clinical oncology (Royal College of Radiologists (Great Britain))* **19,** 397–417 (2007).
125. Seiwert, T.Y., Salama, J.K. & Vokes, E.E. The concurrent chemoradiation paradigm--general principles. *Nature clinical practice. Oncology* **4,** 86–100 (2007).
126. Lawrence, T.S. *et al.* The potential superiority of bromodeoxyuridine to iododeoxyuridine as a radiation sensitizer in the treatment of colorectal cancer. *Cancer research* **52,** 3698–3704 (1992).
127. Cook, G.P. & Greenberg, M.M. A Novel Mechanism for the Formation of Direct Strand Breaks upon Anaerobic Photolysis of Duplex DNA Containing 5-

Bromodeoxyuridine. *Journal of the American Chemical Society* **118,** 10025–10030 (1996).
128. Cook, G.P., Chen, T., Koppisch, A.T. & Greenberg, M.M. The effects of secondary structure and O2 on the formation of direct strand breaks upon UV irradiation of 5-bromodeoxy-uridine-containing oligonucleotides. *Chemistry & Biology* **6,** 451–459 (1999).
129. Chen, T., Cook, G.P., Koppisch, A.T. & Greenberg, M.M. Investigation of the Origin of the Sequence Selectivity for the 5-Halo-2‘-deoxyuridine Sensitization of DNA to Damage by UV-Irradiation. *Journal of the American Chemical Society* **122,** 3861–3866 (2000).
130. Kobyłecka, M., Migani, A., Asturiol, D., Rak, J. & Blancafort, L. Benign decay vs. photolysis in the photophysics and photochemistry of 5-bromouracil. A computational study. *The journal of physical chemistry. A* **113,** 5489–5495 (2009).
131. Sugiyama, H., Tsutsumi, Y., & Saito, I. Sugiyama, H., Tsutsumi, Y., & Saito, I. (1990). Highly sequence-selective photoreaction of 5-bromouracil-containing deoxyhexanucleotides. *Journal of the American Chemical Society* **112,** 6720–6721 (1990).
132. Zheng, Y. & Sheppard, T.L. Half-life and DNA strand scission products of 2-deoxyribonolactone oxidative DNA damage lesions. *Chemical research in toxicology* **17,** 197–207 (2004).
133. E. Rivera, R.H.S. Intermediates in the Reduction of 5-Halouracils by e(aq) -1. *The Journal of Physical Chemistry,* 3966–3971 (1983).
134. Gu, J., Leszczynski, J. & Schaefer, H.F. Interactions of electrons with bare and hydrated biomolecules. From nucleic acid bases to DNA segments. *Chemical reviews* **112,** 5603–5640 (2012).
135. Abdoul-Carime, H., Huels, M.A., Illenberger, E. & Sanche, L. Sensitizing DNA to Secondary Electron Damage. Resonant Formation of Oxidative Radicals from 5-Halouracils. *Journal of the American Chemical Society* **123,** 5354–5355 (2001).
136. Schyman, P., Zhang, R.B., Eriksson, L.A. & Laaksonen, A. Hydrogen abstraction from deoxyribose by a neighbouring uracil-5-yl radical. *Physical chemistry chemical physics : PCCP* **9,** 5975–5979 (2007).
137. Wang, S., Zhao, P., Zhang, C. & Bu, Y. Mechanisms Responsible for High Energy Radiation Induced Damage to Single-Stranded DNA Modified by Radiosensitizing 5-Halogenated Deoxyuridines. *The journal of physical chemistry. B* **120,** 2649–2657 (2016).
138. Chomicz, L., Leszczynski, J. & Rak, J. Electron-induced degradation of 8-bromo-2'-deoxyadenosine 3',5'-diphosphate, a DNA radiosensitizing nucleotide. *The journal of physical chemistry. B* **117,** 8681–8688 (2013).
139. International Crystal Laboratories. Calcium Fluoride (CaF2) Optical Crystals. Available at http://www.internationalcrystal.net/iclsite3/optics_06.htm.
140. V. E. Puchin, A. V. Puchin, M. Huisinga, M. Reichling. Theoretical modelling of steps on the CaF 2 (111) surface. *J. Phys.: Condens. Matter,* 2081–2094.
141. SOLEIL Synchrotron. Available at https://www.synchrotron-soleil.fr/ (2016).
142. Giuliani, A. *et al.* DISCO. A low-energy multipurpose beamline at synchrotron SOLEIL. *Journal of synchrotron radiation* **16,** 835–841 (2009).

143. Giuliani, A. *et al.* A differential pumping system to deliver windowless VUV photons at atmospheric pressure. *Journal of synchrotron radiation* **18,** 546–549 (2011).
144. Allen, F.G. & Gobeli, G.W. Work Function, Photoelectric Threshold, and Surface States of Atomically Clean Silicon. *Phys. Rev.* **127,** 150–158 (1962).
145. Liu, J., Yao, X., Cloutier, P., Zheng, Y. & Sanche, L. DNA Strand Breaks Induced by 0–1.5 eV UV Photoelectrons under Atmospheric Pressure. *J. Phys. Chem. C* **120,** 487–495 (2016).
146. West, P. Introduction to Atomic Force Microscopy Theory, Practice, Applications (2006).
147. Milosavljević, A.R. *et al.* Photoionization of a protein isolated in vacuo. *Physical chemistry chemical physics : PCCP* **13,** 15432–15436 (2011).
148. La Fernandez de Mora, J. Electrospray ionization of large multiply charged species proceeds via Dole's charged residue mechanism. *Analytica Chimica Acta* **406,** 93–104 (2000).
149. Labowsky, M., Fenn, J.B. & La Fernandez de Mora, J. A continuum model for ion evaporation from a drop. Effect of curvature and charge on ion solvation energy. *Analytica Chimica Acta* **406,** 105–118 (2000).
150. Kumar, A. & Sevilla, M.D. Density functional theory studies of the extent of hole delocalization in one-electron oxidized adenine and guanine base stacks. *The journal of physical chemistry. B* **115,** 4990–5000 (2011).
151. Gallandi, L. & Körzdörfer, T. *Ionization energies of the DNA sequences 5'-d(An), n=1-4, 6 and their charged cations calculated with ΔSCF@3BLYP and ΔSCF@LC-ωPBE (ω=0.4)* (2018).
152. Johansson, L.S.O., Landemark, E., Hansson, G.V. & Uhrberg, R.I.G. Resonances in the photoemission cross section of surface states on the Si(100)2 × 1 surface. *Surface Science* **211-212,** 578–585.
153. Fujimoto, K., Sugiyama, H. & Saito, I. Sequence dependent photoreduction of 5-bromouracil-contaning oligonucleotides via electron transfer. *Tetrahedron Letters* **39,** 2137–2140 (1998).
154. Wang, J., Yang, B., Cool, T.A., Hansen, N. & Kasper, T. Near-threshold absolute photoionization cross-sections of some reaction intermediates in combustion. *International Journal of Mass Spectrometry* **269,** 210–220 (2008).
155. Sugiyama, H. & Saito, I. Theoretical Studies of GG-Specific Photocleavage of DNA via Electron Transfer. Significant Lowering of Ionization Potential and 5'-Localization of HOMO of Stacked GG Bases in B-Form DNA. *Journal of the American Chemical Society* **118,** 7063–7068 (1996).
156. Budnik, B.A., Tsybin, Y.O., Håkansson, P. & Zubarev, R.A. Ionization energies of multiply protonated polypeptides obtained by tandem ionization in Fourier transform mass spectrometers. *Journal of mass spectrometry : JMS* **37,** 1141–1144 (2002).
157. Budnik, B.A. & Zubarev, R.A. MH2+· ion production from protonated polypeptides by electron impact. Observation and determination of ionization energies and a cross-section. *Chemical Physics Letters* **316,** 19–23 (2000).
158. Giuliani, A. *et al.* Structure and charge-state dependence of the gas-phase ionization energy of proteins. *Angewandte Chemie (International ed. in English)* **51,** 9552–9556 (2012).

159. Becke, A.D. Density-functional thermochemistry. III. The role of exact exchange. *The Journal of chemical physics* **98,** 5648–5652 (1993).
160. Vydrov, O.A. & Scuseria, G.E. Assessment of a long-range corrected hybrid functional. *The Journal of chemical physics* **125,** 234109 (2006).
161. M. J. Frisch, G. W. Trucks, H. B. Schlegel, G. E. Scuseria, M. A. Robb, J. R. Cheeseman, G. Scalmani, V. Barone, B. Mennucci, G. A. Petersson, H. Nakatsuji, M. Caricato, X. Li, H. P. Hratchian, A. F. Izmaylov, J. Bloino, G. Zheng, J. L. Sonnenberg, M. Hada, M. Ehara, K. Toyota, R. Fukuda, J. Hasegawa, M. Ishida, T. Nakajima, Y. Honda, O. Kitao, H. Nakai, T. Vreven, J. A. Montgomery, Jr., J. E. Peralta, F. Ogliaro, M. Bearpark, J. J. Heyd, E. Brothers, K. N. Kudin, V. N. Staroverov, R. Kobayashi, J. Normand, K. Raghavachari, A. Rendell, J. C. Burant, S. S. Iyengar, J. Tomasi, M. Cossi, N. Rega, J. M. Millam, M. Klene, J. E. Knox, J. B. Cross, V. Bakken, C. Adamo, J. Jaramillo, R. Gomperts, R. E. Stratmann, O. Yazyev, A. J. Austin, R. Cammi, C. Pomelli, J. W. Ochterski, R. L. Martin, K. Morokuma, V. G. Zakrzewski, G. A. Voth, P. Salvador, J. J. Dannenberg, S. Dapprich, A. D. Daniels, O. Farkas, J. B. Foresman, J. V. Ortiz, J. Cioslowski, and D. J. Fox. *Gaussian 09, Revision A.1* (Gaussian, Inc., Wallingford CT, 2009).
162. Allouche, A.-R. Gabedit--a graphical user interface for computational chemistry softwares. *Journal of computational chemistry* **32,** 174–182 (2011).
163. Cauët, E. & Liévin, J. in *Advances in Quantum Chemistry, Volume 52. Theory of the Interaction of Radiation with Biomolecules,* edited by J.R. Sabin (Elsevier, Burlington, 2006), pp. 121–147.
164. Colson, A.O., Besler, B. & Sevilla, M.D. Ab initio molecular orbital calculations on DNA base pair radical ions. Effect of base pairing on proton-transfer energies, electron affinities, and ionization potentials. *J. Phys. Chem.* **96,** 9787–9794 (1992).

Appendix

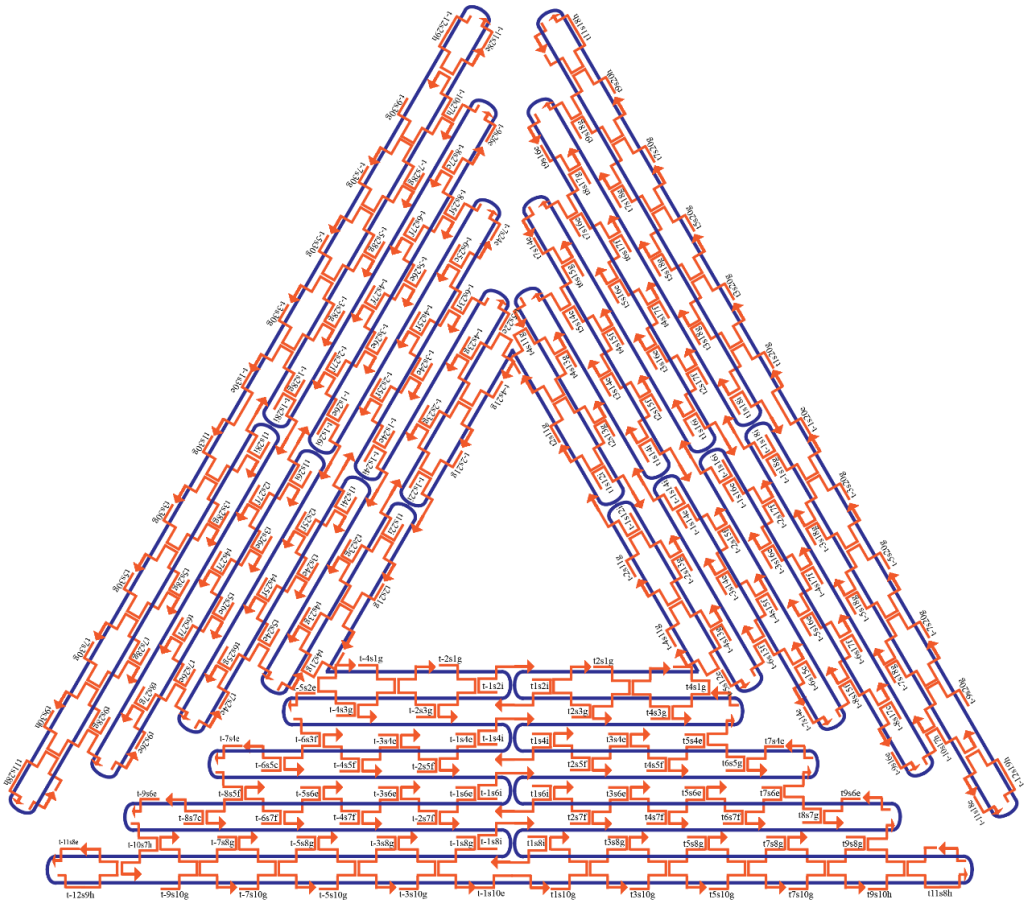

A.1 DNA origami nanostructure map with the scaffold strand marked in blue and the staple strands marked in red; each staple strand has a denotation corresponding to its position; the graphic was created by Alexander Rotaru.

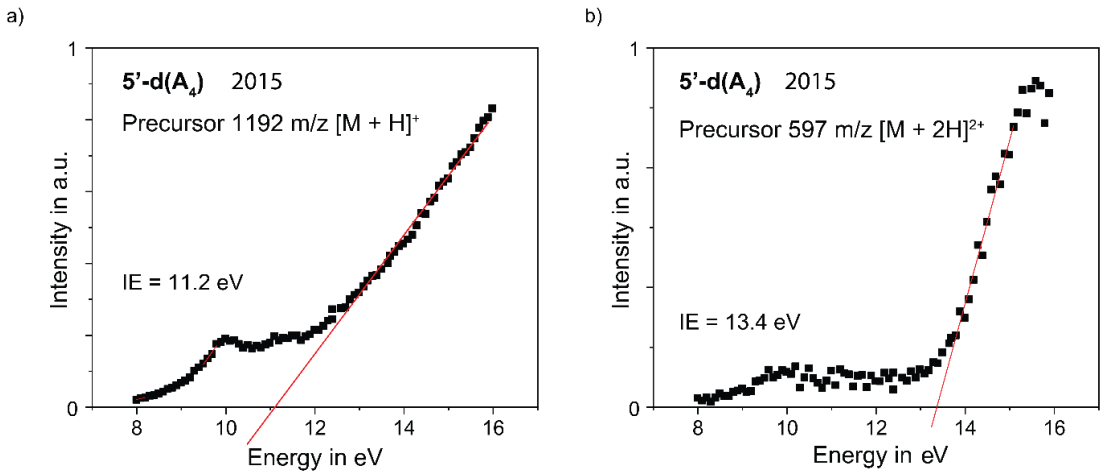

A.2 Intensity trend in arbitrary units (a.u.) of the precursor cations $[M + H]^+$ (a) and $[M + 2H]^{2+}$ (b) of the DNA sequence 5'-d(A_4) correlated to the increasing photon irradiation energy; determination of the IE *via* extrapolation to zero intensity; data from 2015.

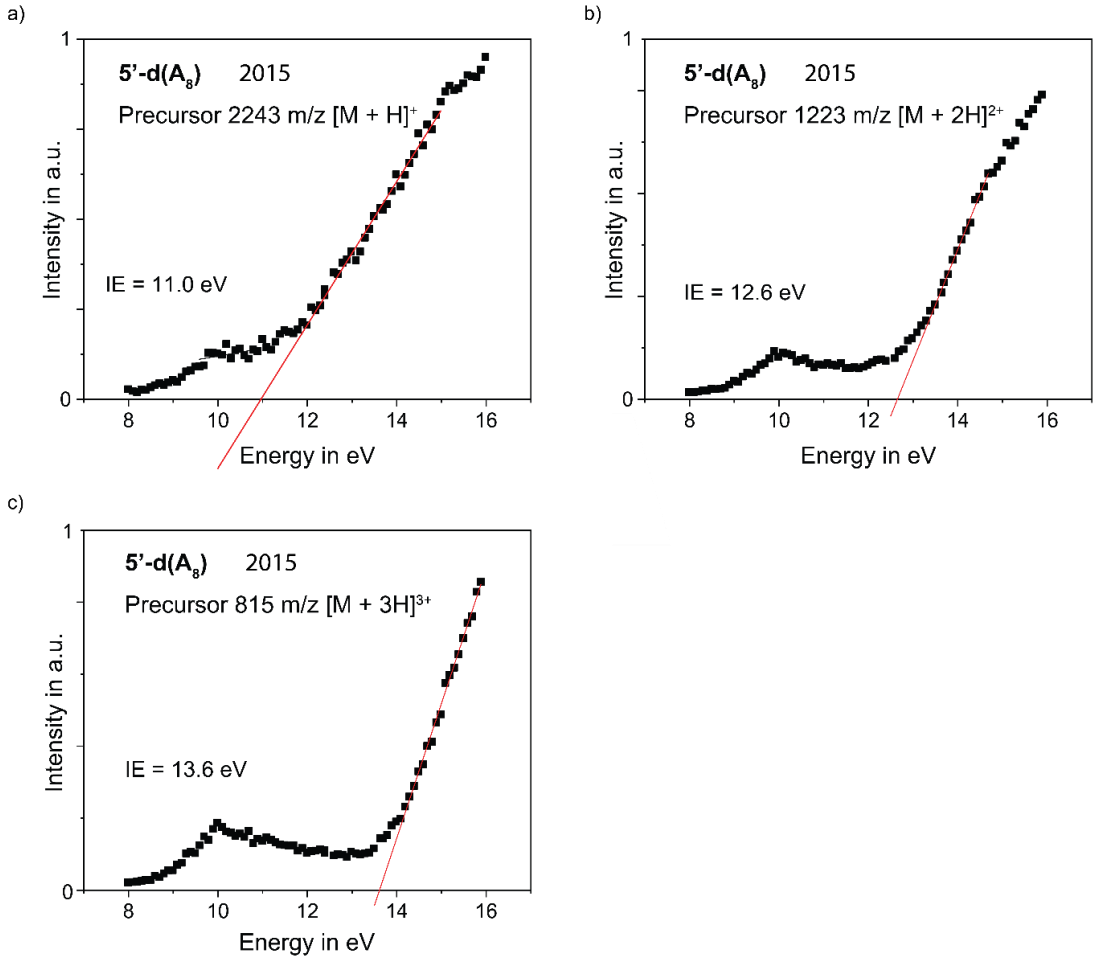

A.3 Intensity trend in arbitrary units (a.u.) of the precursor cations M1+ (a), M2+ (b) and M3+ (c) of the DNA sequence 5'-d(A_8) correlated to the increasing photon irradiation energy; determination of the IE *via* extrapolation to zero intensity; data from 2015.

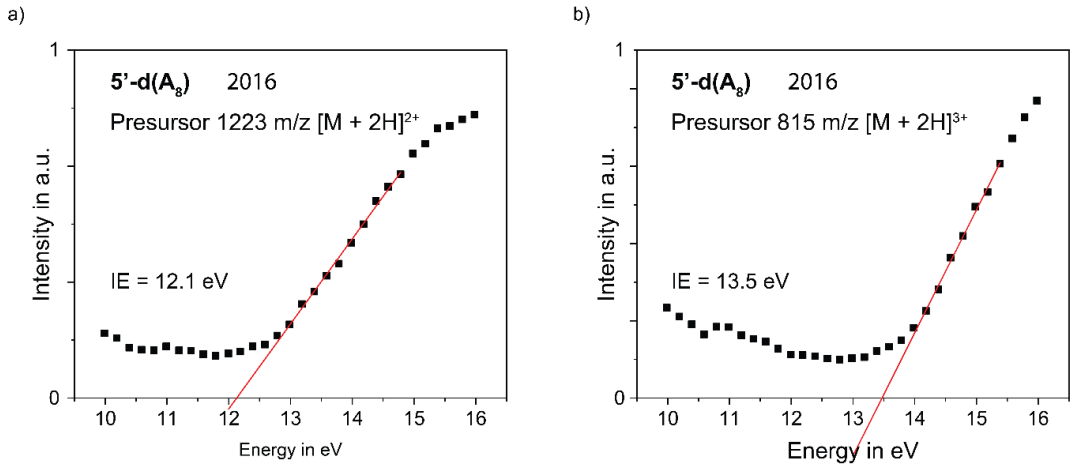

A.4 Intensity trend in arbitrary units (a.u.) of the precursor cations $[M + H]^+$ (a) and $[M + 2H]^{2+}$ (b) of the DNA sequence 5'-d(A_8) correlated to the increasing photon irradiation energy; determination of the IE *via* extrapolation to zero intensity, data from 2016.

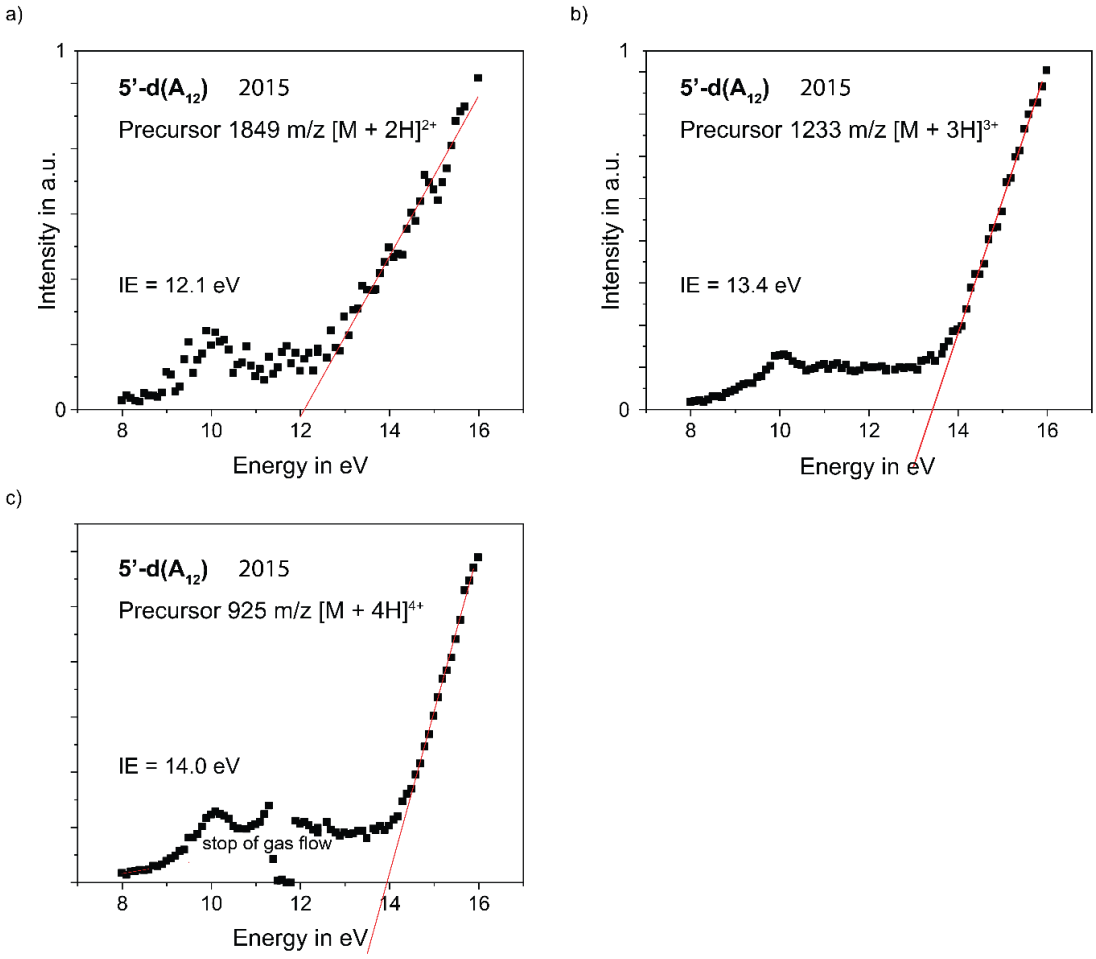

A.5 Intensity trend in arbitrary units (a.u.) of the precursor cations $[M + 2H]^{2+}$ (a), $[M + 3H]^{3+}$ (b) and $[M + 4H]^{4+}$ (c) of the DNA sequence 5'-d(A_{12}) correlated to the increasing photon irradiation energy; determination of the IE *via* extrapolation to zero intensity; data from 2015.

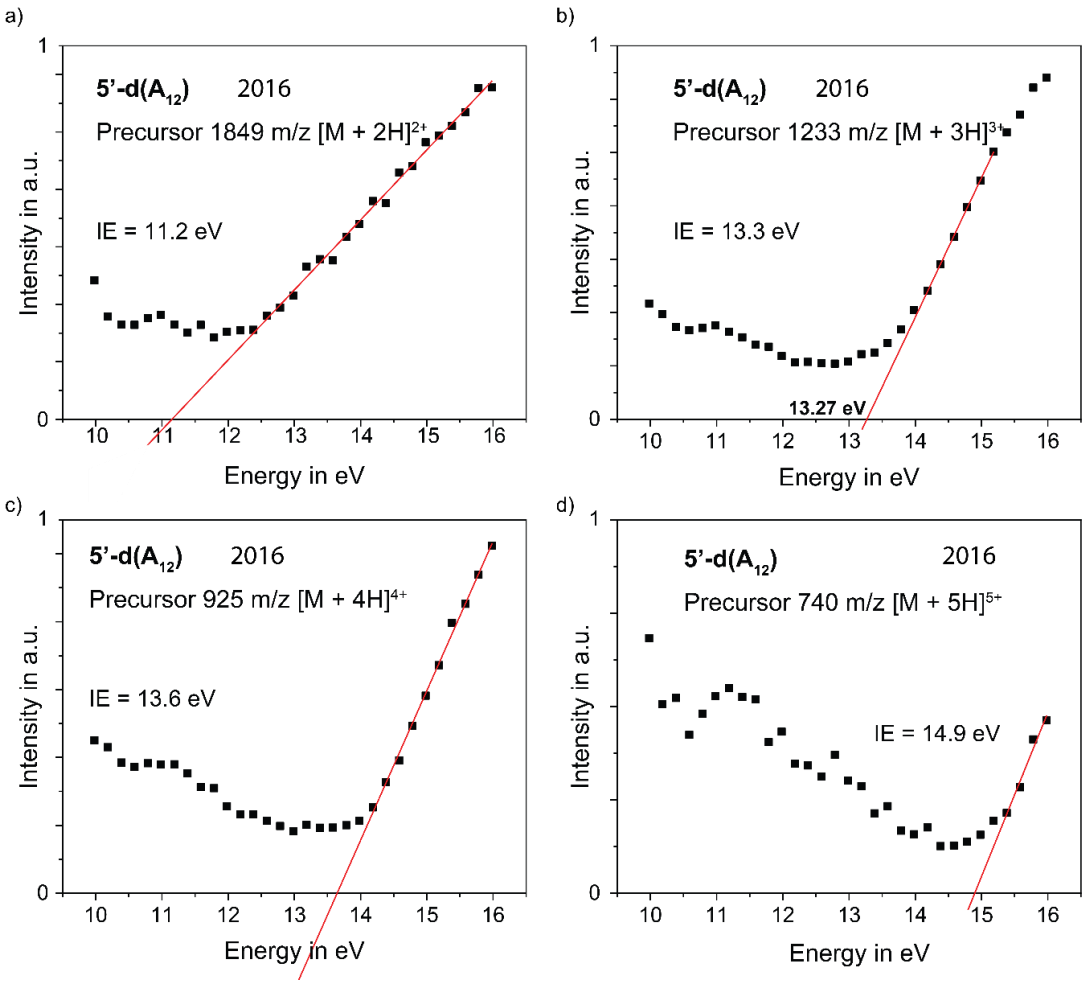

A.6 Intensity trend in arbitrary units (a.u.) of the precursor cations $[M + 2H]^{2+}$ (a), $[M + 3H]^{3+}$ (b), $[M + 4H]^{4+}$ (c) and $[M + 5H]^{5+}$ (d) of the DNA sequence 5'-d(A_{12}) correlated to the increasing photon irradiation energy; determination of the IE *via* extrapolation to zero intensity; data from 2016.

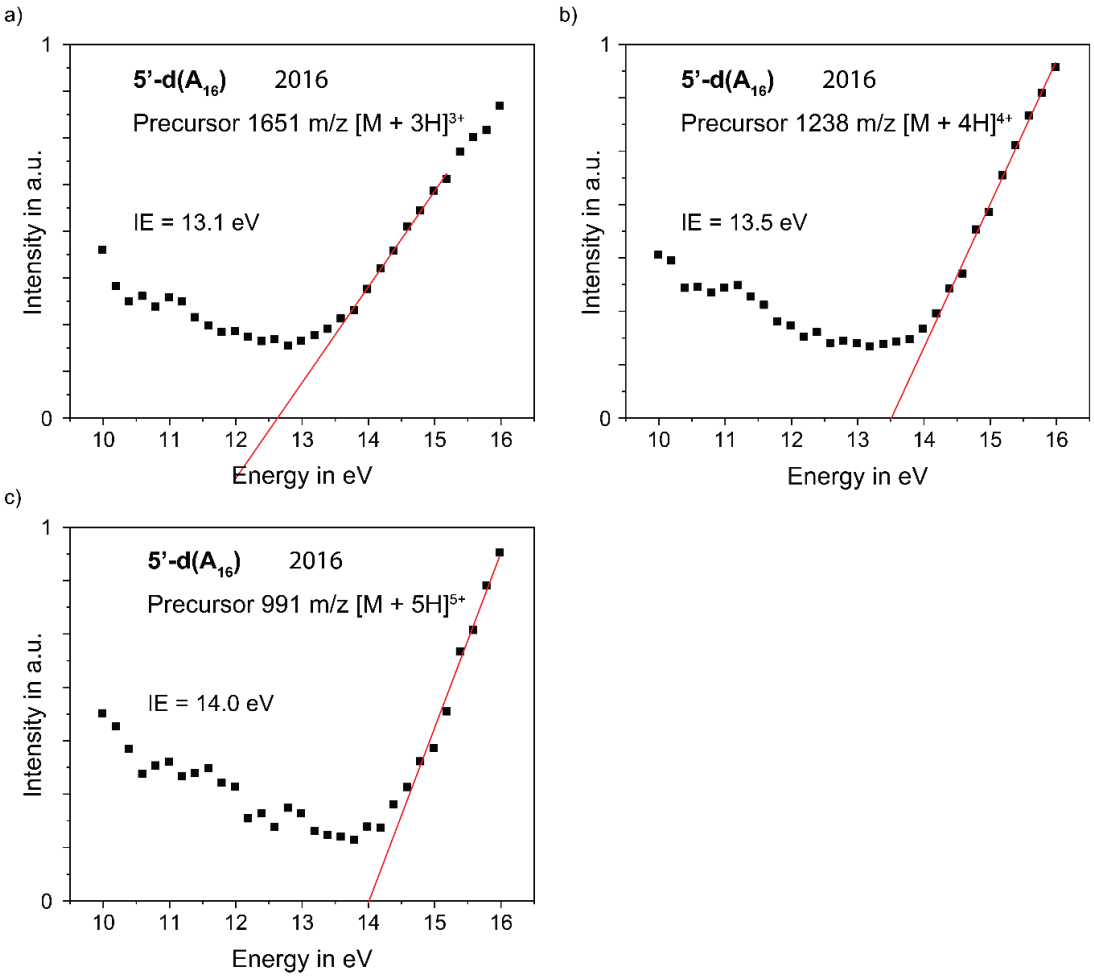

A.7 Intensity trend in arbitrary units (a.u.) of the precursor cations $[M + 3H]^{3+}$ (a), $[M + 4H]^{4+}$ (b) and $[M + 5H]^{5+}$ (c) of the DNA sequence 5'-d(A_{16}) correlated to the increasing photon irradiation energy; determination of the IE *via* extrapolation to zero intensity; data from 2016.

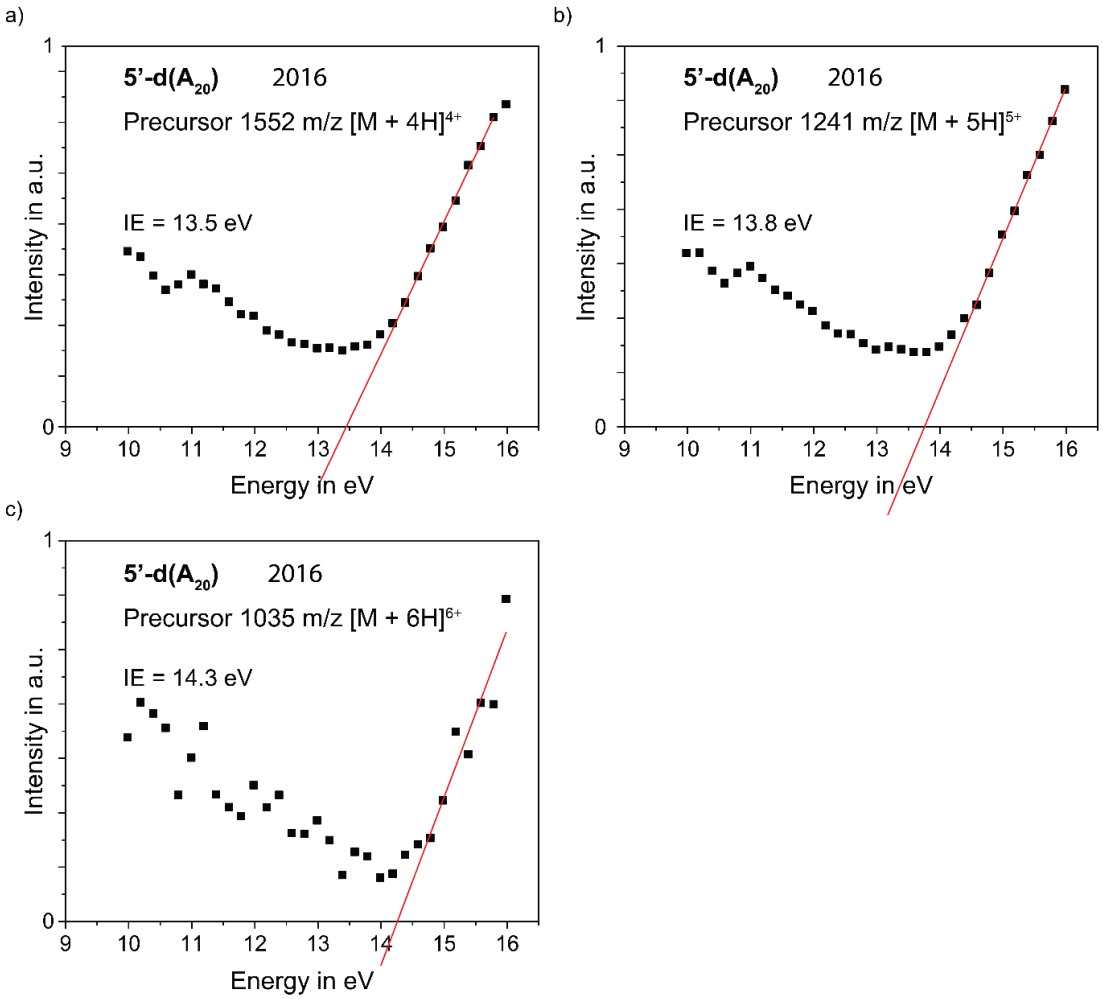

A.8 Intensity trend in arbitrary units (a.u.) of the precursor cations $[M + 4H]^{4+}$ (a), $[M + 5H]^{5+}$ (b) and $[M + 6H]^{6+}$ (c) of the DNA sequence 5'-d(A_{20}) correlated to the increasing photon irradiation energy; determination of the IE *via* extrapolation to zero intensity; data from 2016.

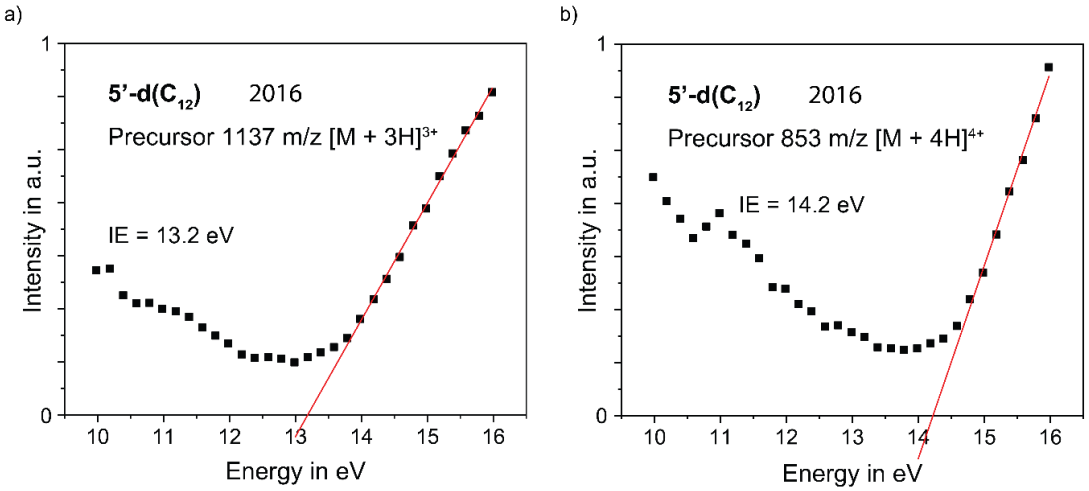

A.9 Intensity trend in arbitrary units (a.u.) of the precursor cations $[M + 3H]^{3+}$ (a) and $[M + 4H]^{4+}$ (b) of the DNA sequence 5'-d(C_{12}) correlated to the increasing photon irradiation energy; determination of the IE *via* extrapolation to zero intensity; data from 2016.

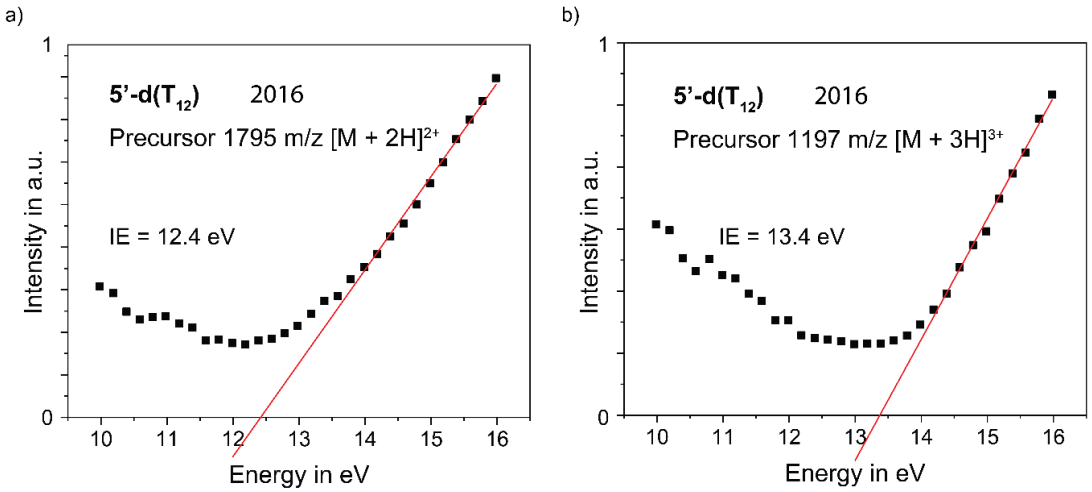

A.10 Intensity trend in arbitrary units (a.u.) of the precursor cations $[M + 2H]^{2+}$ (a) and $[M + 3H]^{3+}$ (b) of the DNA sequence 5'-d(T_{12}) correlated to the increasing photon irradiation energy; determination of the IE *via* extrapolation to zero intensity; data from 2016.

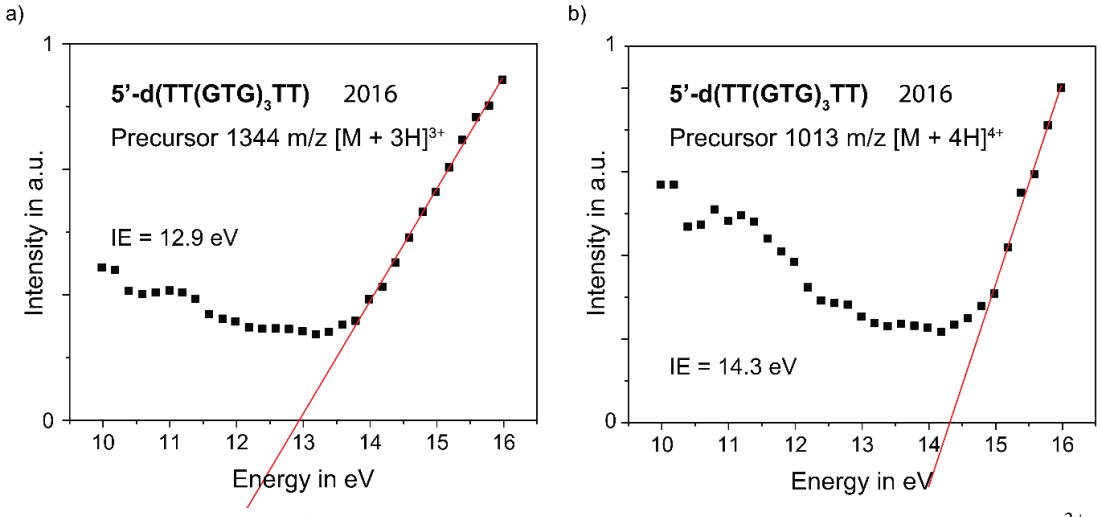

A.11 Intensity trend in arbitrary units (a.u.) of the precursor cations $[M + 3H]^{3+}$ (a) and $[M + 4H]^{4+}$ (b) of the DNA sequence 5'-d(TT(GTG)$_3$TT) correlated to the increasing photon irradiation energy; determination of the IE *via* extrapolation to zero intensity; data from 2016.

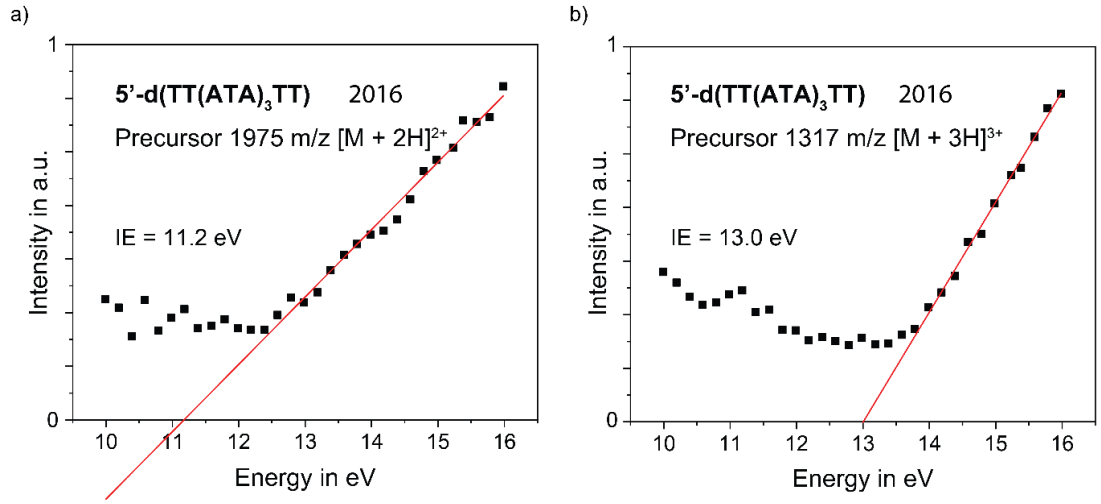

A.12 Intensity trend in arbitrary units (a.u.) of the precursor cations $[M + 2H]^{2+}$ (a) and $[M + 3H]^{3+}$ (b) of the DNA sequence 5'-d(TT(ATA)$_3$TT) correlated to the increasing photon irradiation energy; determination of the IE *via* extrapolation to zero intensity; data from 2016.

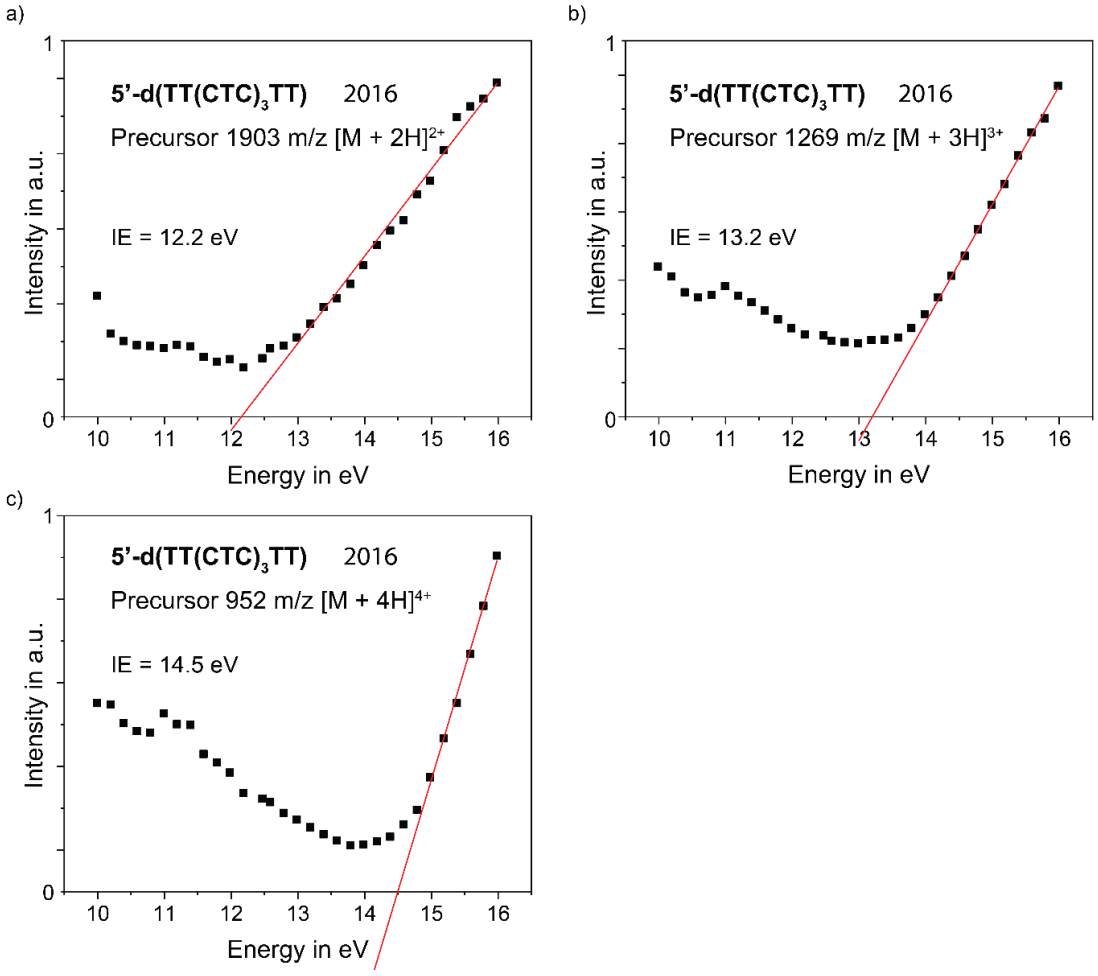

A.13 Intensity trend in arbitrary units (a.u.) of the precursor cations $[M + 2H]^{2+}$ (a), $[M + 3H]^{3+}$ (b) and $[M + 4H]^{4+}$ (c) of the DNA sequence 5'-d(TT(CTC)$_3$TT) correlated to the increasing photon irradiation energy; determination of the IE *via* extrapolation to zero intensity; data from 2016.

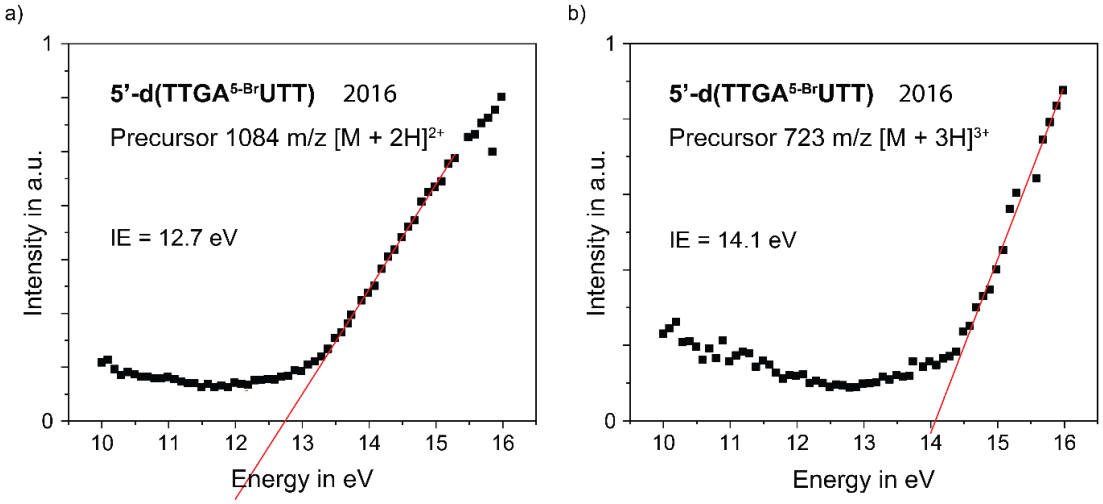

A.14 Intensity trend in arbitrary units (a.u.) of the precursor cations $[M + 2H]^{2+}$ (a) and $[M + 3H]^{3+}$ (b) of the DNA sequence 5'-d(TTGA^{5Br}UTT) correlated to the increasing photon irradiation energy; determination of the IE *via* extrapolation to zero intensity; data from 2016.

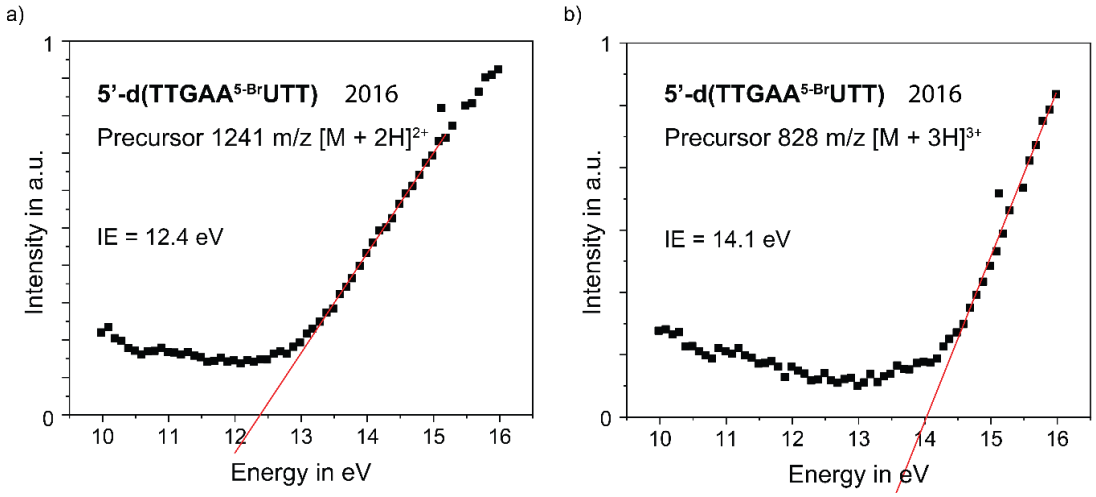

A.15 Intensity trend in arbitrary units (a.u.) of the precursor cations $[M + 2H]^{2+}$ (a) and $[M + 3H]^{3+}$ (b) of the DNA sequence 5'-d(TTGAA^{5Br}UTT) correlated to the increasing photon irradiation energy; determination of the IE *via* extrapolation to zero intensity; data from 2016.

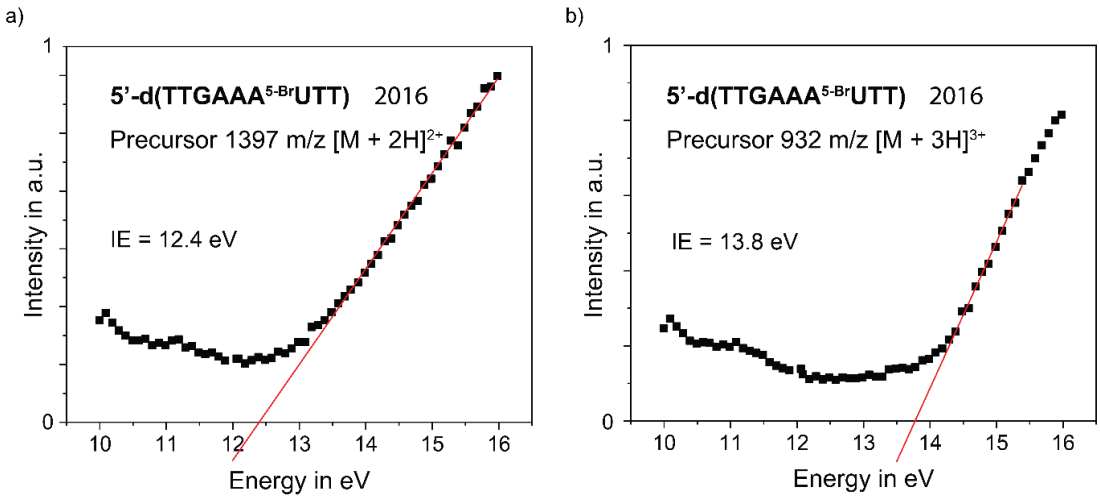

A.16 Intensity trend in arbitrary units (a.u.) of the precursor cations $[M + 2H]^{2+}$ (a) and $[M + 3H]^{3+}$ (b) of the DNA sequence 5'-d(TTGAAA^{5Br}UTT) correlated to the increasing photon irradiation energy; determination of the IE *via* extrapolation to zero intensity; data from 2016.

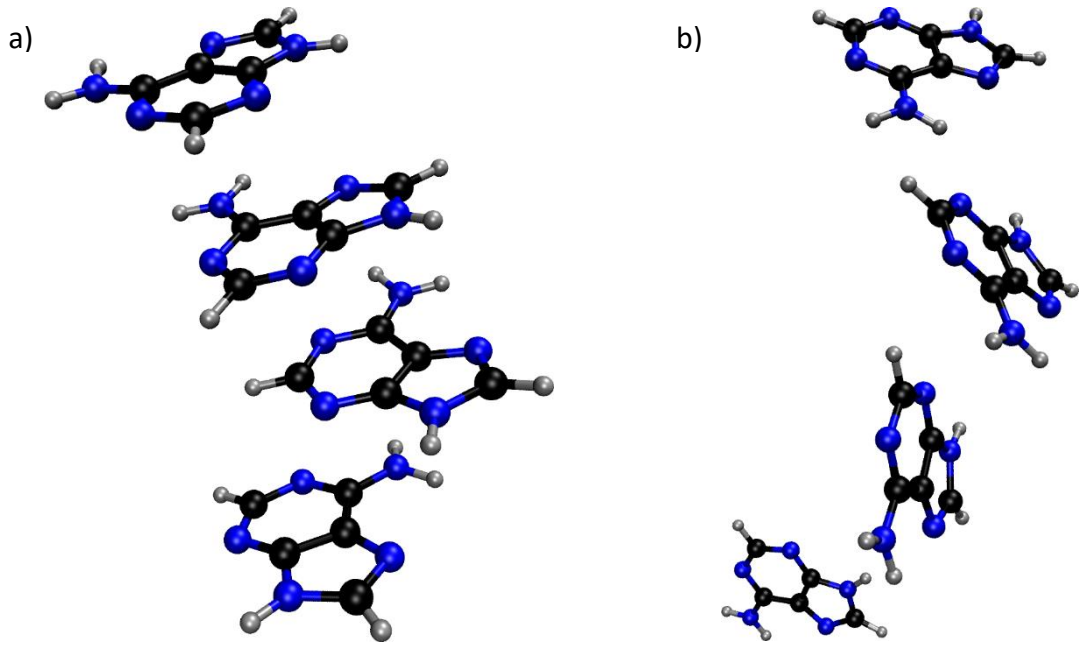

A.17 Geometry predictions of four A nucleobases forming the DNA sequence 5'-d(A_4) at 0 K (a) and 300 K (b) calculated with Gaussian09 [161] (a) and Gabedit 2.4.8 [162] (b) by Gallandi and Körzdörfer [151]; carbon is shown in black, nitrogen in blue and hydrogen in grey.

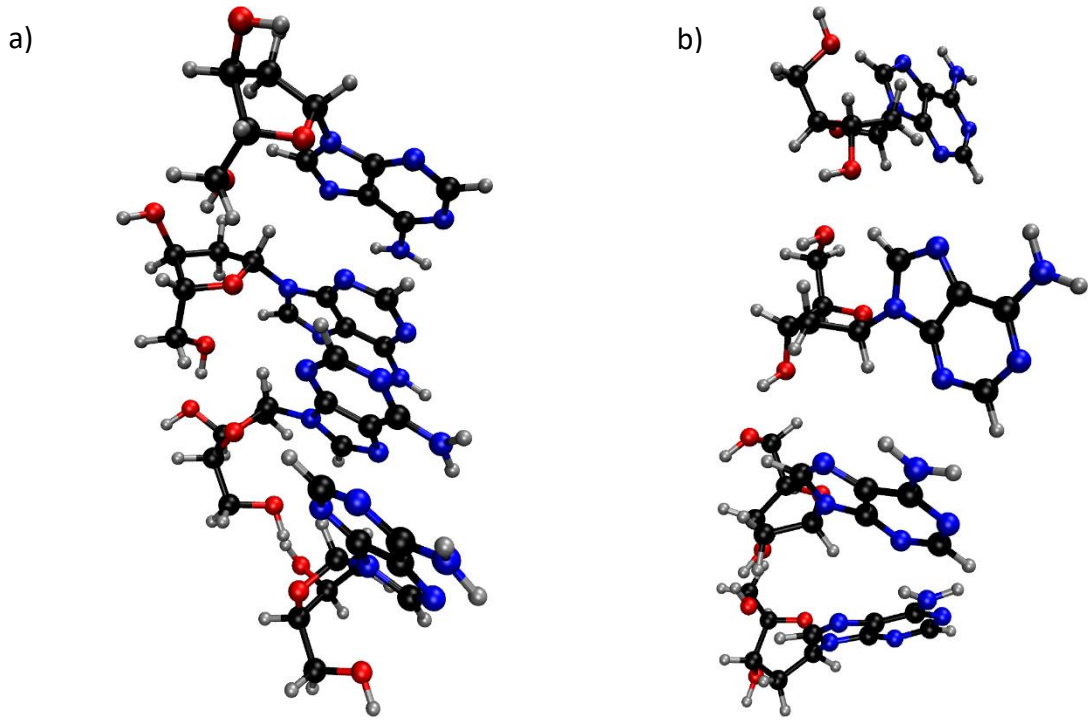

A.18 Geometry predictions of four A nucleobases with the corresponding sugar units forming the DNA sequence 5'-d(A_4) at 0 K (a) and 300 K (b) calculated with Gaussian09 [161] (a) and Gabedit 2.4.8 [162] (b) by Gallandi and Körzdörfer [151]; carbon is shown in black, nitrogen in blue, hydrogen in grey and oxygen in red.

a) b)

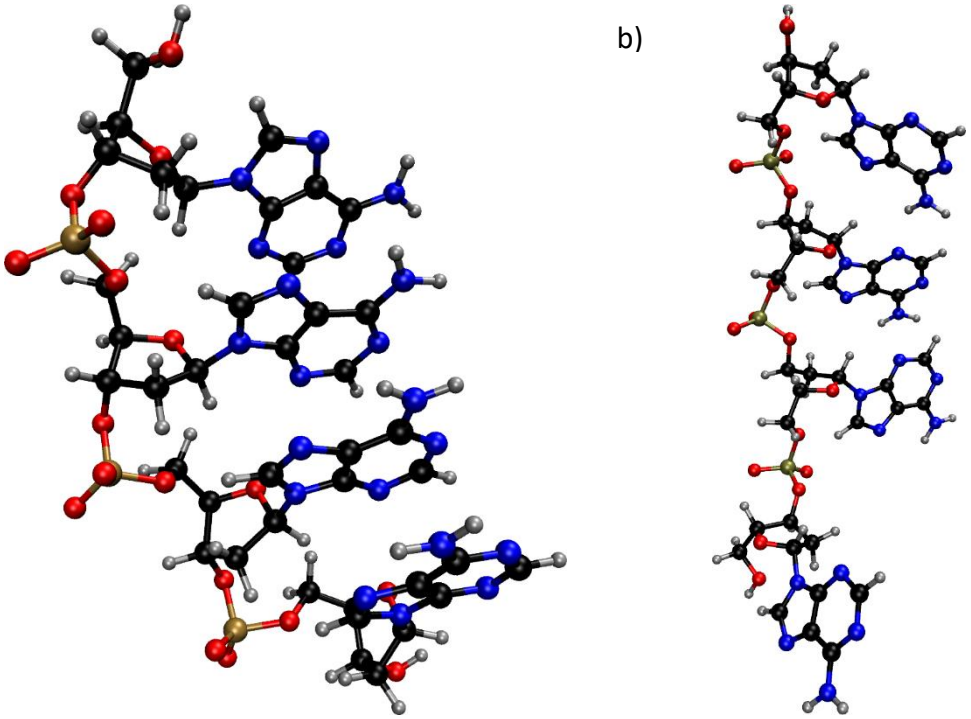

A.19 Geometry predictions of full DNA sequence 5'-d(A_4) at 0 K (a) and 300 K (b) calculated with Gaussian09 [161] (a) and Gabedit 2.4.8 [162] (b) by Gallandi and Körzdörfer [151]; carbon is shown in black, nitrogen in blue, hydrogen in grey, oxygen in red and phosphor in gold.

List of publications

S. Vogel, K. Ebel, R. Schürmann, C. Heck, T. Meiling, A. Guiliani, A. R. Milosavljević, I. Bald, „Vacuum-UV and Low-Energy Electron Induced DNA Strand Breaks – Influence of the DNA Sequence and Substrate" *submitted*.

S. Vogel, K. Ebel, R. Schürmann, C. Heck, A. Guiliani, A. R. Milosavljević, I. Bald, „Vacuum-UV and Low-Energy Electron Induced DNA Strand Breaks – Influence of the Radiosensitizers 5-Bromouracil and 8-Bromoadenine" *in preparation*.

S. Vogel, K. Ebel, A. Guiliani, M. Ranković, A. R. Milosavljević, L. Gallandi, T. Körzdörfer, I. Bald, „Charge-State Dependence of the Gas-Phase Ionization Energies of Short DNA Sequences – Experimental and Computed Studies" *in preparation*.

R. Schürmann, S. Vogel, K. Ebel, I. Bald, "The physico-chemical basis of DNA radiosensitization - Implications for cancer radiation therapy" *Chemistry – A European Journal* **2018**, *24*, 1–10.

T. Meiling, R. Schürmann, S. Vogel, K. Ebel, C. Nicolas, A. R. Milosavljević, I. Bald, "Photophysics and Chemistry of Nitrogen-Doped Carbon Nanodots with High Photoluminescence Quantum Yield" *J. Phys. Chem. C*, **2018**, *122*, 10217–10230.

S. Vogel, J. Rackwitz, R. Schürman, J. Prinz, A. R. Milosavljević, M. Réfrégiers, A. Giuliani, I. Bald, *"*Using DNA Origami Nanostructures to Determine Absolute Cross Sections for UV Photon-Induced DNA Strand Breakage" *Journal of Physical Chemistry Letters* **2015**, *6*, 4589−4593.

M. Girod, S. Vogel, W. Szczerba, A. F. Thünemann, "How Temperature Determines Formation of Maghemite Nanoparticles" *Journal of Magnetism and Magnetic Materials* **2015**, *380*, 163-167.

Talks

S. Vogel und I. Bald "VUV and LEE induced ssDNA strand breaks - dependency on the DNA sequence and the irradiation type" *ARGENT - Advanced Radiotherapy, Generated by Exploiting Nanoprocesses and Technologies*, Paris, France, **2018**.

S. Vogel und I. Bald "VUV-induced damage of DNA probed by synchrotron radiation" *Handlungsfeldkonferenz Optische Analytik*, Berlin, Germany, **2017**.

S. Vogel und I. Bald "Probing DNA radiation damage by means of the DNA origami technique" *Potsdamer Doktorandensymposium der Chemie*, Berlin, Germany, **2017**.

S. Vogel und I. Bald “Sequence-specific ionization potentials of oligonucleotides correlated with VUV- and LEE induced DNA strand breaks” *Workshop on Nano-bio-physics*, Tel Aviv, Israel, **2017**.

S. Vogel und I. Bald “Determination of the ionization threshold of oligonucleotides and sequence-specific VUV-induced DNA strand breaks using the DNA origami technique” *115th General Assembly of the German Bunsen Society for Physical Chemistry*, Rostock, Germany, **2016**.

S. Vogel und I. Bald “Absolute Cross Sections for UV-Induced Sequence-Specific DNA Strand Breaks Determined on the Single-Molecule Level” *Network Meeting of Biomolecular nanostructures for the study of biophysical and biochemical processes*, Potsdam, Germany, **2015**.

Poster

S. Vogel und I. Bald “Sequence-specific ionization potentials of oligonucleotides correlated with VUV-induced DNA strand breaks” *116th General Assembly of the German Bunsen Society for Physical Chemistry*, Kaiserslautern, Germany, **2017**.

S. Vogel und I. Bald “Determination of the ionization threshold of oligonucleotides and sequence-specific VUV-induced DNA strand breaks using the DNA origami technique” *14th International Workshop on radiation damage to DNA*, Melbourne, Australia, **2016**.

S. Vogel und I. Bald “Determination of sequence-specific DNA strand breaks induced by VUV radiation using the DNA origami technique” S*ummer School - Woman in Optics*, Marburg, Germany, **2016**.

S. Vogel und I. Bald „Absolute Cross Sections for UV-Induced Sequence-Specific DNA Strand Breaks Determined on the Single-Molecule Level” *XXIX International Conference on Photonic, Electronic, and Atomic Collisions*, Toledo, Spain, **2015**.

Acknowledgements

Diese Arbeit ist in dem Zeitraum von Januar 2015 bis Juni 2018 an der Universität Potsdam und der Bundesanstalt für Materialforschung und -prüfung entstanden. Viele Menschen haben zum Erfolg dieser Arbeit beigetragen und sowohl fachliche als auch emotionale Unterstützung geleistet. Mein größter Dank gilt Prof. Dr. Ilko Bald, der mir die Möglichkeit gegeben hat, mich im Rahmen meine Doktorarbeit mit dem interessanten Gebiet der DNA Strahlenschädigung in seiner Arbeitsgruppe zu beschäftigen. Ich bin sehr dankbar für seine exzellente Betreuung. Immer offen für Fragen und Vorschläge, hat er dafür gesorgt, dass ich in unseren wissenschaftlichen Diskussionen immer viel gelernt habe. Darüber hinaus ermöglichte er es mir, meine Arbeit auf verschiedenen wissenschaftlichen Konferenzen zu präsentieren und einen einmonatigen Forschungsaufenthalt in der Notre Dame University, Indiana in den USA zu verbringen. Ich werde meine Promotionszeit immer in der besten Erinnerung behalten. Sowohl Prof. Dr. Ilko Bald als auch Privatdozent Dr. Thomas Schlathölter und Privatdozent Dr. Steen Brøndsted Nielsen möchte ich für die Anfertigung der Gutachten zu meiner Doktorarbeit danken.

Ferner gilt mein Dank möchte ich der Graduiertenschule SALSA, die mich nicht nur bei meine Promotion, sondern auch mit vielen Reisen zu Konferenzen und einen einmonatigem Forschungsaufenthalt in den USA unterstützte. Daneben möchte ich mich bei Dr. Aleksandar R. Milosavljevic und Prof. Dr. Sylvia Ptasinska bedanken, die mich in ihrem Labor an der Notre Dame University, Indiana, USA aufgenommen haben.

Großer Dank gilt auch meinen Kollegen Kenny Ebel, Dr. Christian Heck, Dr. Robin Schürmann und Dr. Till Meiling, die zum Teil mehrfach mit mir zum Synchrotron SOLEIL in Frankreich gereist sind, um mich bei der Durchführung meiner Experimente zu unterstützen. Die vielen Nachtschichten und die enge Zusammenarbeit haben viele Ergebnisse gebracht, die in dieser Arbeit präsentiert werden. Vor Ort wurde ich zusätzlich durch den Beamline-Wissenschaftler Dr. Alexandre Guiliani unterstützt, der sich bereits vor unserer Ankunft um den Aufbau des Experiments organisiert hat und vor Ort immer als Ansprechpartner zur Verfügung stand. Für die Betreuung der MS^2 Experimente möchte ich mich ferner bei Dr. Aleksandar R. Milosavljevic und Dr. Milos Ranković bedanken, die mir bei ersten Experimenten betreuend zur Seite standen.

Darüber hinaus möchte ich mich bei meiner Arbeitsgruppe (Youngeun Choi, Dr. Christian Heck, Kenny Ebel, Dr. Robin Schürmann, Dr. Lydia Olejko, Dr. Julia Prinz und Dr. Till Meiling) für die tolle Arbeitsatmosphäre, fachlich Hilfe und kreative Einfälle bedanken. Insbesondere möchte ich mich bei Youngeun bedanken, die mich vor allem in der letzten Phase dieser Arbeit immer unterstützt und mir neuen Mut zugesprochen hat. Dr. Matthias Schenderlein möchte ich ebenfalls danken, dass er sich die Zeit genommen hat, meine Arbeit Korrektur zu lesen.

Zu guter Letzt möchte ich noch meinen Freunden und meiner Familie für die stete Unterstützung danken. Mein besonderer Dank gilt hier meinem Freund Stefan Schmechel, der mit mir durch alle Höhen und Tiefen gegangen ist.

Erklärung

Hiermit versichere ich, dass ich die vorliegende Arbeit selbst verfasst und keine anderen Quellen und Hilfsmittel als die hier angegebenen verwendet habe. Ich versichere, dass diese Arbeit bisher nicht an anderer Stelle zur Erlangung des Doktorgrades eingereicht wurde.

Potsdam, 19.06.2018

Stefanie Vogel